NTNU

Norwegian University of
Science and Technology

Pipeline Integrity Assessment of Dent with Gouge after Trawling Impact

Adrian Haugsand Aadal

Marine Technology
Submission date: June 2017
Supervisor: Sigmund Kyrre Ås, IMT

Norwegian University of Science and Technology
Department of Marine Technology

Preface

This thesis is the final project in the five-year Master's of Science program at the Department of Maine Technology at the Norwegian University of Science and Technology (NTNU) in Trondheim, Norway. The thesis continues preliminary work done in a project thesis course.

The learning outcome of this thesis have been great, and the topic have proven challenging and highly interesting.

This report is written for people with basic knowledge in material science and fatigue mechanics, although the basics are hopefully adequately covered in the report.

Adrian Haugsand Aadal,

Trondheim, 09.06.2017

Acknowledgements

I would like to thank my supervisor Sigmund Kyrre Ås for his guidance and valuable input, for helping to create an exciting project, and for being available whenever I needed assistance.

I would also like to thank Kristian Minde, Emil Bratlie and Kristian Aamodt for making the fatigue tests possible, and for teaching and assisting me whenever I needed it in the lab.

And finally, I would like to thank the boys at the office C1.084 for good times and support during the semester.

Abstract

Damage to pipelines from interaction with trawler-gear affects the long-term integrity of the pipeline, and interference from trawling-equipment on subsea pipelines is a relatively common occurrence. This thesis looks on how a gouge introduced to a dent in the pipe affects the fatigue life, compared to a dent without a gouge. The indentation from trawler-gear is replicated by a test-rig and simulated numerically.

A damage system with a smooth dent containing a gouge is a severe form of mechanical damage on a pipeline, and pipes containing dent with gouge must be replaced according to today's regulations. A brief review of the current practice of pipe damage assessment is done, with methodologies from PETROBRAS, The European Pipeline Research Group and American Petroleum Institute, among others.

The numerical model was made to resemble the conditions of the experimental test-setup to create comparable results. The setup allows denting of small scale pipes, creating dents with or without gouges. An indenter is pushed along the top of the pipe transverse to the pipe longitudinal-axis, resembling trawler-equipment impact. The pipe is first subjected to an incrementally increasing static pressure. The pipe is then subjected to internal pressure cycles with fixed mean and amplitude pressure. The dent geometry is not equal for the experimental and numerical results, and the dent behaves differently under pressure because of different material properties. This makes the comparison more complicated, but the residual stresses from an x-ray diffractor gives good consistent results with the numerical simulation.

A total of ten fatigue tests are carried out for dents with and without a gouge. Assuming a maximum fatigue life of 10^6 pressure cycles, the endurance limit decreases from 44 bar to 36 bar when introducing a gouge, a factor of 18.2 %. This decrease is not as severe as expected in terms of fatigue life. The most critical areas are where the indenter enters and exits the pipe for high pressure, and on the side of the dent shoulder for low pressure. The dents with gouge have the through-crack initiated from the gouge base, which decreases the fatigue life.

Fatigue life is influenced by stress concentrations, which in turn are influenced by the dent geometry. Rerounding of the dent from internal pressure reduces the dent depth, which reduces the stress concentrations. In this thesis, one test is performed with increased rerounding before the fatigue test begins. This more than doubled the number of cycles of the pipe without failing, compared to a similar pipe with no increased rerounding. This indicates that it could be a potential way of repairing dents in term of a fatigue perspective.

This thesis only uses pipes with one geometry, creating dents with one depth. More fatigue tests should be performed to improve the knowledge on the effect of a gouge in the dent. This thesis only investigates possibilities, and could serve as a preliminary study for future fatigue tests.

Sammendrag

Skader på rørledninger fra interaksjonen med trålerutstyr påvirker rørets integritet på lang sikt, og interaksjon mellom trålerutstyr og undervannsrørledninger forekommer relativt ofte. Denne oppgaven ser på hvordan en bulk med kutt i røret påvirker utmattingslevetiden, sammenlignet med en bulk uten kutt. Bulkingen fra trålerutstyret er gjenskapt med en testrigg og simulert numerisk.

Et skadesystem som inneholder en bulk med et kutt er en alvorlig form for mekanisk skade, og rør som inneholder en slik skade må byttes ut ifølge dagens regelverk. Det er gjort en kort gjennomgang av dagens praksis om skadevurdering av rør, med blant annet metoder fra PETROBRAS, The European Pipeline Research Group og American Petroleum Institute.

Den numeriske modellen ble laget for å etterligne forholdene fra det eksperimentelle oppsettet for å få sammenlignbare resultater. Oppsettet tillater bulking av rør i småskala med eller uten kutt. Et bulkelegeme blir dyttet langs toppen av røret på tvers av rørets lengdeakse, som etterligner kollisjon med trålerutstyr. Røret blir først utsatt for inkrementelt økende statisk trykk, før det blir utsatt for indre trykksykler med fastsatt gjennomsnitt og amplitude. Geometrien til bulken er ikke lik for de to testtypene, og oppfører seg forskjellig på grunn av forskjell i materialegenskapene. Dette gjør det mer komplisert å sammenligne resultatene, men restspenningene som måles med røntgendiffraksjon gir konsistente resultater med den numeriske simuleringen.

Totalt ti utmattingstester ble utført for bulker med og uten kutt. Ved å anta et maksimalt utmattingsliv på 10^6 trykksykler, reduseres tretthetsgrensa fra et trykk på 44 bar til 36 bar når et kutt er til stede, en faktor på 18.2 %. Med tanke på utmattingslivet er ikke denne endringen så ille som antatt. De mest kritiske områdene er der hvor bulkelegemet går inn og ut av røret for høyt indre trykk, og på siden av bulken for lavt indre trykk. For bulker med kutt starter sprekkene som går gjennom veggtykkelsen i bunnen av kuttet, som reduseres levetiden sammenlignet med en bulk uten kutt.

Utmattingslivet påvirkes av spenningskonsentrasjoner, som på sin side påvirkes av bulkens geometri. En utpressing av bulken fra indre trykk reduserer bulkdybden, som reduserer spenningskonsentrasjonene. I denne oppgaven blir én test utført med økt utpressing før utmattingstesten starter. Dette mer en doblet antall trykksykler uten å ryke sammenlignet med et lignende rør uten økt utpressing. Fra et utmattingsperspektiv indikerer dette at det kan være en mulig måte å reparere bulken på.

Denne oppgaven bruker bare rør med én geometri, som lager bulker med én dybde. Flere utmattingstester burde utføres for å få økt kunnskap om kuttets effekt i bulken. Oppgaven undersøker bare muligheter, og kan fungere som en førstudie for fremtidige utmattingstester.

Contents

List of Figures

List of Tables

Abbreviations

NTNU	Norwegian University of Science and Technology
EGIG	European Gas pipeline Incident data Group
CONCAWE	European Oil Company Organization for Environment Health and Safety
SCF	Stress Concentration Factor
BHN	Brinell Hardness Number
SN	Stress-Life
JIP	Joint Industry Project
API	American Petroleum Institute
EPRG	European Pipeline Research Group
DOE-B	United Kingdom Department of Energy
ASME	American Society of Mechanical Engineers
DNV	Det Norske Veritas
CSA	Canadian Standards Association
LVDT	Linear Variable Differential Transformer
FEM	Finite Element Method

Nomenclature

σ	Stress	[MPa]
ϵ	Strain	[-]
E	Young's Modulus	[GPa]
σ_y, S_y	Yield Stress	[MPa]
ϵ_e	Elastic Strain	[-]
ϵ_p	Plastic Strain	[-]
H', K'	Plastic Tangent Modulus	[MPa]
σ_u, S_u	Ultimate Tensile Strength	[MPa]
ν	Poisson Ratio	[-]
τ	Shear Stress	[MPa]
γ	Shear Strain	[-]
G	Shear Modulus	[GPa]
σ_x	Axial Stress	[MPa]
σ_θ	Hoop Stress	[MPa]
σ_r	Radial Stress	[MPa]
r, R	Radius	[mm]
t	Thickness	[mm]
D	Diameter	[mm]
p	Pressure	[MPa]
σ_v	von Mises Stress	[MPa]
ϵ_P, ϵ_Q	Principle Strain for Strain Gage	[-]
$\epsilon_1, \epsilon_2, \epsilon_3$	Measured Gage Strain	[-]
θ, ϕ	Angle between Principle- and Directional Measurement	[rad]
ϵ_θ	Strain in Arbitrary Direction	[-]
K_t	Theoretical Stress Concentration Factor	[-]
$\bar{\sigma}_{max}$	Maximum Stress Value	[MPa]
$\bar{\sigma}_{nom}$	Nominal Stress Value	[MPa]

q	Notch Sensitivity Factor	[-]
K_f	Fatigue Stress Concentration Factor	[-]
d	Dent Depth	[mm]
w	Dent Width	[mm]
l	Dent Length	[mm]
$A_{(n,0,1)}$	Regression Parameters	[-]
$\alpha_{(1-4)}$	Curve Fitting Parameters	[-]
$\Delta S, S_r$	Stress Range	[MPa]
$\Delta\epsilon$	Strain Range	[-]
N	Number of Cycles to Failure	[-]
n	Number of Cycles in Stress Range	[-]
S_{max}	Maximum Stress	[MPa]
S_{min}	Minimum Stress	[MPa]
S_m	Mean Stress	[MPa]
R	Stress Ratio	[-]
D	Miner Summation	[-]
D_f	Failure Criterion	[-]
S_n'	Material Endurance Limit	[MPa]
S_n	Endurance Limit	[MPa]
σ_1	Maximum Principle Stress	[MPa]
S_1	Nominal Stress corresponding to σ_1	[MPa]
σ_2	Secondary Principle Stress	[MPa]
ϵ_1	Maximum Principle Strain	[-]
ϵ_N	Nominal Strain corresponding to ϵ_N	[-]
K_σ, K_ϵ	Stress Concentration Factors in Neuber's Equation	[-]
n', b, c	Fitting Parameters in Neuber's Equation	[-]
$N_f, \epsilon_f, \sigma_f$	Fatigue Parameters in Neuber's Equation	[-],[MPa]
A, B, C, D, E, F	Interpolation Coefficients	[-]
Δp	Pressure Range	[psi],[MPa]
$\sigma_a, \bar{\sigma}_a$	Alternating Stress	[MPa]
σ_A	EPRG Stress Parameter	[MPa]
S_e, k_a	PETROBRAS Parameters	[-]
b	PETROBRAS Slope	[-]

Chapter 1

Introduction

1.1 Background

Trawling-equipment interference with subsea pipelines is a relatively common occurrence. Trawling is a technique in fishing where a fish net is towed behind a fishing vessel with an opening in the net in the travelling direction. There are three types of trawling based on how the net is kept open. These are otter trawl, beam trawl and twin trawl [Joh12]. Interaction between a pipeline and trawl gear for the different types are seen in figure 1.1.

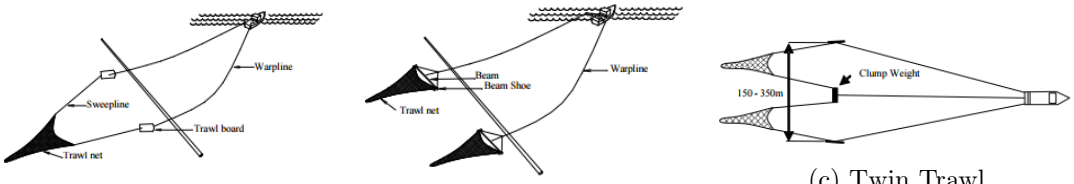

(a) Otter Trawl (b) Beam Trawl (c) Twin Trawl

Figure 1.1: Trawler Pipeline Interaction from [DG10]

Trawling could be performed on all water depth, also across the sea floor called bottom trawling. The equipment used to keep the net open is heavy, and could cause serious damage to pipelines if it is dragged across it. Trawler doors used for otter trawling can be seen in figure 1.2, while clump weights used for twin trawling can be seen in figure 1.3.

Figure 1.2: Different Types of Trawl Doors from [VJE07]

Figure 1.3: Different Types of Clump Weights from [VJE07]

The pipelines have protective measures to handle impact with the trawler equipment, but damage may occur which affects the long-term integrity of the pipe. This damage may result in smooth dents with or without scratches and gouges. Pipelines that develop a scratch or gouge because of such impact must be replaced according to today's rules and regulations, at great cost for the companies. Interference from external factors is relatively common, as seen in table 1.1, which is data taken from reports by the European Gas pipeline Incident data Group (EGIG) for gas, and the European Oil Company Organization for Environment Health and Safety (CONCAWE) for oil [Eli16].

Table 1.1: Distribution of Damage Incidents from [Eli16]

Pipeline:	External interference	Corrosion	Construction defects/ material failures	Ground	Other movement
Gas	35 %	24 %	16 %	13 %	12 %
Oil (Hot)	13 %	81 %	N/A	N/A	6 %
Oil (Cold)	71 %	19 %	N/A	N/A	10 %

1.2 Objective

The objective of this thesis is to look at how gouges introduced into smooth dents affect the fatigue life of the pipe compared to a smooth dent without a gouge, and how a numerical simulation of the dented pipe compares with the stress and strain values found around the real dented pipes. This should help lie the foundation for future fatigue tests.

1.3 Scope and Limitations

The scope of the thesis is to:

- Create dents with and without gouges in pipes of the same geometry.
- Perform fatigue tests on the dented pipes by subjecting it to cyclic internal pressure with fixed mean pressure and amplitude.
- Create an SN-curve of the fatigue tests with and without gouge.
- Perform numerical simulations, replicating the conditions from the indentation and pressurization of the experimental pipes.
- Compare the numerical simulation with stress and strain values found from strain gages and using x-ray diffraction.

The work in this thesis is imitated in that it only uses pipe geometry with one thickness and diameter. The dent depth is also the same for all pipes before the fatigue tests. The gouge is not modelled in the numerical simulation.

1.4 Definition of Terms

Some terminology on damage types in pipelines need to be introduced. The terminology is taken from [CH04].

- **Kinked dent**: a dent which causes an abrupt change in the curvature of the pipe wall (radius of curvature (in any direction) of the sharpest part of the dent is less than five times the wall thickness).
- **Plain dent**: a smooth dent that contains no wall thickness reductions (such as a gouge or a crack) or other defects or imperfections (such as a girth or seam weld).
- **Unconstrained dent**: a dent that is free to rebound elastically (spring back) when the indenter is removed, and is free to reround as the internal pressure changes.
- **Constrained dent**: a dent that is not free to rebound or reround, because the indenter is not removed (a rock dent is an example of a constrained dent).
- **Gouge**: surface damage caused by contact with a foreign object that has removed material from the pipe, resulting in a metal loss defect. The depth of a gouge is equal to the depth of the metal loss plus the depth of any cracking at the base of the gouge.

Chapter 2

Theory

2.1 Elasticity and Plasticity

Elasticity and plasticity are common terms in material science, and defines the material behavior under the influence of stresses. A typical stress-strain relationship for a metal can be seen in figure 2.1. Initially, there is a linear relationship between stress and strain governed by Hooke's law for a one dimensional linear-elastic material, seen in equation 2.1.

$$\sigma = E\epsilon \tag{2.1}$$

Here σ is stress, ϵ is strain, and E is the Young's Modulus. Any strain gained through imposed stress will be fully recovered when the stress is removed. If the stress level is increased, the material can yield. The stress for which this happens is known as the yield stress, σ_y. Yielding occurs at point 1 in figure 2.1. The strain gained after this level will be a combination of linear strain, which is recovered at unloading, and plastic strain, which gives a permanent displacement at unloading. In point 2, the strain will be as in equation 2.2, with an elastic and a plastic contribution.

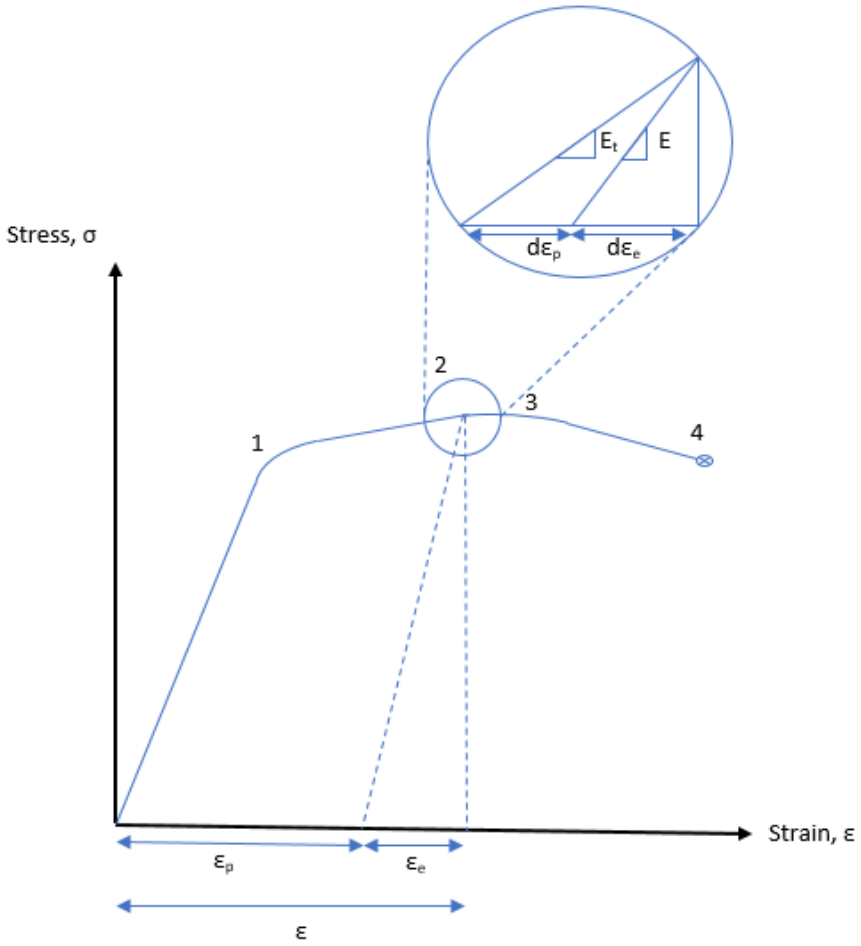

Figure 2.1: Elastoplastic Behavior of a typical Steel Material

$$\epsilon = \epsilon_e + \epsilon_p \tag{2.2}$$

The values $d\epsilon_e$ and $d\epsilon_p$ denotes the change of ϵ_e and ϵ_p respectively. As the material is loaded above the yield strength, a hardening process will occur. If the material had an ideal behavior, the line would be horizontal. The hardening process can be described by $d\sigma$ as in the equations in 2.3,

$$d\sigma = Ed\epsilon_e = H'd\epsilon_p = E_t d\epsilon \tag{2.3}$$

where H' is the plastic tangent modulus seen in equation 2.4

$$H' = \frac{1}{\frac{1}{E_t} - \frac{1}{E}} \tag{2.4}$$

At point 3, the maximum stress in the material occurs. This is known as the ultimate tensile strength, σ_u. Finally, the material fractures in point 4.

Equation 2.1 depicts Hooke's law in one dimension. Figure 2.2 shows the stresses acting on an object in three dimensions.

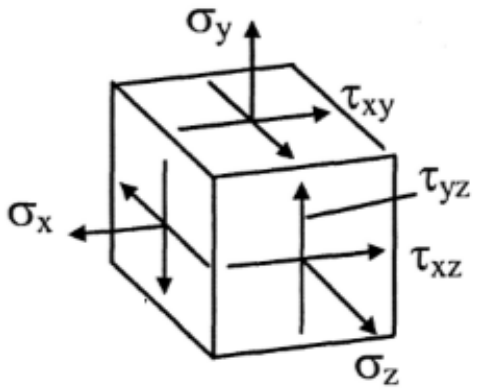

Figure 2.2: Stresses in Three Dimensions from [Ber06a]

The stress in each direction now also has contributions from the other directions through the Poisson ratio ν. The stress concentrations can now be expressed as in equation 2.5.

$$\begin{bmatrix} \sigma_x \\ \sigma_y \\ \sigma_z \\ \tau_{xy} \\ \tau_{yz} \\ \tau_{xz} \end{bmatrix} = \frac{E}{(1+\nu)(1-2\nu)} \begin{bmatrix} 1-\nu & \nu & \nu & 0 & 0 & 0 \\ \nu & 1-\nu & \nu & 0 & 0 & 0 \\ \nu & \nu & 1-\nu & 0 & 0 & 0 \\ 0 & 0 & 0 & \frac{1-2\nu}{2} & 0 & 0 \\ 0 & 0 & 0 & 0 & \frac{1-2\nu}{2} & 0 \\ 0 & 0 & 0 & 0 & 0 & \frac{1-2\nu}{2} \end{bmatrix} \begin{bmatrix} \epsilon_x \\ \epsilon_y \\ \epsilon_z \\ \gamma_{xy} \\ \gamma_{yz} \\ \gamma_{xz} \end{bmatrix} \tag{2.5}$$

This says some things implicitly. Normal stress going in one plane will produce normal strains in three planes, and does not create shear strain in the same plane. Shear stress produces strains in only one plane, and does not produce normal strains in the same plane [SM00].

Another important modulus is the shear modulus, G, which can be expressed as in equation 2.6, and governs the shear stress.

$$G = \frac{E}{2(1+\nu)} \tag{2.6}$$

2.2 Material Hardening

If the material in figure 2.1 is loaded above the yield-strength, plastic behavior will occur. The strain energy received leads to a hardening of the material. This hardening can occur in different ways. Here, *isotropic-* and *kinematic hardening* will be covered.

It must be noted that materials excite complex hardening behavior, and must be firmly tested to acquire the material constants. The hardening behavior is often a combination of multiple models.

The hardening behavior is of importance if the material is going to be loaded multiple times.

Isotropic Hardening

Isotropic hardening is an increase in material strength due to plastic strain. Figure 2.3 shows the stress-strain behavior of a material with isotropic hardening behavior.

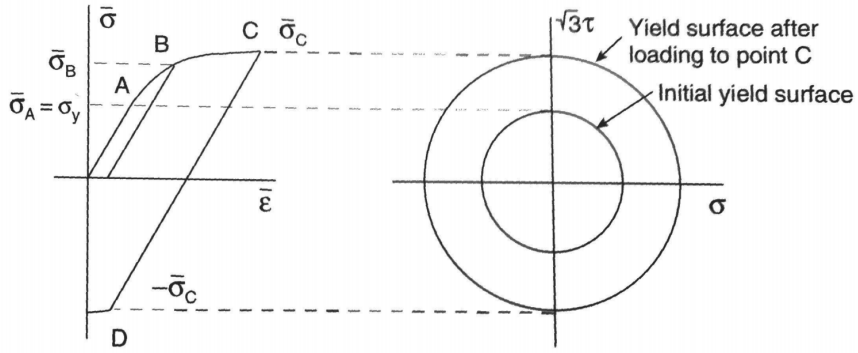

Figure 2.3: Stress-Strain Curve for Isotropic Hardening from [SM00]

If the material is loaded to point B, released and then reloaded again, the material will not start to yield until it reaches point B again. The material "remembers" the hardening and the yield strength has increased. If loading continues up to point C, than $\bar{\sigma}_C$ is considered the new yield strength. If reverse loading is applied, then $-\bar{\sigma}_C$ will be the yield strength. The yield surface has expanded evenly in all directions, and does not translate in space. When cyclic loading is applied, the stresses will increase in each cycle until the deformation is completely elastic. The final stress-calculations will then be completely elastic [SM00].

Kinematic Hardening

Kinematic hardening is different from isotropic hardening in that it is allowed to translate in space, but not increase in size, as seen in figure 2.4.

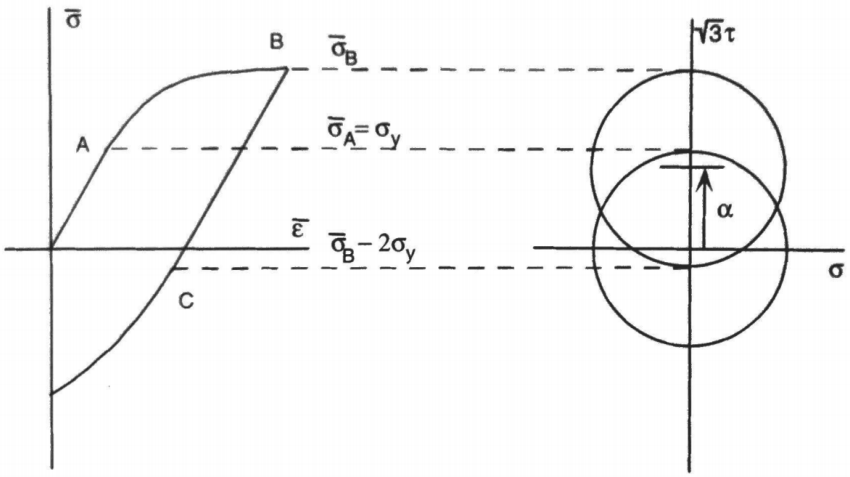

Figure 2.4: Stress-Strain Curve for Kinematic Hardening from [SM00]

The material is loaded to point B resulting in a translation of the yield surface. Unloading to zero will not cause any translation of the yield surface, because it only translates under plastic deformation. Reloading the material will now cause the material to yield in point B. Reversing the loading, the material will yield in point C with a stress equal to $\bar{\sigma}_B - 2\sigma_y$, because the yield surface has moved. Cyclic loading will produce a stable cyclic response if either stress or strain control is used.

Real materials will have behavior from both types of hardening until they become cyclically stable. After that they have kinematic behavior, and can therefore be assumed to have pure kinematic behavior if the transient phase is not of interest [SM00].

2.3 Ratcheting

Ratcheting, or cyclic creep, *"can be defined as the accumulation of plastic deformation and is observed in materials that are subjected to a mean stress"* [SM00]. The total strain value will continue to increase during the cycling. For lower stresses, the ratcheting rate will decrease and eventually become stable. For larger strains, the ratcheting rate will increase in each cycle. Mean stress relaxation is closely related to ratcheting, and occurs during strain-controlled deformation with initial mean stress. Here, the mean stress will tend to move towards zero during the cycling. The rate depends on the plastic

strain range and the level of initial mean stress. The modeling of ratcheting and mean stress relaxation require new material parameters, and no single one is in widespread use [SM00].

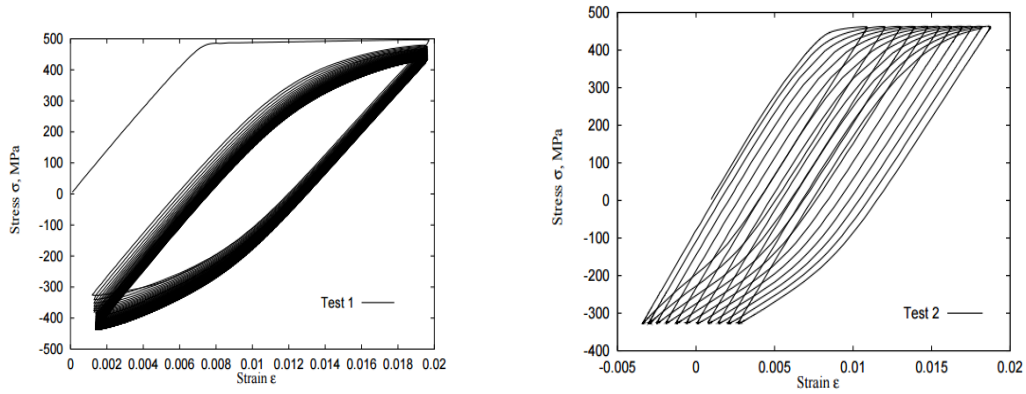

(a) Mean Stress Relaxation under Strain Control (b) Ratcheting under Stress Control

Figure 2.5: Experimental Results showing Ratcheting and Mean Stress Relaxation from [HWB99]

2.4 Pipe Stresses

The stresses in a pipe consist of stress going in the axial direction, σ_x, because of the endcap, stresses going in the hoop direction, σ_θ, as seen in figure 2.6. There is also shear stresses, τ, in the pipe, and stress going in the radial direction, σ_r.

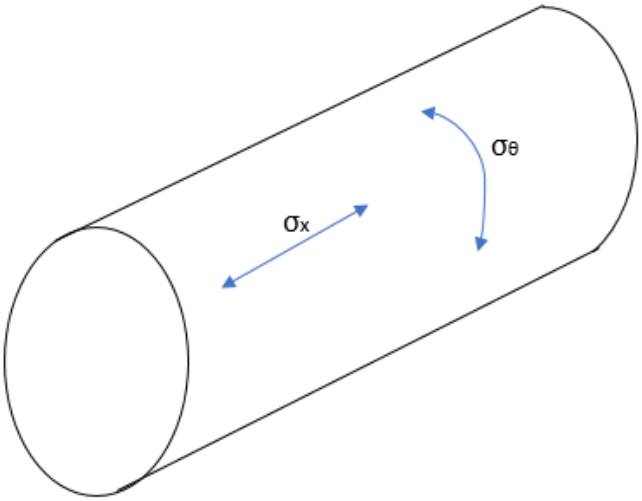

Figure 2.6: Pipe Stresses

For a pipe exposed to both internal pressure, p_i, and external pressure, p_e, the internal and external hoop stress can be seen in equation 2.7 and 2.8,

$$\sigma_{\theta,i} = \frac{(r_i^2 + r_e^2)p_i - 2r_e^2 p_e}{r_e^2 - r_i^2} \tag{2.7}$$

$$\sigma_{\theta,e} = \frac{-(r_i^2 + r_e^2)p_i + 2r_e^2 p_e}{r_e^2 - r_i^2} \tag{2.8}$$

with the largest stress occurring at the inner pipe wall. The general solution at any radius, r, is given for both radial and hoop stress in equation 2.9 and 2.10.

$$\sigma_\theta = \frac{p_i r_i^2 - p_e r_e^2}{r_e^2 - r_i^2} + \frac{(p_i - p_e)r_i^2 r_e^2}{(r_e^2 - r_i^2)r^2} \tag{2.9}$$

$$\sigma_r = \frac{p_i r_i^2 - p_e r_e^2}{r_e^2 - r_i^2} - \frac{(p_i - p_e)r_i^2 r_e^2}{(r_e^2 - r_i^2)r^2} \tag{2.10}$$

The maximum shear stress will occur 45° relative to these stresses and is expressed as in equation 2.11.

$$\tau = \frac{1}{2}(\sigma_\theta - \sigma_r) = \frac{(p_i - p_e)r_i^2 r_e^2}{(r_e^2 - r_i^2)r^2} \tag{2.11}$$

For thin walled pipes the hoop stress and axial stress from endcap can be found from equilibrium considerations, as illustrated in figure 2.7 and 2.8. The equation for the hoop stress can be seen in equation 2.12.

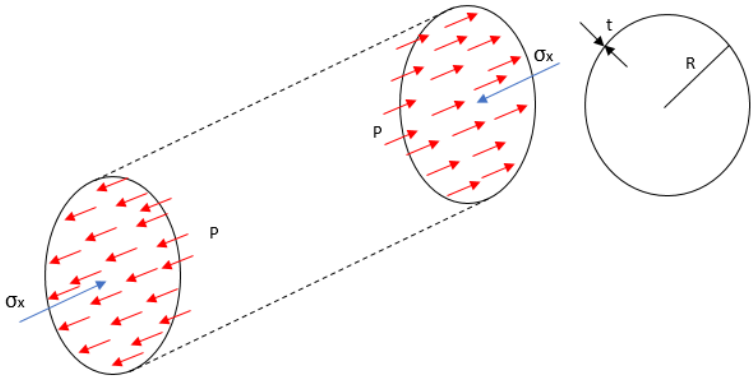

Figure 2.7: Axial Stress Equilibrium from Endcap

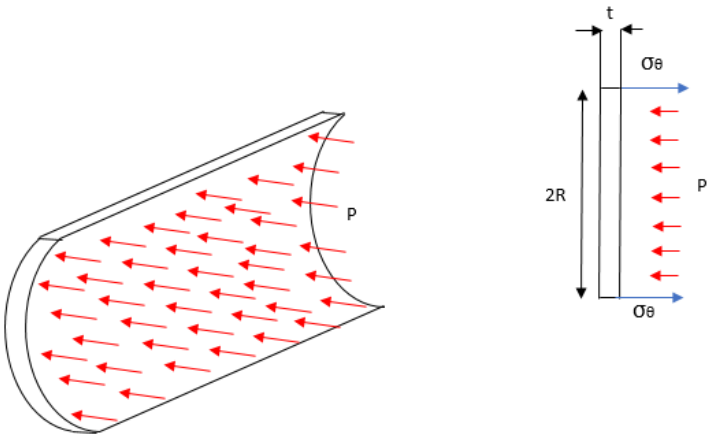

Figure 2.8: Hoop Stress Equilibrium

$$\sigma_\theta = \frac{(r_i + r_e)}{2t}(p_i - p_e) = \frac{R}{t}(p_i - p_e) \tag{2.12}$$

For a thin wall: $R = \frac{1}{2}(D - t)$. For a thick wall the axial stress due to endcap can be seen in equation 2.13, while the thin wall expression can be seen in equation 2.14.

$$\sigma_x = \frac{\pi r_i^2 p_i - \pi r_e^2 p_e}{\pi r_e^2 - \pi r_i^2} \tag{2.13}$$

$$\sigma_x = \frac{\pi R^2 (p_i - p_e)}{2\pi R t} = \frac{R}{2t}(p_i - p_e) = \frac{1}{2}\sigma_\theta \tag{2.14}$$

As seen in the last equation the expression for axial stress is half of the expression for hoop stress. For a thin walled pipe, the von Mises stress, σ_v, becomes as in equation 2.15. All equations taken from [Sæ15].

$$\sigma_v = \sqrt{\sigma_1^2 - \sigma_1\sigma_2 + \sigma_2^2} = \sqrt{\sigma_\theta^2 - \sigma_\theta\sigma_x + \sigma_x^2} = \frac{\sqrt{3}}{2}\sigma_\theta = \frac{\sqrt{3}}{2}\frac{R}{t}(p_i - p_e) \tag{2.15}$$

2.5 Strain Gage

To get a picture on how the stresses are distributed through the pipe in the experimental results, strain gage rosettes will be used. They measure the relative change in electrical resistance through stretching in the pipe material where they are placed, and that is converted to strain values. For this thesis, interesting values to take out is the strains, as well as the stresses in hoop and axial direction. The principle stresses are also interesting, together with the angle between the axial stress and the principle stress. The gage is a rectangular gage measuring in three directions, $(0°, 45°, 90°)$, which is situated on top of each other. For the rest of this section, ϵ_P and ϵ_Q refers to the principle strains, while ϵ_1, ϵ_2 and ϵ_3 refers to the measured gage strains, as seen in figure 2.9.

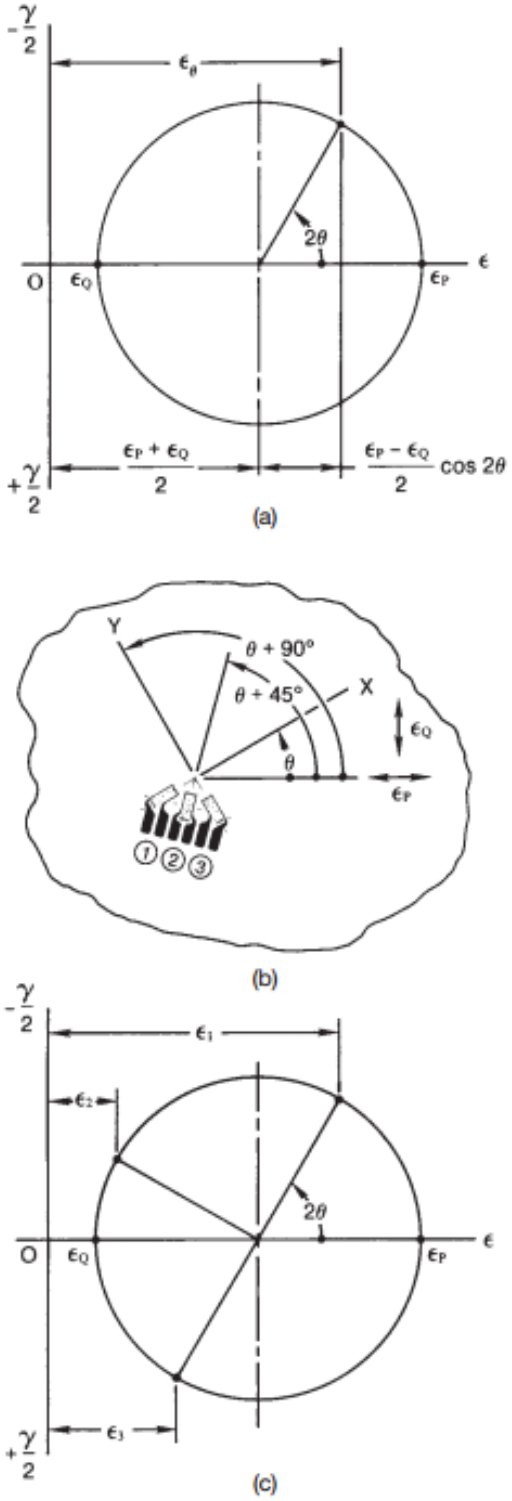

Figure 2.9: Gage Strains from [MM08]

The normal strain in an arbitrary direction, ϵ_θ (not to be mistaken for strain in hoop direction), can be found from equation 2.16.

$$\epsilon_\theta = \frac{\epsilon_P + \epsilon_Q}{2} + \frac{\epsilon_P - \epsilon_Q}{2}\cos 2\theta \tag{2.16}$$

For each direction in the gage, the strain can be found from the equation 2.17-2.19, where θ is the angle to the first principle strain.

$$\epsilon_1 = \frac{\epsilon_P + \epsilon_Q}{2} + \frac{\epsilon_P - \epsilon_Q}{2}\cos 2\theta \tag{2.17}$$

$$\epsilon_2 = \frac{\epsilon_P + \epsilon_Q}{2} + \frac{\epsilon_P - \epsilon_Q}{2}\cos 2(\theta + 45^\circ) \tag{2.18}$$

$$\epsilon_3 = \frac{\epsilon_P + \epsilon_Q}{2} + \frac{\epsilon_P - \epsilon_Q}{2}\cos 2(\theta + 90^\circ) \tag{2.19}$$

If the gage values are known, like in this case, the unknown values can be found from rewriting equation 2.17-2.19 into equation 2.20 and 2.21.

$$\epsilon_{P,Q} = \frac{\epsilon_1 + \epsilon_3}{2} \pm \frac{1}{\sqrt{2}}\sqrt{(\epsilon_1 - \epsilon_2)^2 + (\epsilon_2 - \epsilon_3)^2} \tag{2.20}$$

$$\theta = \frac{1}{2}\tan^{-1}\left(\frac{\epsilon_1 - 2\epsilon_2 + \epsilon_3}{\epsilon_1 - \epsilon_3}\right) \tag{2.21}$$

The $\pm$ sign relates to which one of the principle stresses that are of interest, with $+$ relating to ϵ_P. The angle also needs some interpretation. As it stands now, the angle *"represents the acute angle **from** the principal axis **to** the reference grid of the rosette..."* [MM08]. It could be more convenient to change the angle to be **from** the grid **to** the principle axis. Then simply change the sign, as in equation 2.22. These angles are always referring to the counterclockwise direction if positive.

$$\phi_{P,Q} = -\theta = \frac{1}{2}\tan^{-1}\left(\frac{2\epsilon_2 - \epsilon_1 - \epsilon_3}{\epsilon_1 - \epsilon_3}\right) \tag{2.22}$$

The angle can, however, refer to both principle axes. This ambiguity can be solved by implementing the following rules:

(a) if $\epsilon_1 > \epsilon_3$, then $\phi_{P,Q} = \phi_P$
(b) if $\epsilon_1 < \epsilon_3$, then $\phi_{P,Q} = \phi_Q$
(c) if $\epsilon_1 = \epsilon_3$ and $\epsilon_2 < \epsilon_1$, then $\phi_{P,Q} = \phi_P = -45^\circ$
(d) if $\epsilon_1 = \epsilon_3$ and $\epsilon_2 > \epsilon_1$, then $\phi_{P,Q} = \phi_P = +45^\circ$
(e) if $\epsilon_1 = \epsilon_2 = \epsilon_3$, then there is equal biaxial strain

From figure 2.9, the maximum shear strain can be found to be as in equation 2.23.

$$\gamma_{\text{MAX}} = \epsilon_P - \epsilon_Q \tag{2.23}$$

It would be interesting to get the stresses from the strains. The material needs to be homogeneous, isotropic and linear elastic. Then Hooke's law on biaxial form can be used if E and ν are known properties. Equation 2.24 and 2.25 gives the principle stresses.

$$\sigma_P = \frac{E}{1-\nu^2}(\epsilon_P + \nu\epsilon_Q) \tag{2.24}$$

$$\sigma_Q = \frac{E}{1-\nu^2}(\epsilon_Q + \nu\epsilon_P) \tag{2.25}$$

There are several sources of error in these calculations and the underlying principles. If the temperature varies during the test, this will certainly lead to errors, as it affects the resistance in the strain gage. The material must also have a linear elastic behavior, and plastic behavior might occur during the analysis [MM08].

2.6 Stress Concentration Factor

Large stress concentrations occur in structural areas with cut-outs, welds, notches, corners or other structural details. The stress concentration factor (SCF) is a common way of expressing the local stress concentration. The theoretical SCF can be seen in equation 2.26,

$$K_t = \frac{\bar{\sigma}_{max}}{\bar{\sigma}_{nom}} \tag{2.26}$$

where $\bar{\sigma}_{max}$ is the maximum stress value, while $\bar{\sigma}_{nom}$ is the nominal (engineering) stress value for an undamaged pipe with the same dimensions as the damaged pipe. This equation can take the von Mises equivalent stress, and allows direct reading from the SN-curve [SIB14]. This theoretical SCF is independent of the material, and a notch

sensitivity factor, q, is introduced to account for the part material. This allows the calculation of the fatigue stress concentration factor seen in equation 2.27,

$$K_f = q(K_t - 1) + 1 \tag{2.27}$$

where q is a value from zero to one. The most conservative assumption is when $q = 1$, and represents a completely homogeneous material.

The reason for using this SCF is that the material rarely is perfectly homogeneous and smooth. There already exists internal and surface stress raisers in the specimen, so that the effect of a notch will be smaller than the theoretical SCF would predict. The value of K_f can also be seen as a fatigue strength reduction factor of the notch and can be interpreted as in equation 2.28 [LJ63].

$$K_f = \frac{\text{endurance limit of specimen without the notch}}{\text{endurance limit of specimen with the notch}} \tag{2.28}$$

Figure 2.10 shows general curves for K_f when K_t are known.

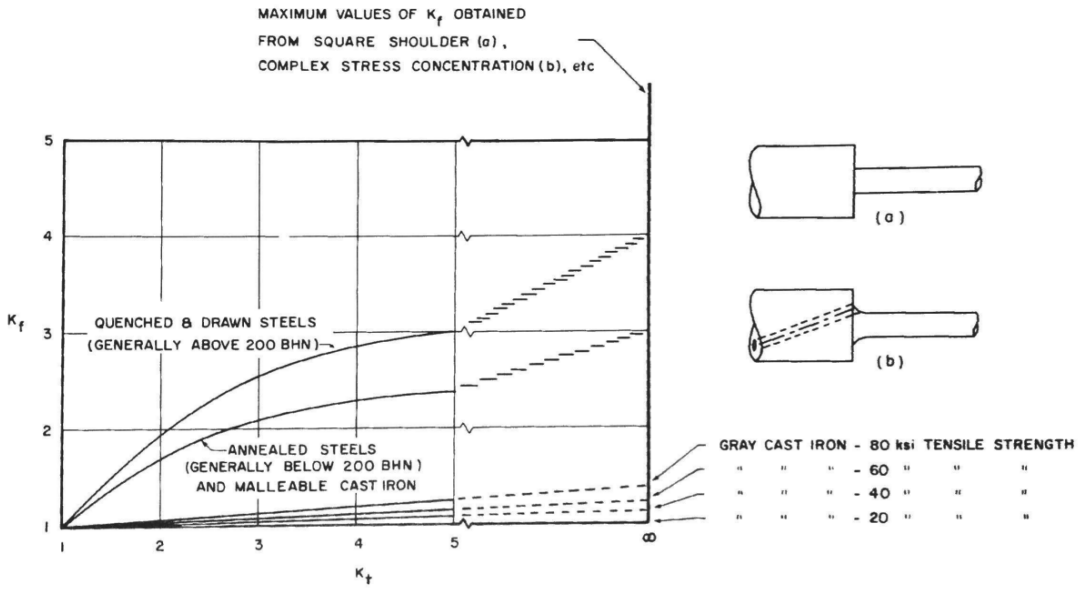

Figure 2.10: General Curves of K_f for known K_t from [LJ63]

The figure indicates that finer steel types are much more impacted by the presence of a notch than lower grade steel and iron. The figure is a rough method of obtaining K_f, and more accurate methods exists. The most accurate way of obtaining K_f is from using test data for the same material and general geometry to compare the difference. A

second method is by calculating it from K_t as in equation 2.27. In figure 2.11, different values of the notch sensitivity factor, q, are stated [LJ63].

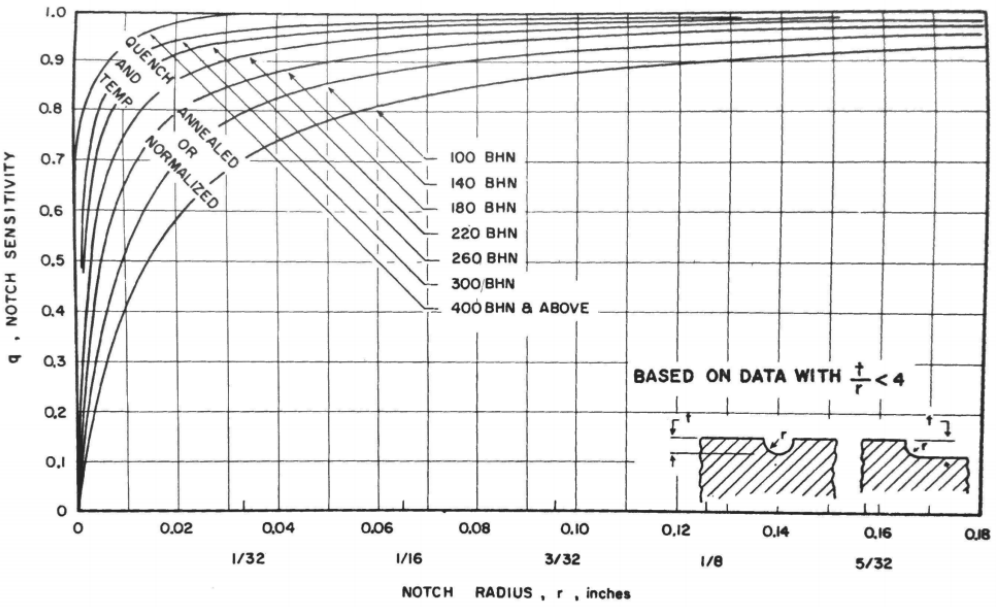

Figure 2.11: Notch Sensitivity Curves from [LJ63]

The notch sensitivity is a function of material hardness (BHN) and notch geometry. The material used in this project has a hardness in the lower end of the scale.

Since the SCF depends solely on part geometry, it is important to determine this geometry accurately. Analytically, the SCF is a function of dent depth, width, length, in addition to the diameter and radius of the pipe, as seen in equation 2.29.

$$K_t = F\left(\frac{D}{t}, \frac{d}{D}, \frac{l}{w}, \frac{t}{w}\right) \tag{2.29}$$

These parameters can be seen illustrated in figure 2.12 and 2.13.

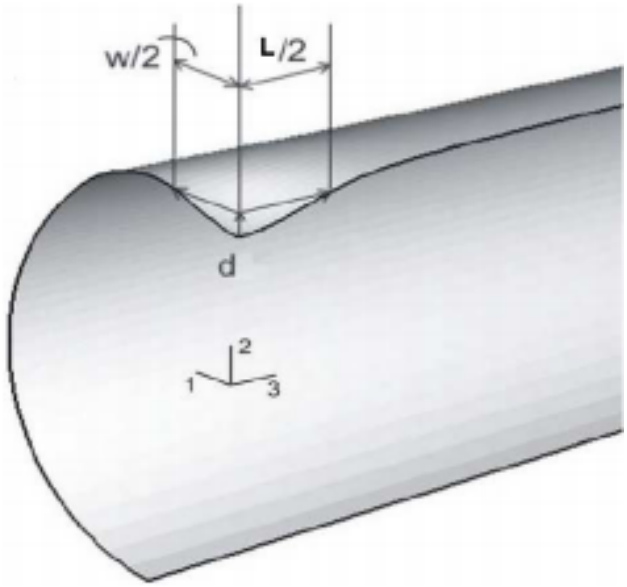

Figure 2.12: First Illustration of Dent Parameters from [SIB14]

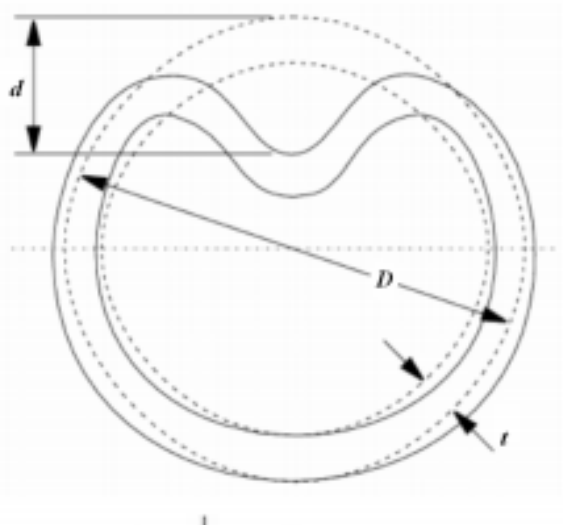

Figure 2.13: Second Illustration of Dent Parameters from [SIB14]

The analytical SCF-function can be expressed as in equation 2.30

$$K_t = \sum_{n=0}^{\infty} A_n \left[\left(\frac{D}{t} \right)^{\alpha_1} \left(\frac{d}{D} \right)^{\alpha_2} \left(\frac{l}{w} \right)^{\alpha_3} \left(\frac{t}{w} \right)^{\alpha_4} \right]^n \tag{2.30}$$

It is also important to know the stress at various levels through the thickness, as well as the maximum stress often found at the surface. This is because the strength may decrease more rapidly than the stress, which means that the most critical point will be located below the surface. This stress variation through the thickness is known as the stress gradient [LJ63].

2.7 Spring Back and Rerounding

Introducing a dent to a pipe is both an elastic and a plastic process. When the indenting object is removed the elastic displacement will be recovered, and this process is called *Spring back*. *Rerounding* is a process where the dent depth is reduced because of internal pressure. This reduction can be elastic, with no permanent change, and plastic, with permanent change in the depth. If the pipe is subjected to cyclic internal pressure it experiences incremental rerounding behavior, until the deformation becomes pure elastic response. The spring back and rerounding behavior depends on pipe geometry and shape, material properties and whether or not the pipe is pressurized when indented. The stress concentration factor depends on the dent depth, and will therefor also be affected by the spring back and rerounding behavior. Tests made to study spring back and rerounding indicates that:

- Long dents spring back and reround more than short dents.
- The middle of the dent is more affected than the edges of the dent.
- Smooth dents spring back and reround more than kinked dents or dents with sharp changes in curvature.
- Dents made in pressurized pipes spring back more than dents made in unpressurized pipes with the same maximum depth.
- The dent will continue to reround as the internal pressure increases.
- Spring back is affected by the lateral support around the circumference of the pipe near the dent at the time of indentation.
- Thin walled pipes spring back and reround more than thicker walled pipes.

[CH04]

2.8 Fatigue

Fatigue life can be presented by a stress-life diagram, often called an SN-curve. In the diagram, stress or strain range ($\Delta S, \Delta\epsilon$) are plotted versus cycles to failure (N). The SN-curve is derived from material tests under cyclic load. Figure 2.14 shows an SN-curve with a fatigue limit. Values with stress/strain-range below the fatigue limit is assumed to not cause damage.

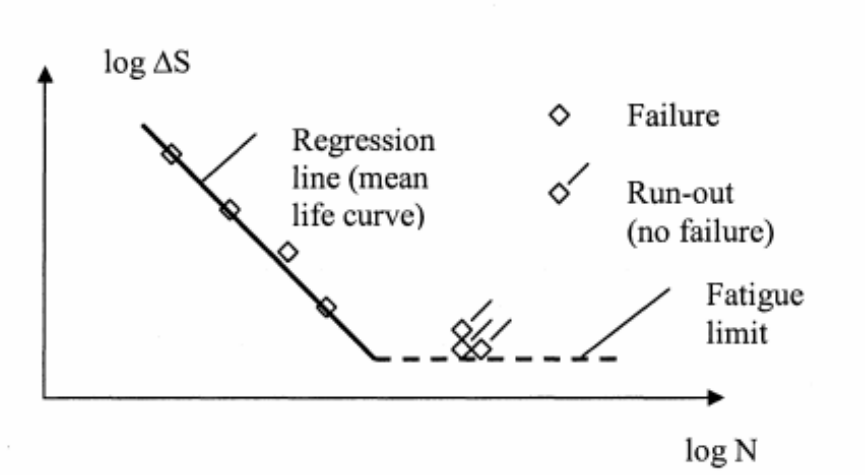

Figure 2.14: Stress-Life Diagram with Fatigue Limit from [Ber06b]

Terms relating to fatigue loading can be seen in figure 2.15,

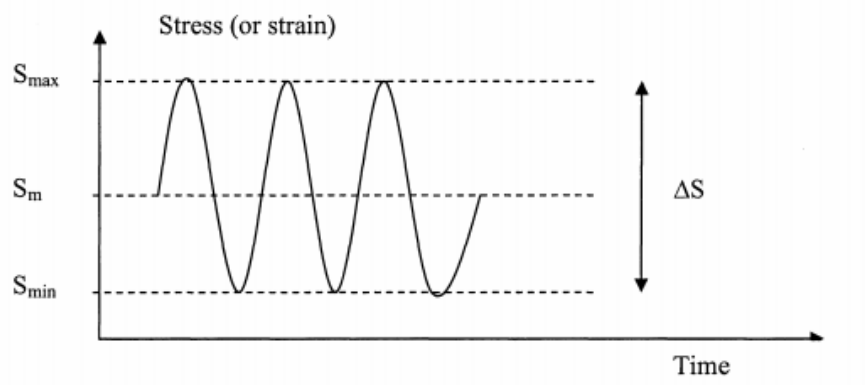

Figure 2.15: Terms relating to Fatigue Loading from [Ber06b]

where S_{max} is the maximum stress in the cycle, S_{min} is the minimum stress in the cycle and S_m is the mean stress. The stress range is $\Delta S = S_{max} - S_{min}$, and the stress ratio is $R = \frac{S_{min}}{S_{max}}$. They are related to each other as seen in equation 2.31.

$$S_m = \frac{\Delta S}{2}\left(\frac{1+R}{1-R}\right) \tag{2.31}$$

Cumulative fatigue damage can be calculated using the Miner summation. The basic assumption behind this method is that the damage in each cycle is constant at a given stress range, given as $D = \frac{1}{N}$. The failure criterion is given as $D_f \geq 1$. If the load history contains several stress ranges, $S_{r,i}$, with a number of cycles, n_i, the damage sum is given as the sum of all the damage contributions, $D = \sum_i \frac{n_i}{N_i}$ [Ber06b].

2.9 Fatigue Limit

The fatigue limit, or endurance limit, is the point for which the stress cycle does not cause fatigue damage. This limit is often set to be between 10^6 and 10^7 cycles for ferrous alloys. In [LJ63], Lipson and Juvinall approximates the endurance limit for steel as in equation 2.32,

$$S'_n = 0.50 \times S_u \tag{2.32}$$

where S_u is the ultimate tensile strength and S'_n is the material endurance limit. The approximation is valid for steel with tensile strength up to 200.000 psi = 1379 MPa. This endurance limit is for a unnotched, polished steel subjected to completely reversed stress-cycles imposed by bending. For gray iron, the endurance limit is between 0.35 and 0.50 of the ultimate tensile strength. For most sections, a value of 0.40 will be safe to use [LJ63]. An example of an endurance limit can be seen in the SN-curve in figure 2.16.

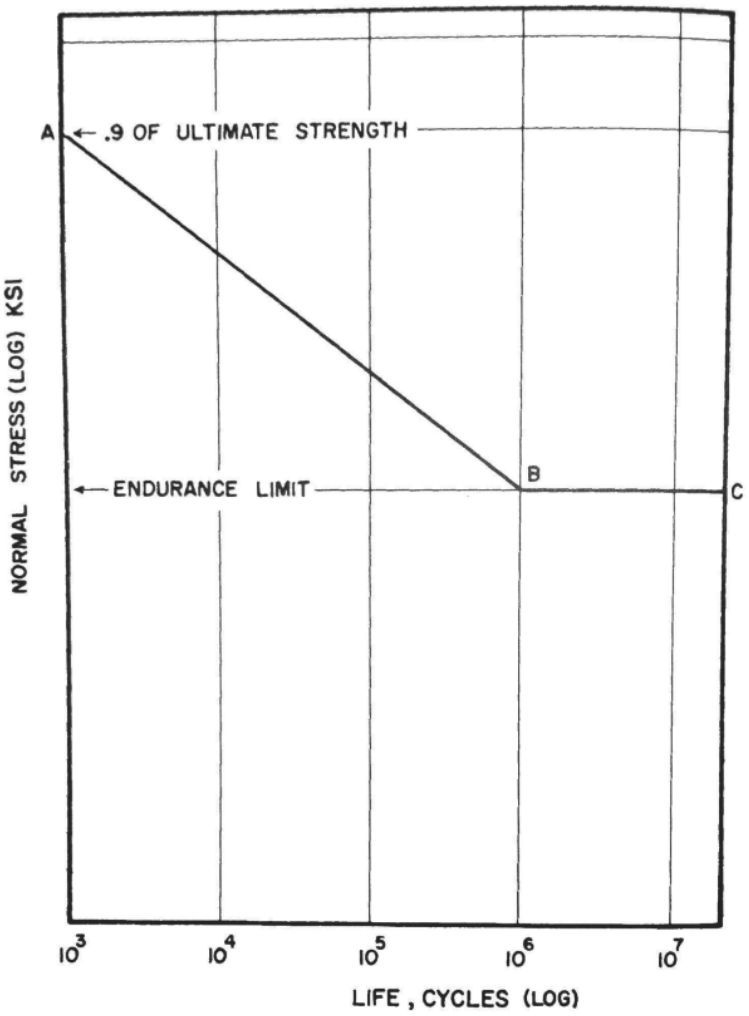

Figure 2.16: Endurance Limit for Steel from [LJ63]

In reality, very few machined or structural members are unnotched, polished and only subjected to reversible bending stress. The endurance limit must therefore be corrected for loading type, section size and surface of the material. Typical endurance limits for different steel and iron types can be seen in figure 2.17.

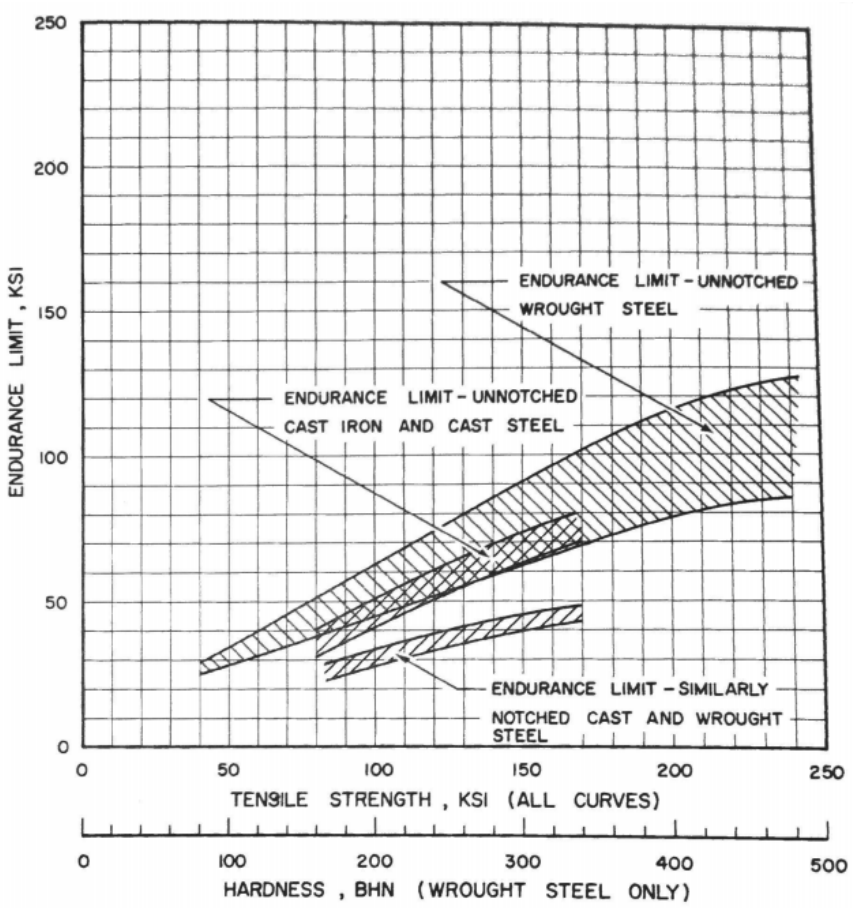

Figure 2.17: Endurance Limit for Different Steel and Iron Types from [LJ63]

The effect of surface finish can be seen in figure 2.18a, and the endurance strength reduction due to surface finish can be seen in figure 2.18b.

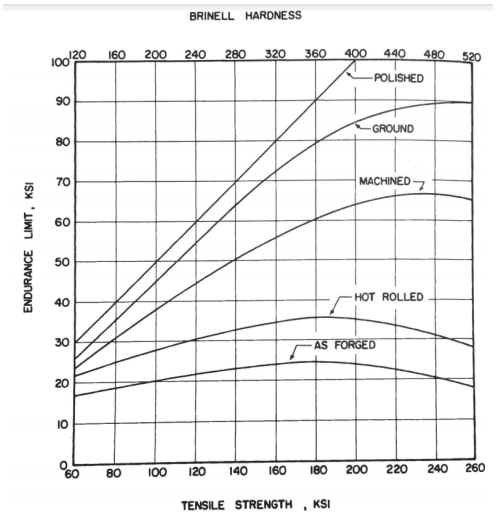

(a)

Effect of Surface Finish on Endurance Limit from [LJ63]

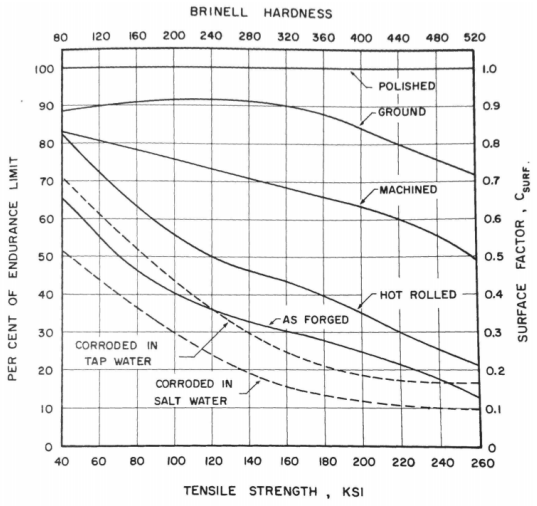

(b)

Reduction of Endurance Strength due to Surface Finish from [LJ63]

Figure 2.18

The effect of load type can be seen in figure 2.19.

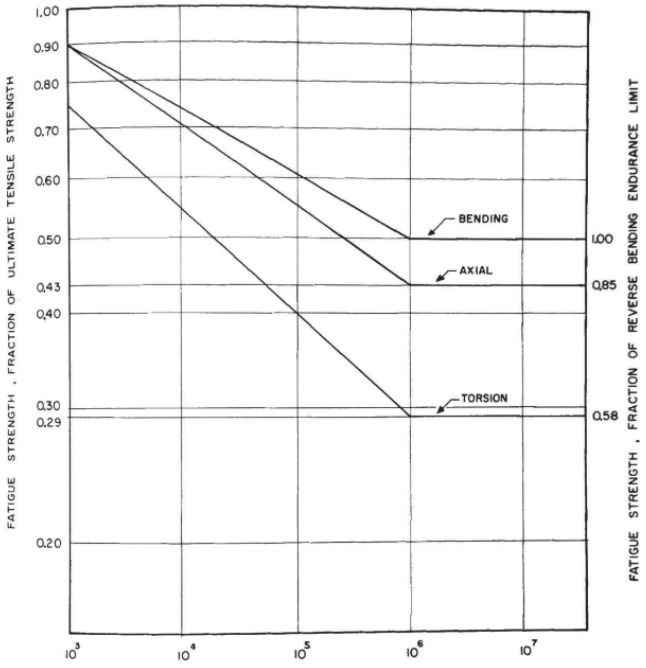

Figure 2.19: Effect of Load Type on Endurance Limit from [LJ63]

The load in this project, which is internal pressure in the pipe, will give a combination of all three stress-types.

2.10 Goodman Diagram

All the above considerations have been for completely reversed loading. In most practical situations, and for the fatigue considerations in this project, that will not be the case. This can be corrected for by using a Goodman diagram. A modified Goodman diagram is seen in figure 2.20.

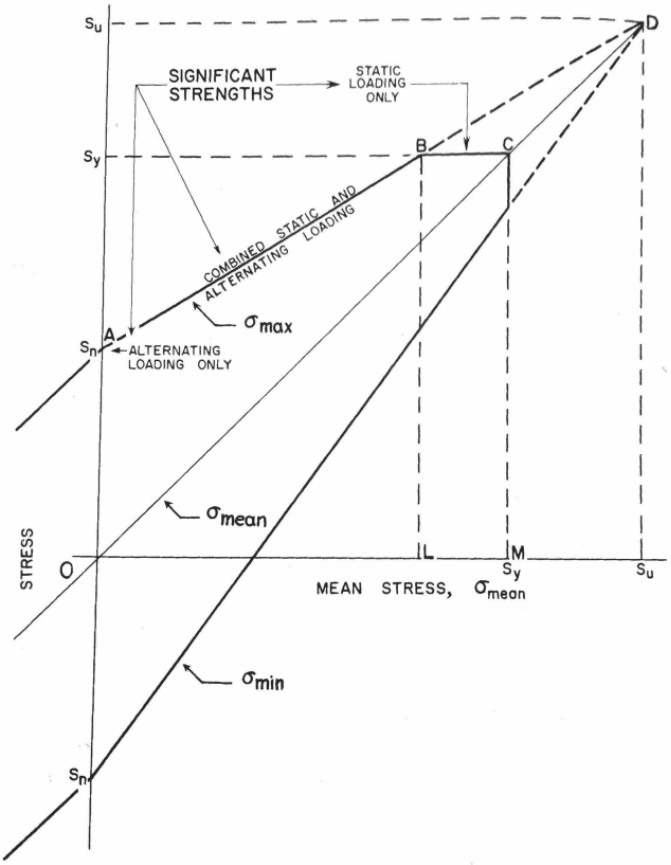

Figure 2.20: Modified Goodman Diagram for Wrought Steel from [LJ63]

Both axis have the same value. The endurance limit for completely reversible loading is set on the left-hand side. The intersection point between the ultimate strengths is located in point D. The lines from the endurance limits up to point D represents the lines of maximum and minimum allowable stress for infinite life. As long as the stress cycle remains within these lines, the part will not experience fatigue failure. The Goodman

diagram have been corrected for yield strength effects, as seen by the lines representing the yield strength. This figure is completely equivalent to figure 2.21, where mean stress is plotted versus alternating stress.

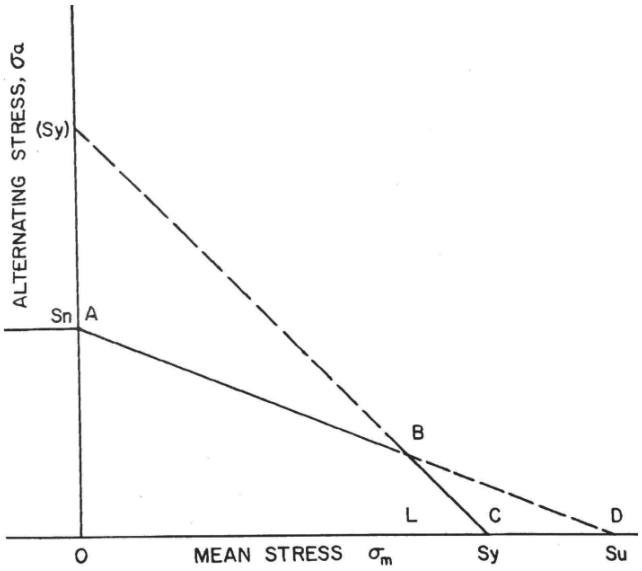

Figure 2.21: Alternate Goodman Diagram for Wrought Steel from [LJ63]

The yield stress line meeting in point C in figure 2.20 can be seen as the 45° line in figure 2.21. The points C and D corresponds to stresses for static yielding and static ultimate fracture respectively. The line AD represents the modified Goodman criterion for fatigue fracture. Line BC represents any fluctuating stresses with maximum stress equal to the yield stress. The use of these diagrams allows the problem to be modified from a case with completely reversed load, to a problem with fluctuating load and mean load not equal to zero [LJ63].

Different effects contribute to making the actual experimental failure line lie above the line for maximum allowable stress, and below the line for minimum allowable stress. These lines have concave shapes and start of at the endurance limit points, and ends up together in point D. This means that the lines for maximum and minimum allowable stresses to failure are conservative, in the way that they underestimate the range for which fatigue failure does not occur.

2.11 Iterative Fatigue

Normal fatigue damage assessment follow a sequential pattern with the steps necessary to calculate the effect on the fatigue life, as illustrated in figure 2.22. Some methods calculate the damage indirectly using remote loads or stresses scaled to account for the

notch. These remote stresses are often nominal stresses, and thus these methods are often called "nominal" or "local" methods.

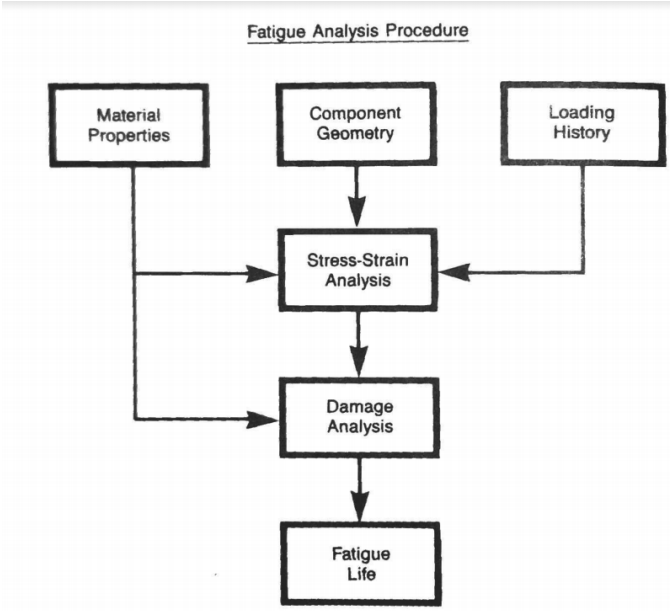

Figure 2.22: Fatigue Analysis Procedure from [Ric+88]

The fatigue life predictions are made using theoretical or elastic stress concentration factors, like equation 2.26, or here in equation 2.33,

$$K_t = \frac{\sigma_1}{S_1} \tag{2.33}$$

where σ_1 is the maximum principal stress in a notch and S_1 is the corresponding nominal stress. It is important to consider the effects of multiaxial behavior, and it needs to be consistency between nominal stresses and nominal strains defined. Alternatively the fatigue stress concentration factor, equation 2.28, can be used.

These methods also need a basis in notch stress analysis. Inelastic behavior will be accounted for directly in these methods, and one way of doing this is to apply Neuber's rule in what is called a "universal" notch analysis. Neuber's rule is stated in equation 2.34,

$$K_t = (K_\epsilon \times K_\sigma)^{1/2} \tag{2.34}$$

where $K_\epsilon = \epsilon_1/\epsilon_N$ and $K_\sigma = \sigma_1/S_1$, with ϵ_1 being the maximum principle strain and ϵ_N being the nominal strain defined consistently with S_1. Neuber rewritten for fatigue

becomes as equation 2.35, and inserting the expressions and rearranging as equation 2.36.

$$K_f = (K_\epsilon \times K_\sigma)^{1/2} \tag{2.35}$$

$$K_f^2 = \frac{\Delta\sigma_1}{\Delta S_1} \times \frac{\Delta\epsilon_1}{\Delta\epsilon_N} \tag{2.36}$$

Assuming nominally elastic conditions, the equation can be written as in 2.37.

$$\frac{\Delta S_1^2 K_f^2}{4E} = \frac{\Delta\sigma_1}{2} \times \frac{\Delta\epsilon_1}{2} \tag{2.37}$$

This is an equation with two unknowns, the local stress and strain, from the imposed stress range, ΔS, the material constant, E, and the empirical/theoretical value of K_f/K_t. The solution can be found as illustrated in figure 2.23, where the Neuber's equation can be solved against the stress-strain relationship. The solution can therefore be made in the inelastic domain, using elastic material properties.

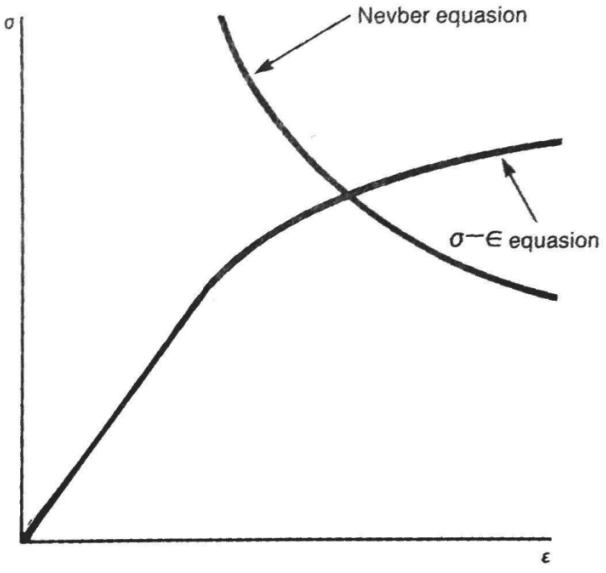

Figure 2.23: Solution to Neuber's Equation from [Ric+88]

The solution acquired is an approximation, and does not work well for some materials and geometries. The solution does not work well for plates with a central hole, depending on the nominal stress and material.

An equation of a cyclic stress-strain curve, for example equation 2.38, can be substituted into Neuber's equation to form the expression in equation 2.39.

$$\frac{\Delta\epsilon}{2} = \frac{\Delta\sigma}{2E} + \left(\frac{\Delta\sigma}{2K'}\right)^{1/n'} \tag{2.38}$$

$$\frac{\Delta S_1^2 K_f^2}{4E} = \frac{\Delta\sigma^2}{4E} + \frac{\Delta\sigma}{2}\left(\frac{\Delta\sigma}{2K'}\right)^{1/n'} \tag{2.39}$$

The latter equation cannot be solved directly, and thus require a process of trial and error, or an iterative approach. Once the stress is determined, the strain value can be found from equation 2.38. Once the strain is found, the fatigue life can be found from a common strain-life equation like equation 2.40, which also needs to apply trial and error or iterations.

$$\frac{\Delta\epsilon}{2} = \left(\frac{\sigma_f'}{E}\right)(2N_f)^b + \epsilon_f'(2N_f)^c \tag{2.40}$$

Fatigue damage and fatigue life is calculated using Miner's rule. This procedure requires several material properties to be known [Ric+88].

Chapter 3

Assessment Methodologies

Many different empirical methods exist for assessing dents and defects in pipelines. One of the more substantial works came in 1998, when a group of companies formed a Joint Industry Project (JIP) to review pipeline defect assessment methods. The aim was to have a guidance manual to consult when assessing pipeline defects [CH01].

Table 3.1: Table of Availability of Assessment Method by Defect Type and Loading from [CH01]

	internal pressure (static)	internal pressure (cyclic)	external pressure	axial force	bending moment	combined loading
defect-free pipe	YES	YES	YES	YES	YES	YES
corrosion	YES	YES	NO	YES	YES	YES
gouges	YES	YES	NO	YES	YES	YES
plain dents	YES	YES	NO	NO	NO	NO
kinked dents	NO	NO	NO	NO	NO	NO
smooth dents on welds	NO	YES	NO	NO	NO	NO
smooth dents and gouges	YES	YES	NO	NO	NO	NO
smooth dents and other types of defect	YES	YES	NO	NO	NO	NO
manufacturing defects in the pipe body	YES	YES	NO	YES	YES	YES
girth weld defects	YES	YES	NO	YES	YES	YES
seam weld defects	YES	YES	NO	YES	YES	YES
cracking	YES	YES	NO	YES	YES	YES
environmental cracking	YES	YES	NO	YES	YES	YES

Notes:

1. **Red** denotes cases where specialist assistance is required.
2. **Yellow** denotes cases where specialist assistance may be required.

Table 3.1 shows the availability of assessment method by the defect and loading type. The method may not be available for all combinations of defect type, orientation and

loading. Red cases requires specialist assistance, while yellow cases denotes that a specialist may be required.

A series of fatigue tests were carried out by [SIB14], to compare five different plain dent fatigue assessment methodologies. The results of the methods were compared and correlated using a classic Palmgren-Miner cumulative fatigue damage rule. The tests were carried out with two different pressure cycles. The five different methodologies include two versions of the American Petroleum Institute (API) Publication 1156, the European Pipeline Research Group (EPRG) 1995, EPRG 2000, and PETROBRAS.

3.1 API 1156

This methodology uses tabulated values of SCF obtained from finite element simulations. The SCF converts directly from pressure into stress. The method considers two slenderness-ratios, (D/t) = 34 and 68, and two indenter-geometries, dome and long bar. The mean pressure is considered the SCF, and have three conditions; low-, high-, and full-range. The SN-diagram uses two curves, taken from the standards United Kingdom Department of Energy (DOE-B) and modified American Society of Mechanical Engineers (ASME) standard, to determine the number of cycles to failure. The expression for the SCF can be seen in equation 3.1, with d/D as percentage-values. The interpolation coefficients can be seen in table 3.2.

$$K = A + B\left(\frac{d}{D}\right) + C\left(\frac{d}{D}\right)^2 + D\left(\frac{D}{t}\right) + E\left(\frac{d}{D}\right)\left(\frac{D}{t}\right) + F\left(\frac{d}{D}\right)^2\left(\frac{D}{t}\right) \tag{3.1}$$

Table 3.2: Table of Interpolation Coefficients from API 1156 [SIB14]

	DOME Pressure Range			LONG BAR Pressure Range		
	Low	**High**	**Full**	**Low**	**High**	**Full**
A	11.200	9.275	7.630	-14.350	-15.898	-11.556
B	-15.950	-11.300	-14.387	-16.388	6.089	-3.864
C	0.650	0.925	1.557	1.738	0.109	1.719
D	0.682	0.632	0.587	0.358	0.774	0.616
E	0.588	0.453	0.583	1.196	0.338	0.723
F	-0.017	-0.029	-0.049	-0.087	-0.032	-0.095

The SN-curves can be seen in equation 3.2 from DOE-B, and equation 3.3 from modified ASME, with Δp in *psi*.

$$N = 4.424 \times 10^{23} (K\Delta p)^{-4} \tag{3.2}$$

$$N = \exp\left(43.944 - 2.971 \ln\left(K\frac{\Delta p}{2}\right)\right) \tag{3.3}$$

3.2 EPRG

The European Pipeline Research Group have developed two empirical methodologies, predicting the fatigue-life of dented pipes. These are the previously named EPRG 1995 and 2000. Both methods use hoop stress and a SCF to calculate the fatigue life. The hoop stress and SCF is calculated based on dent depth. EPRG 2000 is an empirical model-fitting from 131 fatigue tests. The SCF is for smooth dents without gouges. The mean stress is considered using Gerber's equation. The SCF for EPRG 2000 can be seen in equation 3.4,

$$K = 1 + 2\sqrt{d^{1.5}\frac{t}{D}} \tag{3.4}$$

with d in mm, and σ_A is given in equation 3.5,

$$\sigma_A = \frac{\sigma_a}{1 - \left(\frac{\sigma_m}{S_u}\right)^2} \tag{3.5}$$

and N is given in equation 3.6.

$$N = 5622 \left[\frac{S_u}{2\sigma_A K}\right]^{5.26} \tag{3.6}$$

The EPRG 1995 methodology can be seen in equations 3.7 and 3.8, with stress in MPa and d in mm.

$$K = 2.871\sqrt{d\frac{t}{D}}, \qquad B = \frac{\frac{\sigma_a}{S_u}}{\left[1 - \frac{\sigma_m}{S_u}\right]^{0.5}} \tag{3.7}$$

$$2\sigma_A = S_u\left[B(4 + B^2)^{0.5} - B^2\right], \qquad N = 1000\left[\frac{S_u - 50}{2\sigma_A K}\right]^{4.292} \tag{3.8}$$

3.3 PETROBRAS

Together with the technical university in Rio de Janeiro, they predict fatigue life of dented pipelines by using stress-life fatigue design equations. The SCF is determined in the linear elastic domain, and the tensile strength of the material infers the SN-curve. This method also uses Gerber's equation selected based on experimental results. The best SN-curve correlation with tensile tests are found from fatigue tests on dented pipe samples. The endurance limit is assumed to be 10^6 in this method. Detailed finite element simulations are used to find the best fit for the SCF. The dent geometry is important, and the dent can be classified as spherical, transverse, longitudinal or short longitudinal. The PETROBRAS interpolation coefficients can be seen in table 3.3.

Table 3.3: Table of Interpolation Coefficients from PETROBRAS [SIB14]

Dent Type	Geometry	*A*	*B*
Spherical	$0.9 < \frac{L}{w} < 2$	2.40	0,737
Transverse	$\frac{L}{w} \leq 0.9$	2.11	0.853
Longitudinal	$\frac{L}{w} \geq 2,\ \frac{L}{d} \geq 3\left(\frac{D}{t}\right)^{0.37}$	1.38	2.398
Short Longitudinal	$\frac{L}{w} \geq 2,\ \frac{L}{d} < 3\left(\frac{D}{t}\right)^{0.37}$	6.50	0.825

The SCF can be seen in equation 3.9,

$$K = A + B\left(\frac{d}{D}\right)\left(\frac{D}{t}\right)^{1.14} \tag{3.9}$$

with N in equation 3.10,

$$N = \left[\frac{\bar{\sigma}_a}{C\left(1 - \left(\frac{\bar{\sigma}_m}{S_u}\right)^2\right)}\right]^{\frac{1}{b}} \tag{3.10}$$

using the parameters in equation 3.11 and 3.12.

$$k_a = 56.1 \times S_u^{-0.719}, \qquad S_e = 0.5 \times S_u \frac{k_a}{K} \tag{3.11}$$

$$C = S_u + 345, \qquad b = \frac{1}{6} log_{10}\left(\frac{S_e}{C}\right) \tag{3.12}$$

The method from PETROBRAS do not consider plastic effects in fatigue life, since they likely occur in the first few cycles. The method also uses von Mises stress, where the others use hoop stress, accounting for multi-axial stress behavior.

The different methodologies are compared in the handy table put together by [SIB14] seen in 3.4.

Table 3.4: Table compering the Different Methodologies from [SIB14]

	API	EPRG 1995 2000	PETROBRAS
SN curve	From standards, independent of the pipe material	From standard, derived from Su	From design rule, considers Su and K
Stress concentration factor - K	Elasto-plastic FEM simulation	Empirical fitting	Linear elastic FEM simulation
Mean stress	Included in K	Empirical Gerber	Gerber's Equation
Dent measurement	Unpressurized	Unpressurized	Under pressure
Dent geometry	Two types	Only depth considered	Four types

The conclusion from the fatigue tests was that the API method using the DOE-B curve and EPRG 2000 predicted a fatigue-life much smaller than the observed lifetime, and varied greatly in each experiment. The API method using the ASME curve predicted a fatigue-life larger than the actual life, making it unsafe. The EPRG 1995 and PETROBRAS methodologies got the best correlation, with a small number of unsafe predictions and generally consistent behavior. EPRG 1995 have the best correlation, but is not recommended to use beyond 10^5 cycles. PETROBRAS does not have this restriction [SIB14].

In [Eli16], multiple acceptance criteria from standards were compared. The included standards are:

- API 1156 from [AK99]

- ASME B31.4 Code from [ASM93]
- ASME B31.8 Code from [ASM04]
- EPRG 2000 from [Roo+00]
- Det Norske Veritas (DNV) from [DG10]
- Canadian Standards Association (CSA) from [Rac08]

A summary of the acceptance criteria can be seen in table 3.5.

Table 3.5: Table compering the Acceptance Criteria for some Standards, from [Eli16]

	Plain Dents		Dents with
	Constrained	**Unconstrained**	**cracks or gouges**
API 1156 (1997)	Upto 6 % of D, > 2 % requires fatigue assessment		Not allowed
ASME B31.8 (2014)	Upto 6 % of D or not exceed 6 % strain		Not allowed
ASME B31.4 (1992)	Upto 6 % of D or strain level upto 6 % for OD > 4"		Not allowed
	Up to 6 mm in pipes with D < 4"		
DNV (2010)	3.5 % of D with low impact frequency		Not allowed
EPRG (2000)	≤ 7 % of D at a hoop stress of 72 % SMYS		Not allowed
CSA - Z662 (1999)	Upto 6 mm for ≤ 101.6 mm D or		Not allowed
	< 6 % of D for > 101.6 mm		

Dents with gouge are not allowed in any of these methodologies.

3.4 Dents with Gouge

A damage system with a smooth dent containing a gouge is a severe form of mechanical damage to a pipeline, which lowers the burst strength compared to a plain dent and a gouge in an undented pipe. According to [CH04] there were approximately 242 published tests (pr. 2004) of burst strength of smooth dents containing gouges. Most of these tests have, however, been machined notches in dents, rather than gouges.

The tests introduce the gouge in various ways, both in pressurized and unpressurized condition, introducing the dent before the gouge or the gouge before the dent, and introducing them at the same time. Introducing the gouge in an unpressurized state creates deeper gouges than what is usually observed in practice. Introducing the gouge prior to the dent increases the probability of cracking in the gouge. The most realistic way

of introducing the gouge is to introduce it at the same time as the dent in a pressurized pipe under dynamic conditions [CH04]. In this thesis, the gouge and dent are introduced at the same time in an unpressurized pipe.

The behavior of a dent containing a gouge is highly complex and is a geometrical unstable structure. The gouge itself may have cracking which effect the dent and material as well. The movement of the dent with gouge might also initiate or promote growth of cracks. The failure of this system usually involves high plastic strain with plastic flow and ductile tearing, wall thinning, outwards motion of the dent, and crack initiation and growth. According to [CH04] there were approximately 81 published full-scale fatigue tests (pr. 2004), and all the gouges were machined notches or slots. An overview of these tests can be seen in figure 3.1.

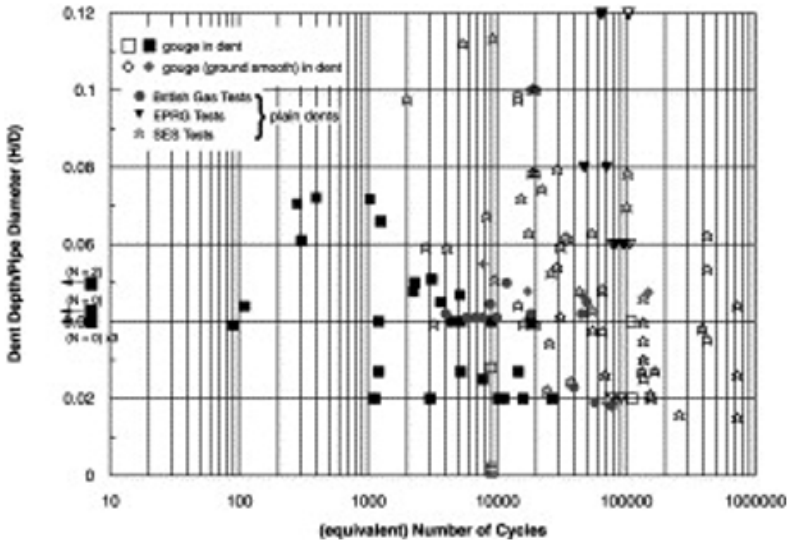

Figure 3.1: Fatigue Tests with Dents with Gouge from [CH04]

According to [CH04], the fatigue life of a smooth dent with a gouge can reduce the fatigue life with a factor of one hundred compared to a plain dent. The short life is due to a combination of crack growth from the gouge and ductile tearing of the dent. Experiments show that the fatigue life can be increased if the gouge is dressed, removing any initiated crack and hardened layer in the gouge. There are no standard recommending any practice in the case of a dented gouge and there are no method for reliably predicting the fatigue life of a gouged dent, or a covered gouged dent [CH04].

Chapter 4

Method

4.1 Indentation

Several small-scale fatigue tests are done during this project. The first part of the process is to simulate an interaction between trawler-equipment and the pipe. This is done by restraining the pipe with metal clamps, while pushing an indenter-object through a hole in the clamps. There are two different heights possible for indentation, varying the depth of the dent. There are also two different indenter types, one with a blunt profile and one with a sharp profile. The geometry specifications can be seen in figure 4.1, and the finished indenters can be seen in figure 4.2. There is a small imperfection at the tip of the indenter. This imperfection creates a sharp gouge in the dent if it faces the pipe. The imperfection can be seen in the red circle in the figure. The indenter test-setup was created as a part of the Master's thesis of Agnes Karin Eliassen [Eli16].

To reduce friction between the indenter and the pipe, the pipe in cleaned with an industrial cleaning remedy, and the indenter is lubricated with industrial grease. This reduces the possibility of creating other imperfections in either the pipe or the indenter itself, and reduces the amount the material of the pipe is dragged across the surface.

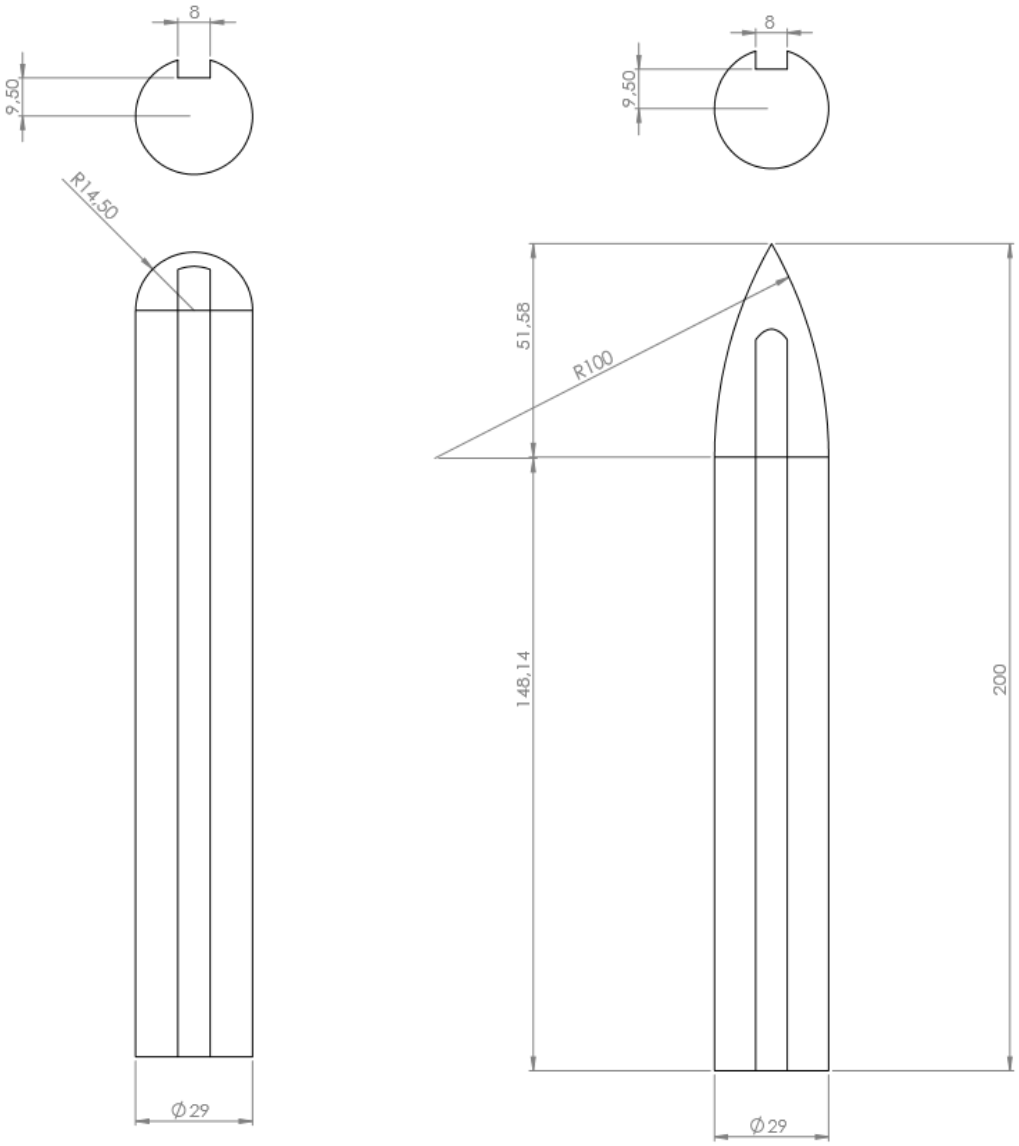

(a) Blunt Indenter Type from [Eli16]

(b) Sharp Indenter Type from [Eli16]

Figure 4.1: Illustration of Indenter Types used in Experimental Tests

(a)
Blunt Indenter

(b)
Sharp Indenter Type

Figure 4.2: Indenter Types used in Experimental Tests

An illustration of the indentation is shown in figure 4.3, while the clamp and rig used to drive the indenter through can be seen in figure 4.5. The dents created without and with gouge can be seen in figure 4.4a and 4.4b.

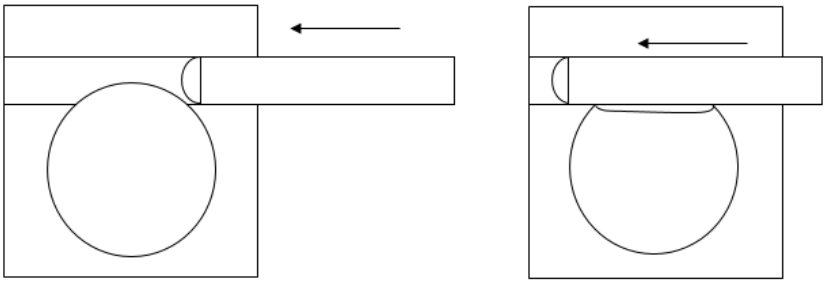

Figure 4.3: Illustration of Pipe Indentation

(a) Dent without Gouge

(b) Dent with Gouge

Figure 4.4: Dent with and without Gouge

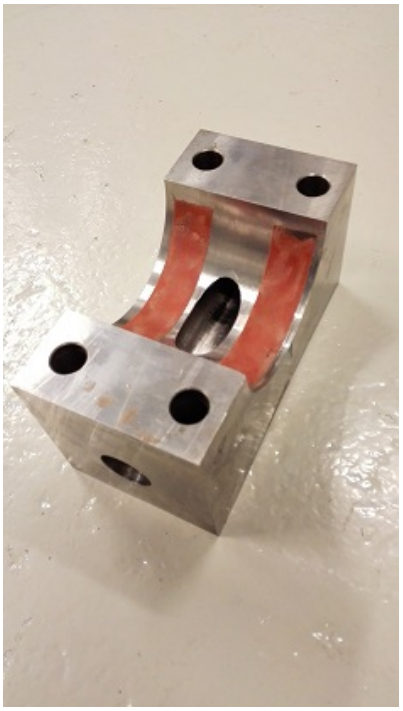

(a)
Clamp used for Pipe Indentation

(b)
Indenter Pressure Rig

Figure 4.5: Pipe Denting Equipment

The pipe used in the thesis have the geometry seen in table 4.1.

Table 4.1: Pipe Geometry

Outer Diameter D	Thickness t
100 mm	2 mm

The indented pipe is now ready for the fatigue tests.

4.2 Fatigue

The indented pipe is now filled with hydraulic oil and rigged up to a pump, supplying pressure to the pipe. The instrumentation can measure temperature inside the pipe and compare it to a control temperature. It also measures pressure, the position of the piston supplying pressure, the load on the piston, as well as three-directional strain from the strain gage placed on five different locations. Another strain gage can be placed at a distance from the dent to measure the development of the nominal strain values. A Linear Variable Differential Transformer (LVDT)-device measures the movement of the dent. In figure 4.6 the placement of the strain gages can be seen, as well as the LVDT. The arrow to the left of the figure indicates the direction of the indentation.

(a) Placement of Gage

(b) Placement of LVDT

Figure 4.6: Placement of Gages and LVDT

The gages are placed where they are because these are the areas of the largest stress concentrations, as well as the area with largest change in stress. Figure 4.7 shows the distribution of von Mises stress measured in the top of the elements in the numerical model. The largest stresses are at the points where the indenter enters and exits the pipe. Figure 4.8 shows the von Mises stress in the pipe as colour contours for both

indenter types, with the sharp indenter type being to the left, while the blunt is on the right. Red areas indicate large stress and blue areas small.

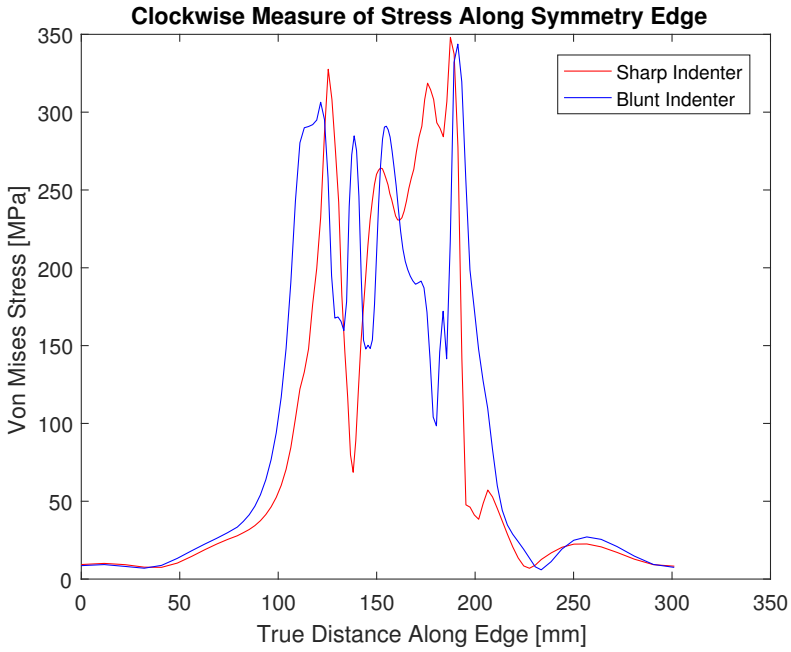

Figure 4.7: Stress along the Symmetry Cross-Section

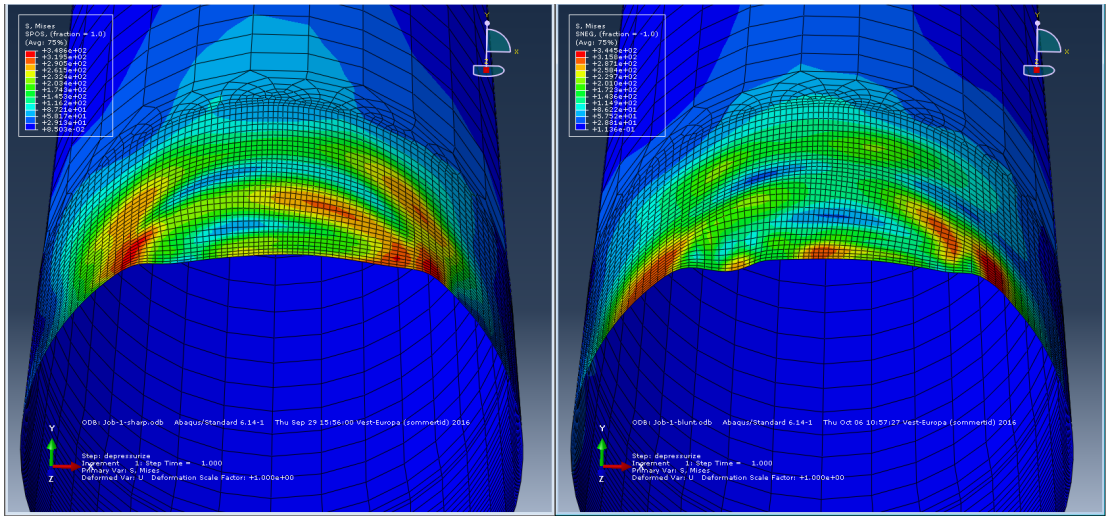

Figure 4.8: Stress Distribution at the Dent

The main goal of the fatigue tests is to look at the impact of gouges in the dent. Several

tests are performed at different pressures for dents with and without gouges. The test is comprised of two parts. In the first part of the test, the pressure is gradually increased up to the maximum pressure of the dynamic test in increments equally spaced, going back to zero for each pressure increase. This initial static pressure test is done to get an idea of the pipe response, and to get initial rerounding to make the dynamic test more dominated by elastic response. In the second part, the pressure is cycled between the maximum pressure and the minimum pressure, which is equal to $\frac{1}{10}$ of the maximum pressure, around the mean value.

4.3 Material Tests

Material tests were made on some selected samples after the fatigue tests were finished. This was done to get details on the material properties of the steel used for the fatigue tests, and comparing the properties for tests subjected to different conditions. The tests are cut out of the pipe as material strips, which are worked into a straight sample. The material is stretched, measuring the load and strain. This determines the material properties of the pipe. The Young's modulus is determined from the linear stress-strain relationship as the rate of change. The yield stress is determined as the point where the measured values deviate more than 0.2 % from the linear value found using the Young's modulus. The ultimate tensile strength stress is the largest stress achieved during the test.

4.4 3D-Scan

The program *Autodesk ReMake* is used to generate a 3D-model of the dented pipe. Models were generated before and after the initial static test, and after the fatigue test were finished. An average of between 30-50 pictures were taken for each 3D-model. The program recognizes patterns between the pictures and constructs the model based on these patterns, so more pictures will create a more detailed and accurate model. Glossy and reflective surfaces make the picture recognition hard, so the pipe was sprayed with white paint, with small droplets of black paint to create a pattern and to reduce the reflectivity of the steel. A 3D-model of pipe 9 can be seen in figure 4.9.

Figure 4.9: 3D-Model of Pipe 9 before Pressure

The creation and modeling worked well for the pipes before the strain gages were attached. The strain gages with the wiring created more complexity, and the models became unusable. A lot more pictures should be taken to compensate for the added complexity. Figure 4.10 shows pipe 4 after the strain gages were attached. The gages, wire and tape makes the surface unrealistically uneven, and makes it hard to take useful measurements of the geometry.

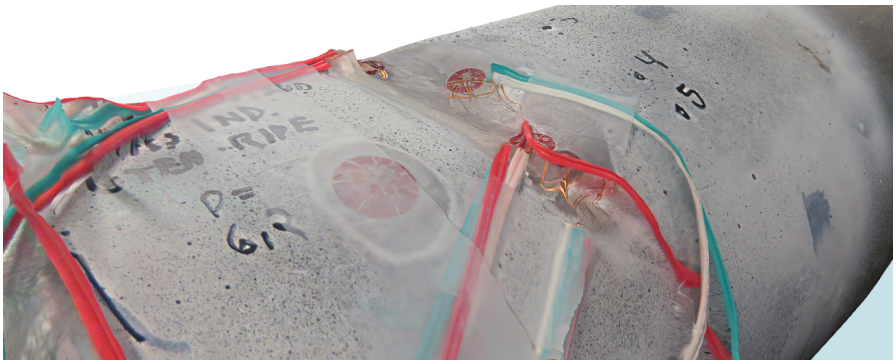

Figure 4.10: 3D-Model of Pipe 4 with Strain Gages

The 3D-models were used to extract the dent geometry before and after static pressure for some pipes to compare with the numerical model.

4.5 X-Ray Diffraction

X-ray diffraction was used to determine the residual stresses in the pipe after the fatigue tests were finished. The method can be used to find residual stresses from measuring strain in the crystal lattice assuming a linear elastic distortion of the crystal lattice plane. The x-rays work over an area and will therefor take measurement over many grains and

crystals, with the total amount depending on the grain size and geometry of the beam. The beam will penetrate the material, although the stress result should be considered as near surface. The total penetration depends on the anode, the material and the beam angle relative to the material. The measured strain is therefore an average over a few μm of material depth.

The x-rays diffract between the different atomic planes in the material, and there is a clear relationship between the appearing diffraction and the distance between these planes, and each material have its distinct diffraction pattern. The change in distance between the planes in the material is directly linked with the straining of the material, so measuring the diffraction change deduces the strains [Fit+05]. The diffractor used in this thesis is a portable system, with beam and detectors as seen in figure 4.11a. The actual diffractor used can be seen in figure 4.11b.

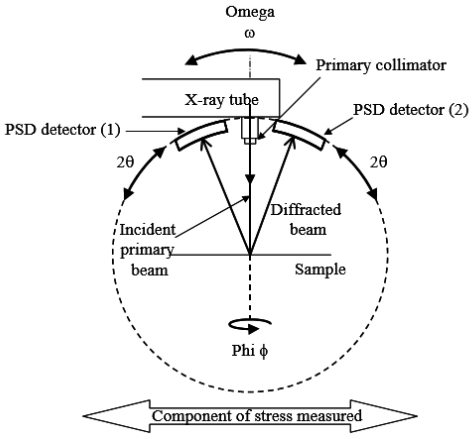

(a)
Illustration of X-Ray Diffractor from [Fit+05]

(b)
X-Ray Diffractor

Figure 4.11: X-Ray Diffractor

Before using the diffractor the material needs to be cleaned, preferably by some degreasing agent to remove any glue or tape rests that could lead to a loss of intensity. Surface paint should also be avoided. The strain gages are carefully removed, since any work done on the pipe in this region would change the residual stresses. It is also important to try to focus straight down on the material and to try to avoid angles. This could of course be difficult on the curved dent.

4.6 Numerical Method

A 3D model is made using the Finite element program (FEM) *ABAQUS*. The model is made to resemble the conditions from the experiments, completed with clamps, endcap plates, an indenter and the pipe. The endcap plate is a thick steel plate welded to the ends of the pipe, also connected to the instrumentation. The model is based on the model used by [Eli16].

The tests are done using an elastoplastic material with isotropic hardening properties. The material values used in the model can be seen in table 4.2. A general value of the modulus of elasticity for steel is used, while the ultimate tensile strength, σ_u, are based on material tests done by [Eli16]. The stress-strain curve can be seen in figure 4.12.

Table 4.2: Material Properties in *ABAQUS*

E	σ_y	ν	σ_u
207 GPa	289.15 MPa	0.3	399.49 MPa

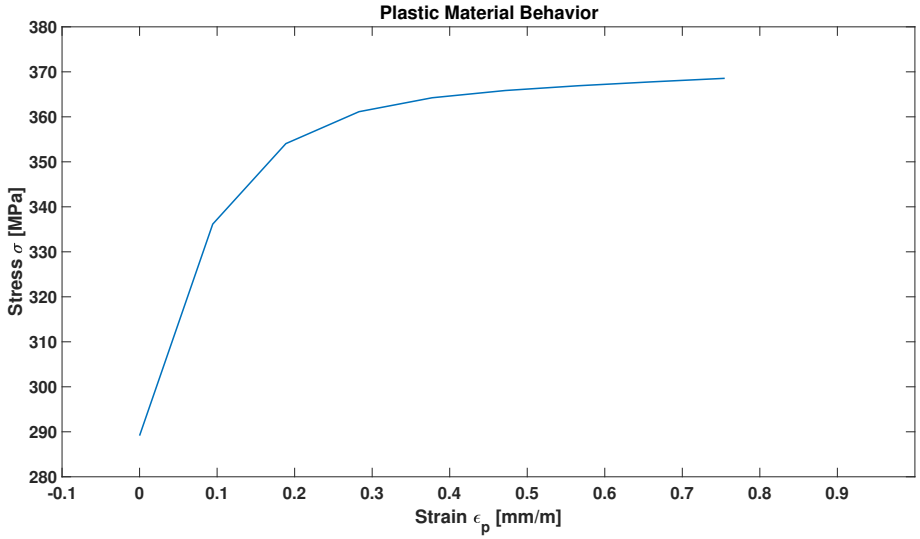

Figure 4.12: Plastic Behavior of Stress-Strain Curve

The clamps and indenters are modeled as rigid R3D4 elements in ABAQUS. The pipe and encap are modeled using shell elements. Figure 4.14 and 4.13 shows the numerical model from the front and behind with the various components. Symmetry is used at the mid-cross-section to save computational time.

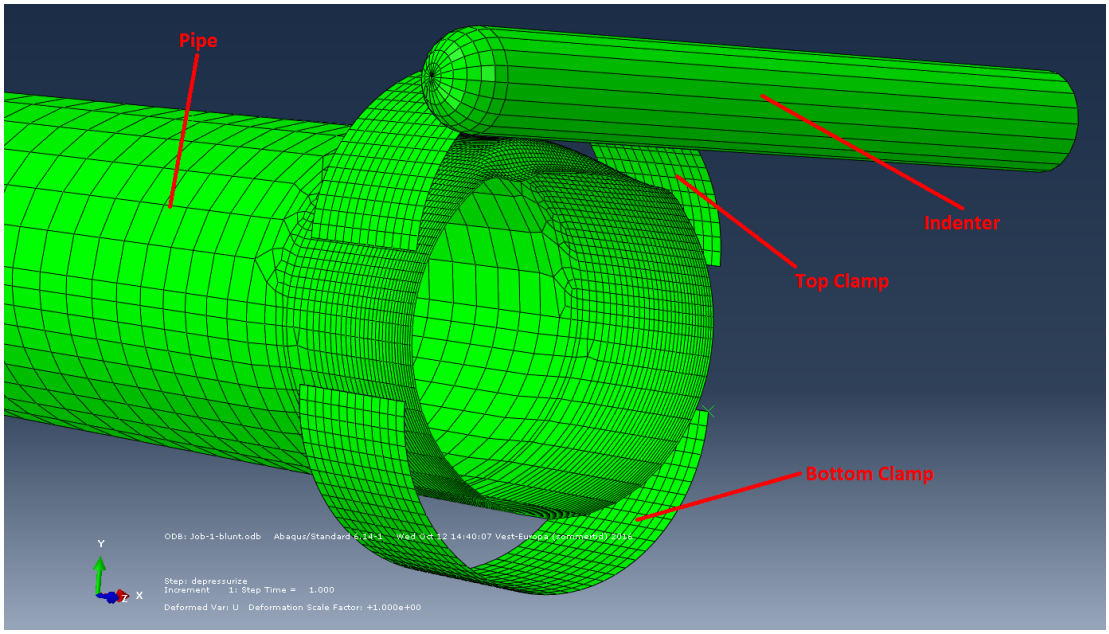

Figure 4.13: Model seen from the Front

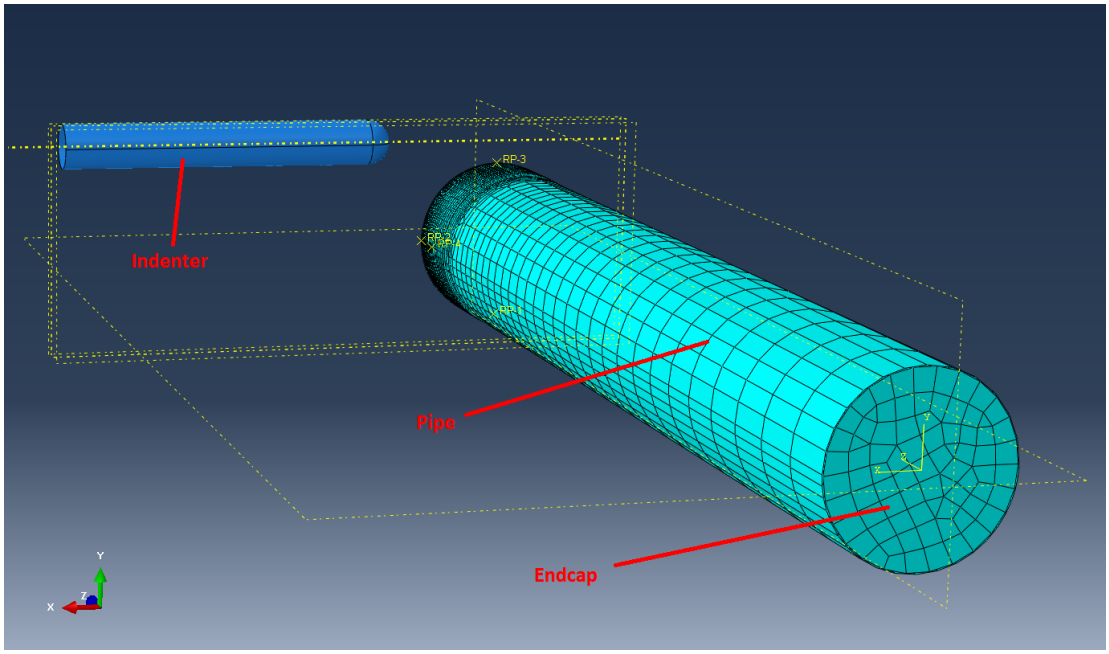

Figure 4.14: Model seen from Behind

The two indenter-types are modeled in the program, and can be seen in figure 4.15.

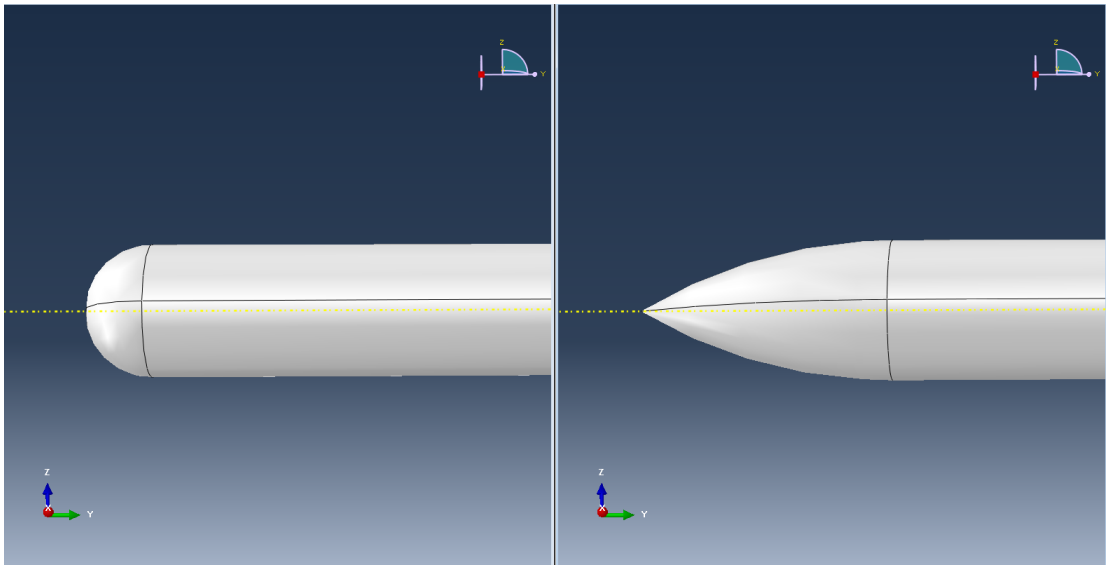

Figure 4.15: The Two Indenter Types

Symmetry boundary conditions are applied to the symmetry cut-out in figure 4.13. Key points at the endcap and in the pipe at the top and bottom clamps are restrained. These boundary conditions restrain the pipe enough to be able to do the computations. The analysis is done in several steps. The first step establishes the boundary conditions. In the next step, the clamps are applied, creating a stress in the clamped region. In the third step, the indenter is moved along a prescribed path, deforming the pipe at small increments. In the fourth step the indenter and clamps are removed. In the final step, the pipe is pressurized until yielding, rerounding the dent.

Chapter 5

Results

5.1 Experimental Results

5.1.1 Strain Measurements

As mentioned in section 4.1, the indentation process is able to control some different variables. These are whether industrial grease is used to lower friction, the distance to the center of the pipe, whether a gouge is made, and which indenter type is used. All tests are made with the sharp indenter type and all indentations were made at a short distance from the pipe center. The maximum static pressure is equal to the maximum dynamic pressure in all cases except for test 10. The rest of the combinations are stated in table 5.1, together with the internal pressure used and the number of cycles achieved during the fatigue test.

Table 5.1: Test Matrix

Test	Grease	Gouge	Static Pressure [bar]	Pressure [bar]	Number of Cycles
1	No	No	100	10-100	18 840
2	No	Yes	100	10-100	19 980
3	Yes	No	100	10-100	16 800
4	Yes	No	70	7-70	112 100
5	Yes	Yes	80	8-80	42 570
6	Yes	Yes	70	7-70	95 500
7	Yes	Yes	60	6-60	111 000
8	Yes	No	60	6-60	205 700
9	Yes	Yes	50	5-50	274 900
10	Yes	No	105	6-60	588 500 +

The number of cycles refers to the number of pressure cycles until a leak appears in and around the dent. It is difficult to determine this number exactly, because the amount of oil penetrating the pipe thickness is small. The crack often appeared while no one was around to confirm the leak. The number in the table is determined from the total number registered by the rig before the pump reaches its minimum position due to the leak. The cylinder has an internal leak which has a linear behavior, and cylinder position is logged, so the leak can be spotted from the development of the slope of the leak. When the slope starts increasing, the pipe must have a leak somewhere. The number in the table is a rounded off guess of when the pipe wall has been penetrated. Figure 5.1 shows a zoomed in picture of the development of the mean of the pump-cylinder position for test 3 during its end-life. The sudden drop in the mean value indicates that the oil suddenly leaked out somewhere in the pipe.

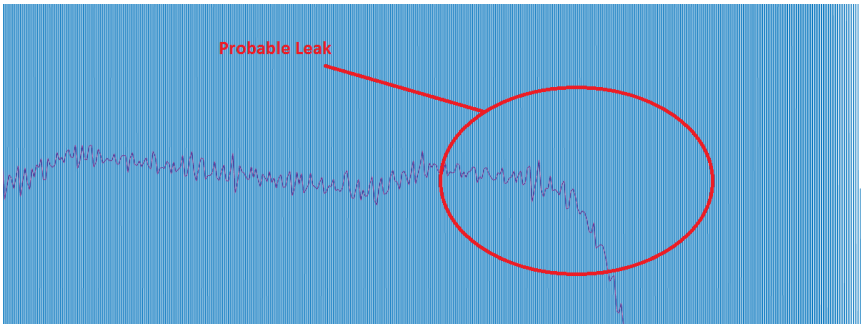

Figure 5.1: Indication of Probable Leak in the Pipe

Figure 5.2 shows the SN-curve for the fatigue tests for the pipes with and without gouges.

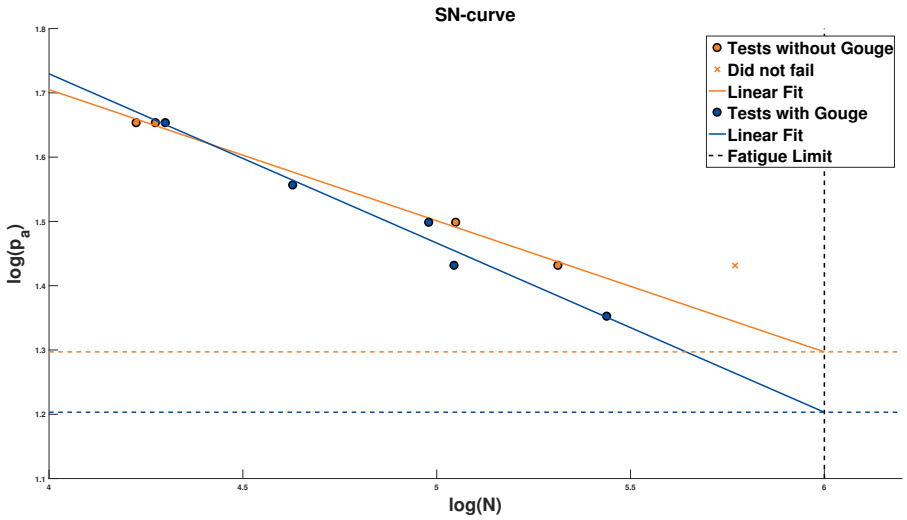

Figure 5.2: SN-Curve for the Fatigue Tests

A logarithmic straight line is fitted to the point for both dents with and without gouge. The tests with gouge fail before the tests without gouge. There is some deviation from the line along the whole figure, but the straight line represents a least square adaption. A standard value of 10^6 is chosen for the fatigue limit for the material and geometry for these tests, although this needs to be verified. The test that did not fail is not applicable for comparison with the other tests without gouge, because of the difference in static pressure. The fatigue limit implies that the limit pressure amplitude for a case without gouge is 19.8 bar, and with gouge 16.0 bar. This equals a pressure range of $4.4 - 44$ bar without gouge and $3.6 - 36$ bar with gouge. The gouge reduces the maximum pressure of the fatigue limit by 18.2 %.

During the test, a lot of variables are measured. Pressure, temperature, cylinder position and load, and strain measured from the strain gages. The gage placement was briefly showed in section 4.2, but for reference the gage placement is illustrated in figure 5.3. For test 2 the gages were put in reverse order, so gage 5 will be the same as gage 1 for the others while gage 4 will be as gage 2.

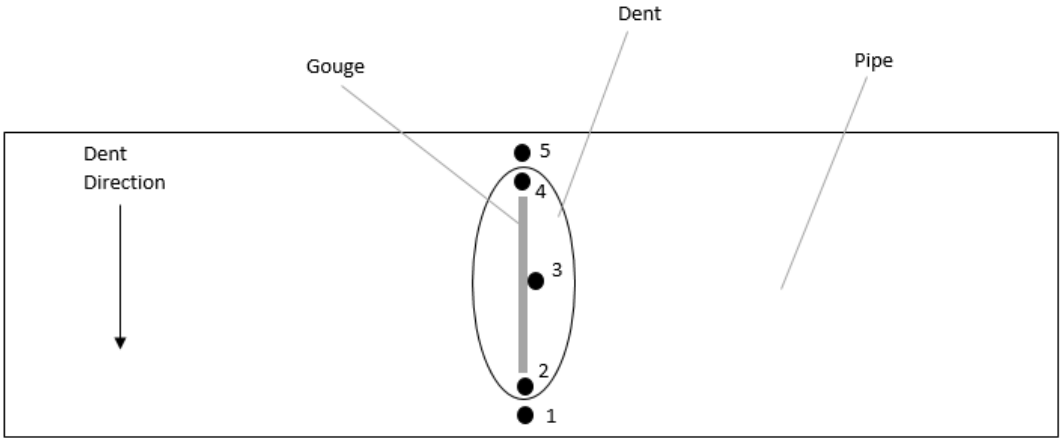

Figure 5.3: Illustration of the Gage Placement

The data is logged and post-processed in the program *catmanEasy-AP*, and the plots are made in *Matlab*. All plots from the strain gages can be found in the appendix. Figure 5.4 shows the strain data for gage 3 from test 3. The strains are measured in the axial and hoop direction, as well as 45° between them.

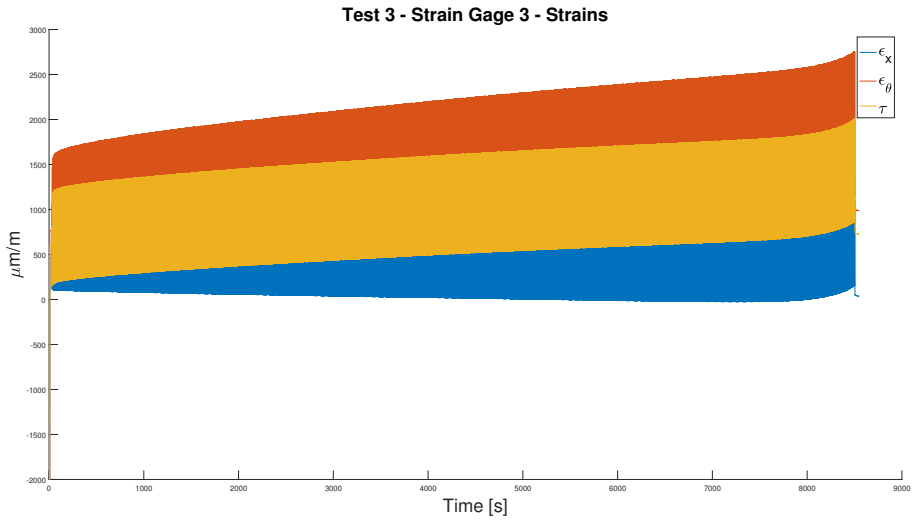

Figure 5.4: Strain for Test 3 at Gage 3

In this plot, the hoop strain is larger than the axial strain. Both strains increase during the test, and are generally large. The mean strain development for all the tests at gage 3 for axial and hoop direction is shown in figure 5.5 and 5.6. These plots have been

converted to the same length, so that they represent the full life development of the strain values. The values of the higher-pressure tests increase during the lifetime, while the lower-pressure tests quickly reach and remain at a specific value. Notice that the red color represents tests without gouge, while blue represents tests with gouge. The green line is test 10, which has a different static pressure than the other tests.

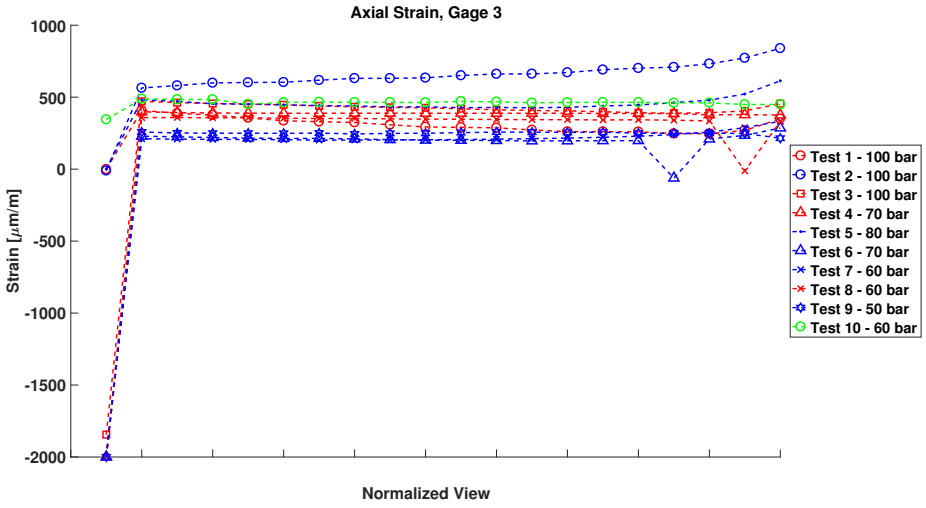

Figure 5.5: Mean Axial Strain at Gage 3

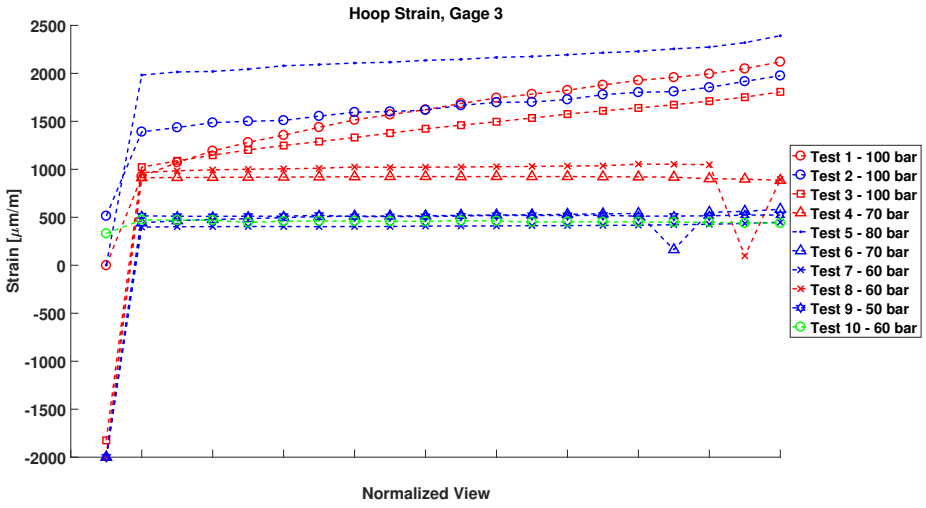

Figure 5.6: Mean Axial Strain at Gage 3

The strain values are larger for larger pressure, and have more plastic effects. The main exception to this is test 5, which has the largest hoop strain values. Test 5 behaves

strange for many of the gages, so it is possible that there is a problem with the gages for this test. There is no clear difference between the gages with and without gouge, except that it seems the strain values are larger for the tests without (red).

At the beginning of the test, some of the values are very low. That is because the gage is not yet active during the test, and the default minimum value is logged. There is also some strange behavior at the end-life for test 6 and 8, where they have a sudden dip in value. The reason for this is that the mean value has been influenced by a test pause, as seen in figure 5.7 for axial strain in test 6.

Figure 5.7: Axial Strain for Test 6

Another example of strange data for the normalized strain life of all the test comes when looking at test 2 for axial strain at gage 1 and 2. The axial mean strain values for gage 2 can be seen in figure 5.8. The mean value changes value and jumps into compression during the test. The same behavior is also observed for test 6 and 7, although not as violent.

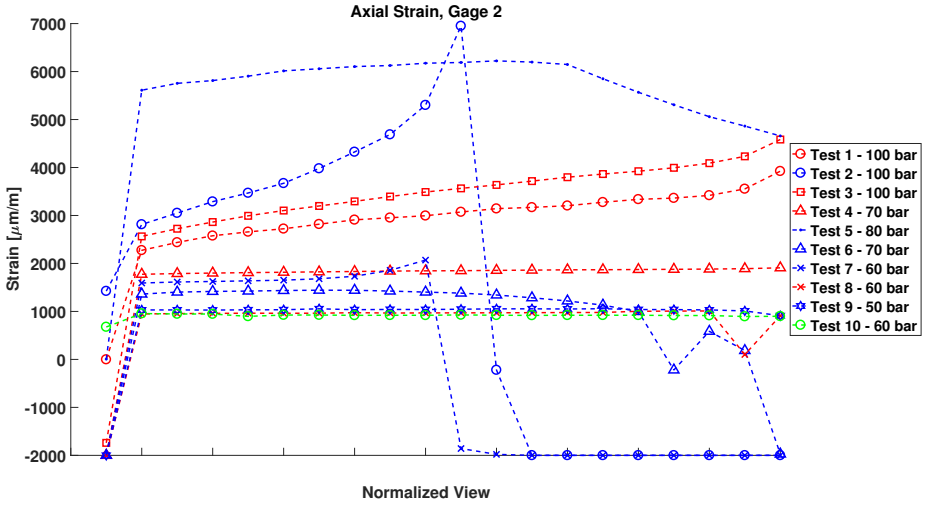

Figure 5.8: Mean Axial Strain at Gage 2

Some gages failed during the test, as in this case for test 2, as seen in figure 5.9, which corresponds to the strange behavior above. There are several causes for failure that have been identified during the tests. One reason is that the gage has been over-strained, destroying further data gathered by the gage. The glue holding the gage to the pipe could slip or crack during the test. The wires from the gage could have been mistakenly glued to the pipe, giving false data or destroying the gage. The LVDT-measuring device also slipped during some of the tests, interfering with gage 3. In some cases, one of the wires came loose from the gage during or before the test, making the gage fail to collect information. More detail about the individual tests are stated in section 5.2.

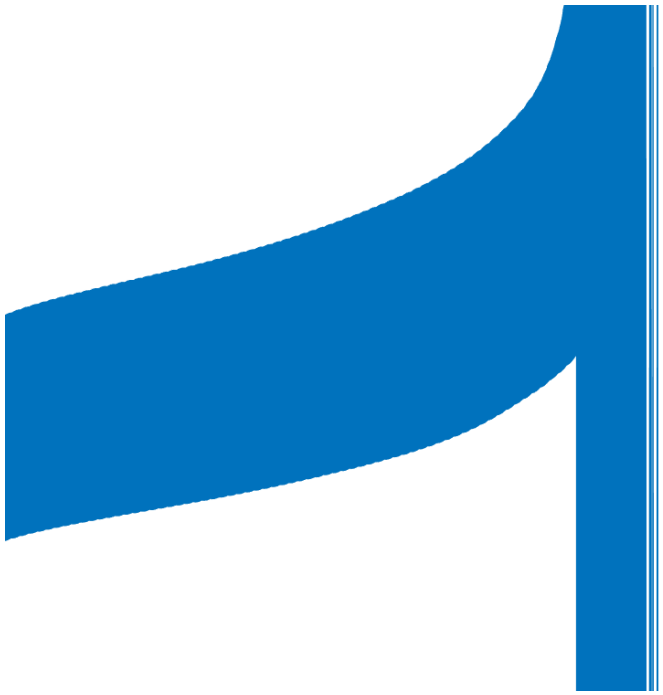

Figure 5.9: Axial Strain for Test 2 at Gage 2

5.1.2 Crack Location and Direction

The crack location and direction are important because it can tell something on how the stress concentration are in and around the dent. The cracks were spotted directly during the fatigue tests looking at the leak in the pipe. For the more extensive tests it was more difficult to spot the crack with the naked eye, so UV-light was used to find the crack. The hydraulic oil was fluorescent under UV-light, as well as another fluorescent liquid used for this purpose. Figure 5.10 shows a crack detected using UV-light. Table 5.2 shows the crack location and direction for the tests, while figure 5.12 shows the location and direction of the cracks (not at scale).

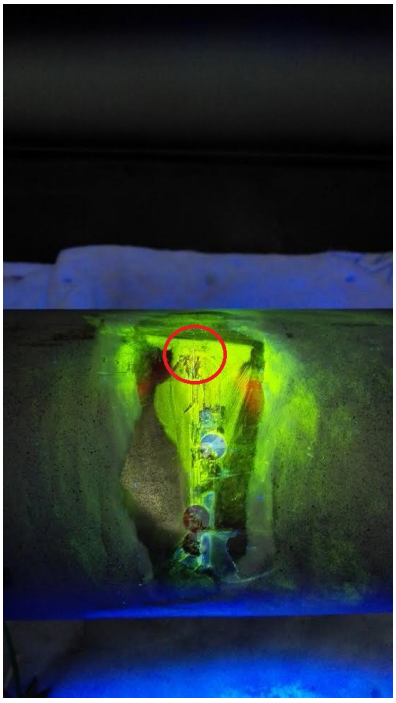

Figure 5.10: Detected Crack under UV-Light

Test 2 and test 7 were inspected under microscope, as seen in figure 5.11a and figure 5.11b. This gives a detailed view of the crack if the general position is already known. It is clear from the microscope imagery that the crack starts at the gouge and crosses the sharp curvature of the entrance/exit of the dent. The gouge can be seen in the bottom of the figure.

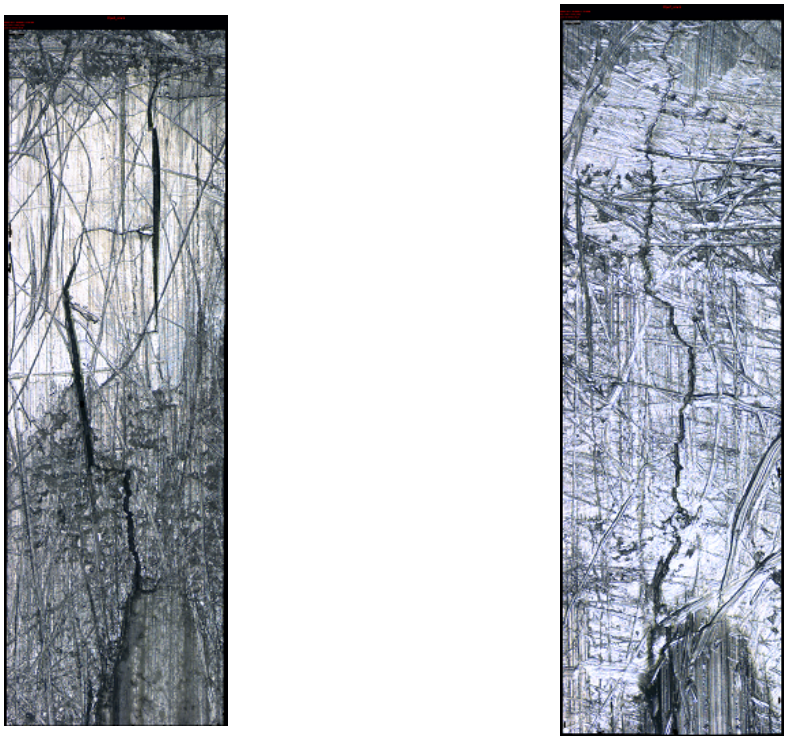

(a) Pipe 2

(b) Pipe 7

Figure 5.11: Detecting Cracks using Microscope

Table 5.2: Crack Location and Direction

Test	Gouge	Pressure [bar]	Crack Location	Crack Direction
1	No	10-100	At Gage 5	Axial
2	Yes	10-100	From Gouge to Gage 2	Hoop
3	No	10-100	At Gage 5	Axial
4	No	7-70	Outside Gage 3	Axial
5	Yes	8-80	Below Gage 1	Axial
6	Yes	7-70	From Gouge to Gage 2	Hoop
7	Yes	6-60	From Gouge to Gage 2	Hoop
8	No	6-60	Outside Gage 3	Axial
9	Yes	5-50	Outside Gage 3	Axial
10	No	6-60	Did Not Fail	Did Not Fail

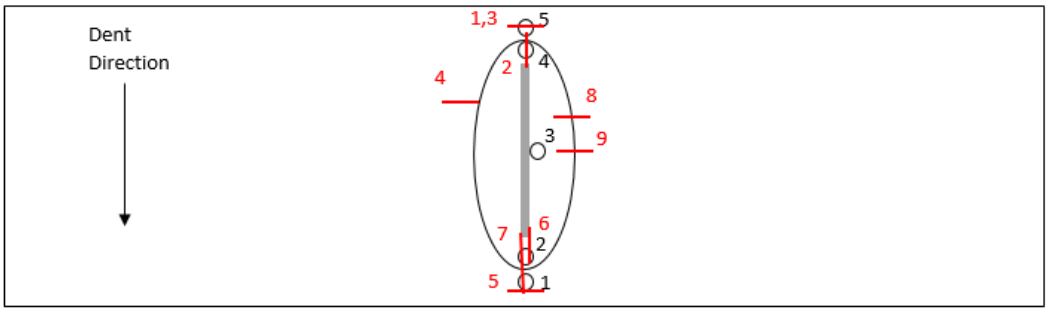

Figure 5.12: Crack Location and Direction

Note again that gage 2 for test 2 is located at the same place as gage 4 for the other tests. The side of the dent where the indenter enters and exits during indentation seems to be the most critical area for fatigue, since most tests failed in this region. It is interesting that the two test that lasted the longest both failed on the dent shoulder instead of around the entrance/exit of the dent. Test 4 also failed in this region. This indicates that the stress concentrations were too small around the sharp entrance/exit compared to the dent shoulder, and other factors became dominant. The cracks from the tests with gouge are initiated by the gouge around the critical areas. They also fail earlier than the tests without gouge, which indicates that the gouge has a significant effect on the crack initiation.

For a normal pipe without any defects the hoop stress is larger than the axial stress in the pipe wall, concentrating the stress around cracks forming in the axial direction. This means that the cracks that appear in a pipe without a dent should form in the axial direction. Many of the tests have cracks forming in the axial direction, but some also have cracks forming in the hoop direction. These three tests all have a gouge. It is possible that the gouge gives additional stress concentrations in the axial direction, which causes the cracks to form in the hoop direction. The cracks could also simply be initiated by the gouge itself, due to small imperfections and damage deeper down in the thickness.

5.1.3 Dent Geometry

The dent geometry was affected by the pressure variation in each cycle, as well as having permanent change during multiple cycles. The radial displacement of the dent was measured with an LVDT-device registering the change while the pressure-cycles were applied. The device was placed in close proximity to gage 3, as seen in figure 4.6b.

During some of the tests the device slipped from the original position. The data from the device should therefore be used with caution. An example of this can be seen in figure 5.13 where the device started to slip on one side and moved during the test. The measurements in themselves are correct, but the area where the device measures changes during the test.

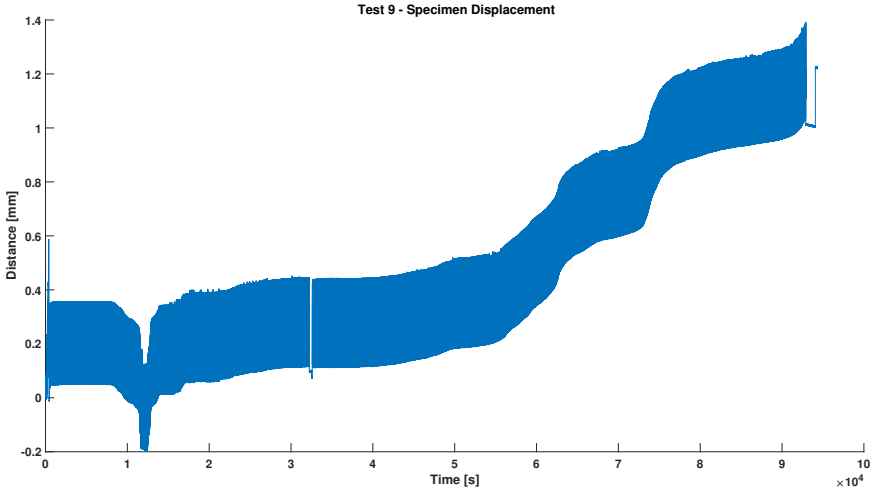

Figure 5.13: Dent Displacement for Test 9

Figure 5.14 shows the development of test 3 and figure 5.15 shows test 4. Both are tests with grease and without gouge. The difference is that test 3 have a pressure of 100 bar while test 4 have 70 bar. Both values are reset after the initial static pressure-increase.

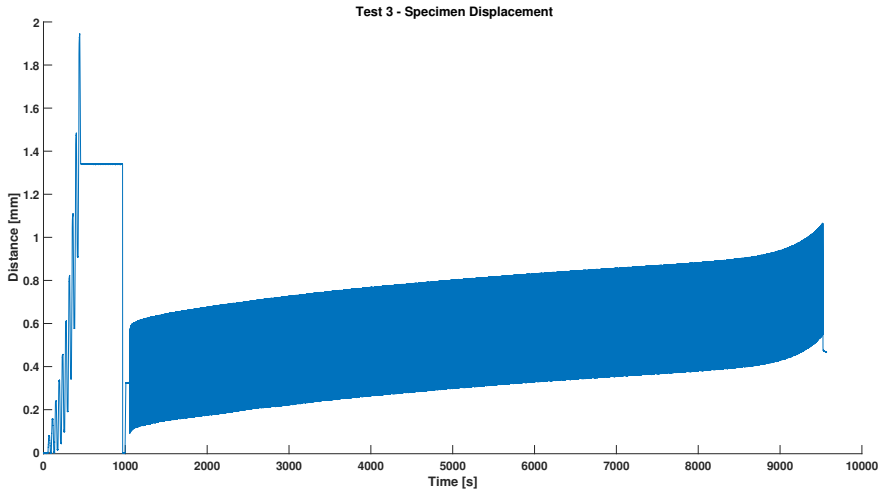

Figure 5.14: Dent Displacement for Test 3

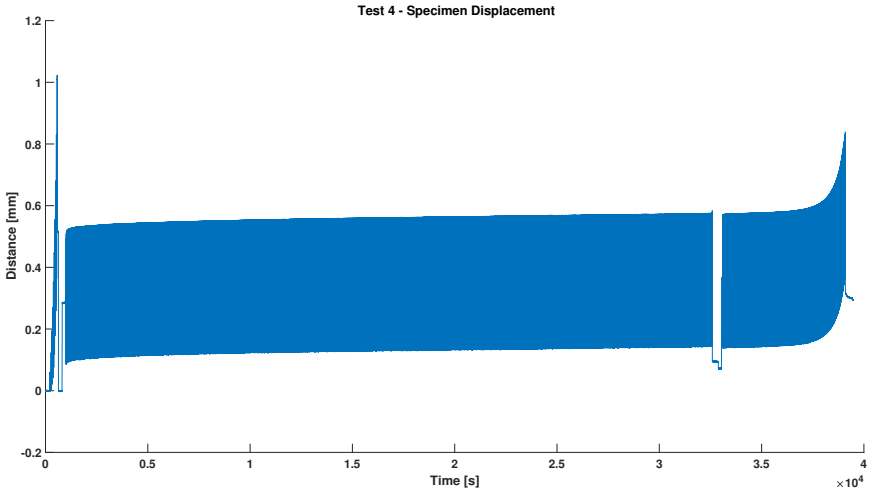

Figure 5.15: Dent Displacement for Test 4

Test 3 had a radial displacement of 1.94 mm during the initial phase, while the maximum radial displacement during the dynamic cycles reached 1.06 mm. The final displacement after the pressure was reduced was 0.47 mm. As a comparison, the radial displacement of test 4 reached 1.02 mm during the initial phase, 0.84 mm during the dynamic phase, and 0.30 mm after the pressure was reduced. This shows that the magnitude of the internal pressure has a large impact on the radial displacement. This can also be seen in figure 5.16 for test 10 which had 60 bar of maximum internal dynamic pressure. The

initial static phase has a greater impact on the rerounding than the dynamic phase afterwards. Test 10 had a larger initial pressure than dynamic pressure to see the effect of rerounding on fatigue life, but unfortunately the LVDT-data was not recorded for the initial phase. It was, however, observed that the LVDT had a change of 3 mm after the initial pressurization. The dynamic pressure gave a maximum radial displacement of 0.27 mm.

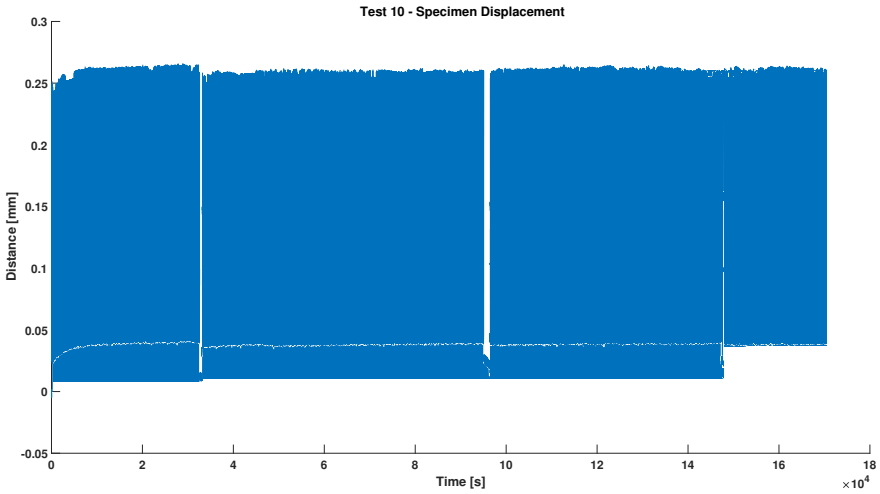

Figure 5.16: Dent Displacement for Test 10

The dent geometry was checked for the 3D-model of test 3 and 8. These were chosen because the 3D-models were of high quality, and they represent one test with high pressure and one with low pressure. The program *Rhinoceros 5* was used to extract the geometry from the 3D-models in *Autodesk ReMake*. Figure 5.17 shows the geometry change after static pressure for test 3 and 8 in the symmetry cross-section, while figure 5.18 shows the dent geometry going out of the dent.

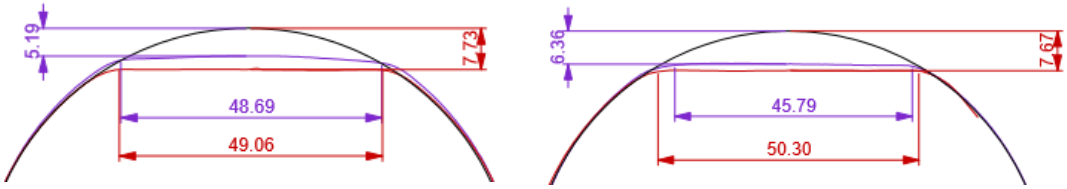

(a) Test 3 (b) Test 8

Figure 5.17: Geometry Change in Symmetry Cross-Section from 3D-Model for Test 3 and 8

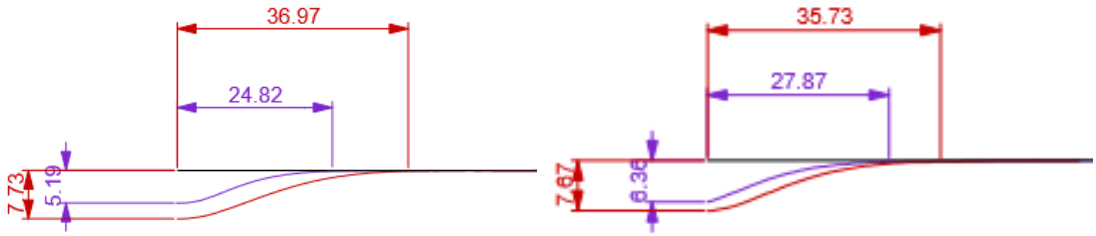

(a) Test 3 (b) Test 8

Figure 5.18: Geometry Change Orthogonal out of the Dent from 3D-Model for Test 3 and 8

This shows the rerounding of the two tests after the static pressure phase. The dent depth and length is stated in table 5.3.

Table 5.3: Dent Geometry from 3D-Model

Test:	Scan:	Depth [mm]	Length [mm]	Width [mm]
3	First	7.73	36.97	49.06
	Second	5.19	24.82	48.69
8	First	7.67	35.73	50.30
	Second	6.36	27.87	45.79

This makes the total static displacement of test 3 from the 3D-model 2.54 mm compared to the value 1.94 mm from the LVDT-device. The total static displacement of test 8 is 1.31 mm. The LVDT-placement could be slightly off from the midpoint of the dent where the 3D-model values were taken from. The calibration of the LVDT-device could be off, which could also slightly affect the measurement. The accuracy of the 3D-model could also be a source of error. The first measurement for both test should be the same, since no pressure is applied and the same indenter was used. There is a 0.8 % difference for the dent depth, a 3.4 % difference for the half-length, and a 2.5 % difference for the width for the first scan. The half-length is difficult to determine exactly based on the figures above. Here, it is taken as the point when the dent starts to curve with the pipe curvature from the straight line of the dent. The width is also difficult to determine. The width changes more for test 8, but this could be due to the 3D-model accuracy as well.

5.1.4 Gouge Geometry

The geometry of the gouge is of interest, and was determined using a microscope. Figure 5.19a and 5.19b shows the gouges as patches of microscopic images for test 2 and 7.

(a) Test 2

(b) Test 7

Figure 5.19: Microscopic Image of the Gouge in Test 2 and 7

The gouge can be seen as two or three distinct cuts into the material following the dent. This is made more clear in figure 5.20a and 5.20b, showing the topology as a color-map.

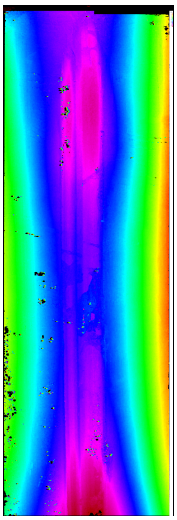

(a) Test 2

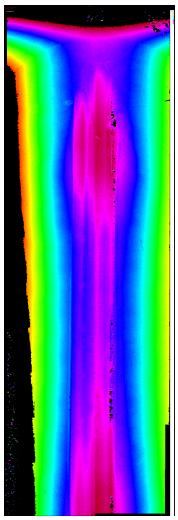

(b) Test 7

Figure 5.20: Color-Map of Topology for Test 2 and 7

Here the cuts are clearer. The color-map has brighter purple areas at the bottom and top of the figure. This is due to the curvature of the dent. Finally, the actual dent depth were measured using the microscope over a line orthogonal to the dent in the middle of

these figures. These measurements can be seen in figure 5.21 and 5.22.

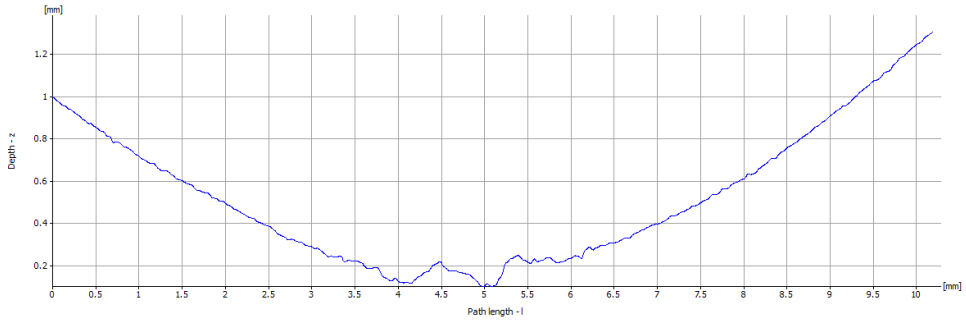

Figure 5.21: Microscopic Measurement of Gouge Depth for Test 2

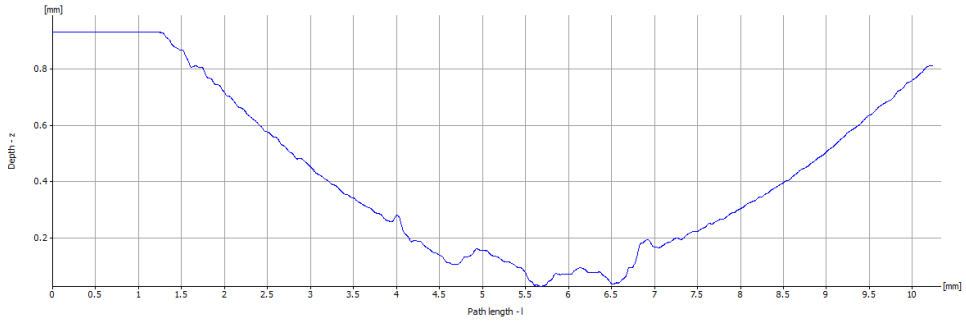

Figure 5.22: Microscopic Measurement of Gouge Depth for Test 7

The gouge can be seen as the unevenness in the bottom of these curves. Using the scale embedded in these images the gouge geometry can be seen in table 5.4.

Table 5.4: Gouge Geometry

Test	Width [mm]	Depth [mm]	Length [mm]
2	2.64 - 2.86	0.215	43.1
7	2.85 - 2.93	0.191	43.1

The depth is measured from the bottom of the dent itself. It should be noted that finding these values were hard, since it is difficult on a microscopic level to determine exactly were the different properties should be measured from. The geometry also changes along the dent, hence the measure range. The depth is measured at the middle of the gouge to the shoulder.

The small difference in width and depth of the gouge indicates that there has been some wear of the indenter during the tests. The gouge has become wider and shallower.

5.1.5 Reference Gage

A reference strain gage was placed on test 1, 2 and 9, sufficiently far enough from the dent to be influenced from the stress concentrations, and thus giving an idea of the nominal strain values. Figure 5.23 shows the nominal strains from test 1. The red line in the middle of the figures are the maximum value for the underlying stress/strain.

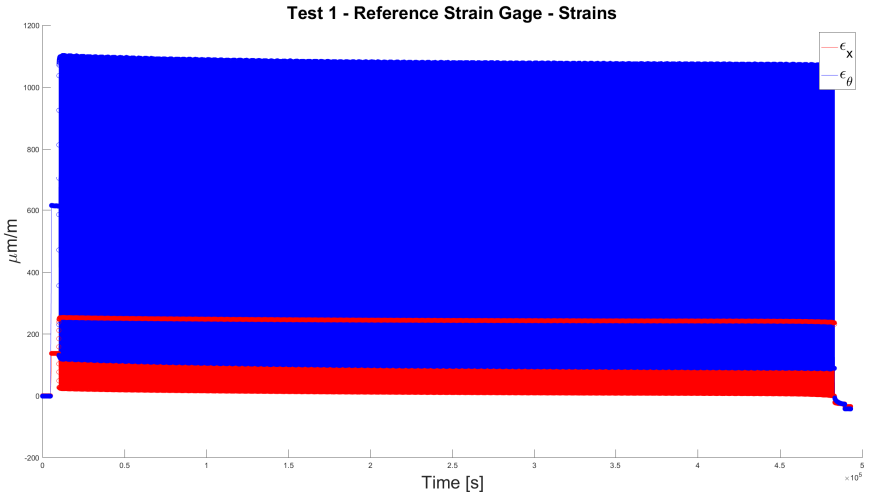

Figure 5.23: Nominal Strain for Test 1

The strain values do not increase during the test, and so linear-elastic theory is valid. The corresponding stresses can be seen in figure 5.24.

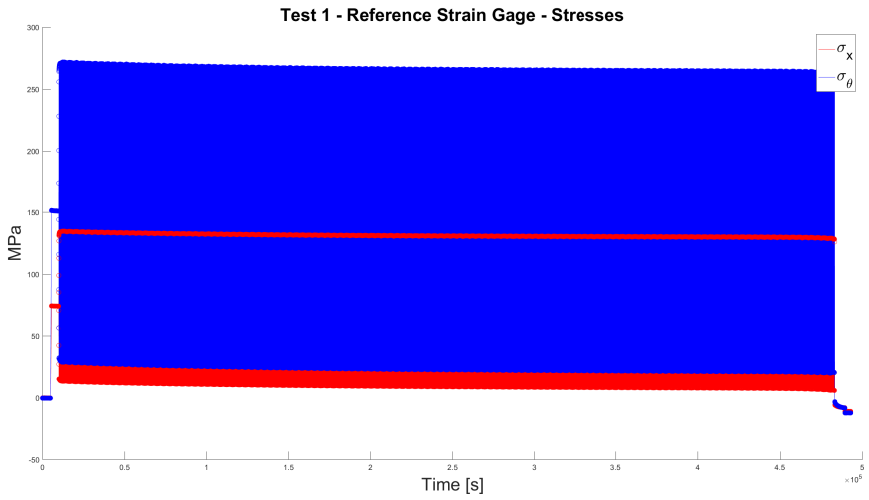

Figure 5.24: Nominal Stress for Test 1

The maximum stress value is found to be approximately 267 MPa for hoop and 132 MPa for axial direction. Using equation 2.14 for stress in a thin walled pipe, the theoretical value becomes 245 MPa for hoop and 122.5 MPa for axial direction. These values are both lower than the observed values. This could be due to using wrong Young's modulus, or that the geometry is slightly different from the stated diameter and thickness.

The values from the other gages compared with the reference strain can be seen in figure 5.25 and 5.26. This gives an idea of how the strains/stresses are concentrated around the dent.

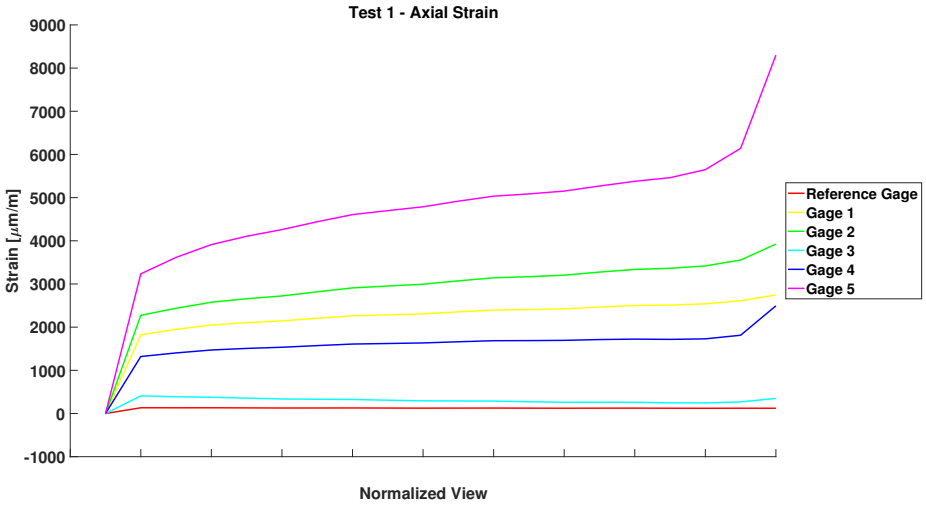

Figure 5.25: Mean Axial Strains for Test 1

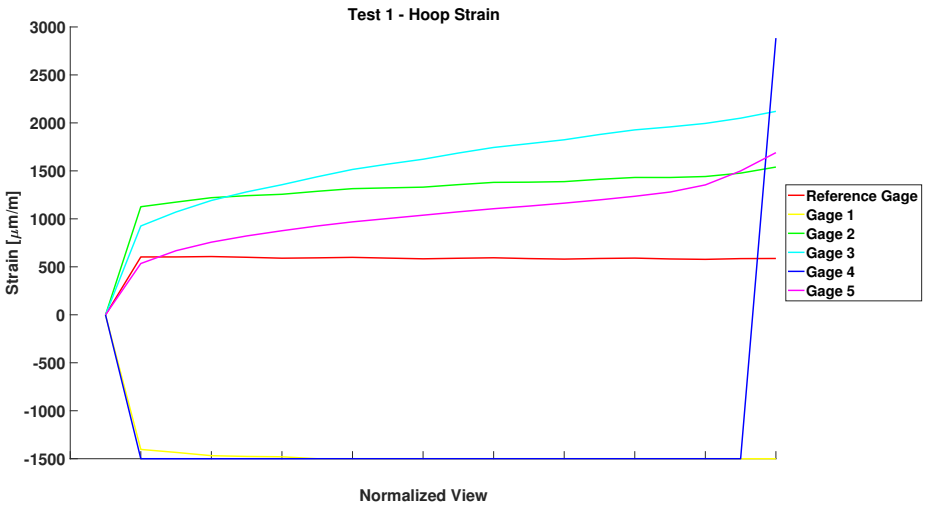

Figure 5.26: Mean Hoop Strains for Test 1

The concentrations are significant around the dent, with the largest values around the dent edges (gage 1,2,4,5). In this figure, the values for gage 4 is broken in hoop direction.

5.1.6 Stress Calculations

The strain is converted to stress using the equations in section 2.5. This gives the mean for the same gage as the strain measurements, seen in figure 5.27 and 5.28.

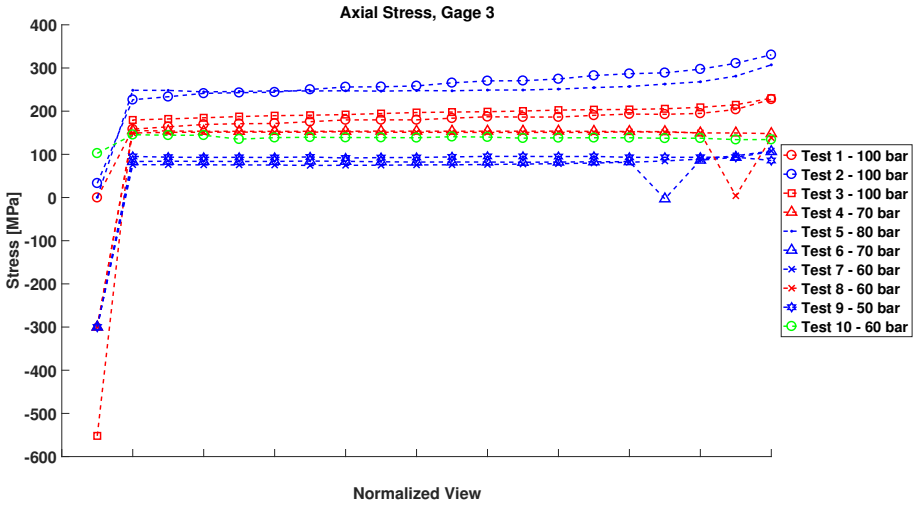

Figure 5.27: Mean Axial Stress at Gage 3

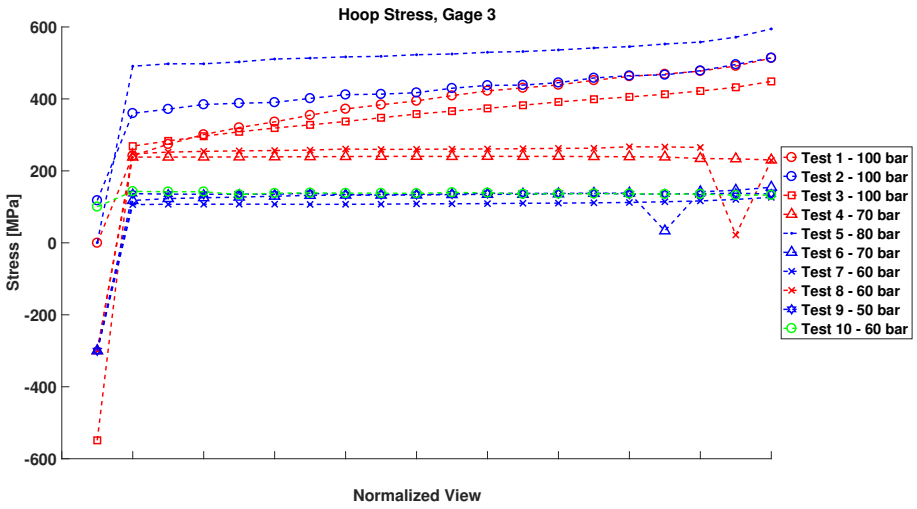

Figure 5.28: Mean Hoop Stress at Gage 3

These values behave more or less fine initially, with the exception of test 5, which are much larger than the other tests during the whole duration. This is probably because of some issue with the gages for this test. The mean stress is, however, large for all the tests. This is the mean values, meaning that the maximum values for some of the tests will reach far beyond the yield strength of the material, stated in table 4.2, in all cycles according to these plots. Some values will also reach beyond the ultimate tensile strength of the material. The values also increase during the duration of the tests for some of the high-pressure tests. This is okay for the strain values because of plastic effects, as well as geometry change of the dent during the cycles. It is strange behavior for the stress values. As the pressure reaches its minimum value in each cycle, so should the stress go down to a minimum value, which should not change much during each cycle. The stress calculations in section 2.5 are for linear-elastic behavior, and there is clearly plastic behavior during the test. The stress distribution for gage 3 can be seen in figure 5.29. The lower hoop-stress value is gradually increasing during the test, as the hoop strain is increasing. Other methods should therefore be considered for computing the stress, like the method discussed in section 2.11 or similar methods.

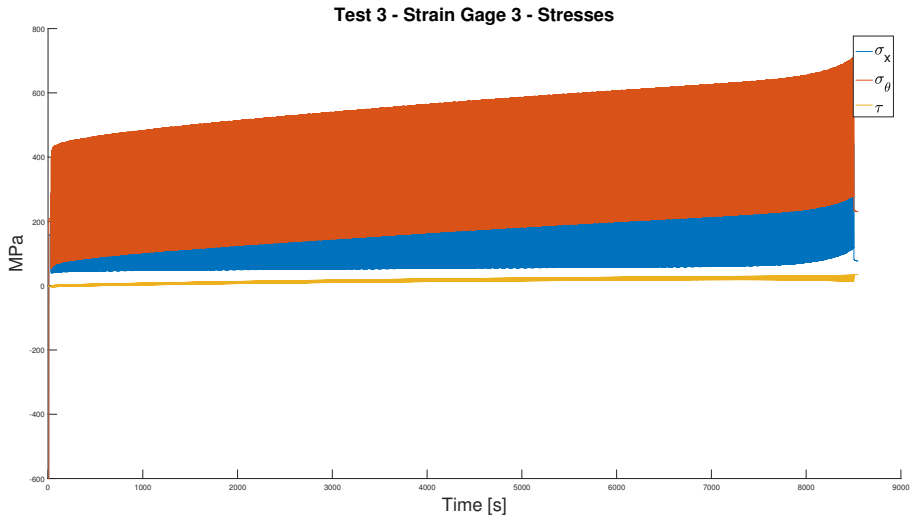

Figure 5.29: Stress for Test 3 at Gage 3

5.1.7 Stress-Strain Relationship

Plotting the stress-strain relationship during the pressure cycles gives an indication of how the relationship changes, and if there are any ratcheting or cyclic creep effects. The gradually increasing stress values are also investigated further with these relationships. Figure 5.30 shows the stress-strain relationship from the reference gage for test 2.

Figure 5.30: Stress-Strain Relationship at Reference Gage for Test 2

As seen here, the stress and strain change very little relative to each other. The entire fatigue life of the test is compressed into the straight lines seen in the figure. If there were any change the values would move along the axis, as seen during cyclic creep and ratcheting. It can also be seen that there is a small change in the relationship between the axial stress and strain. This could be compared to the stress-strain relationship from the other gages in test 2, for instance for gage 1 as seen figure 5.31. This stress-strain relationship is nothing like the straight line in figure 5.30, with more ratcheting effects, as well as much larger values.

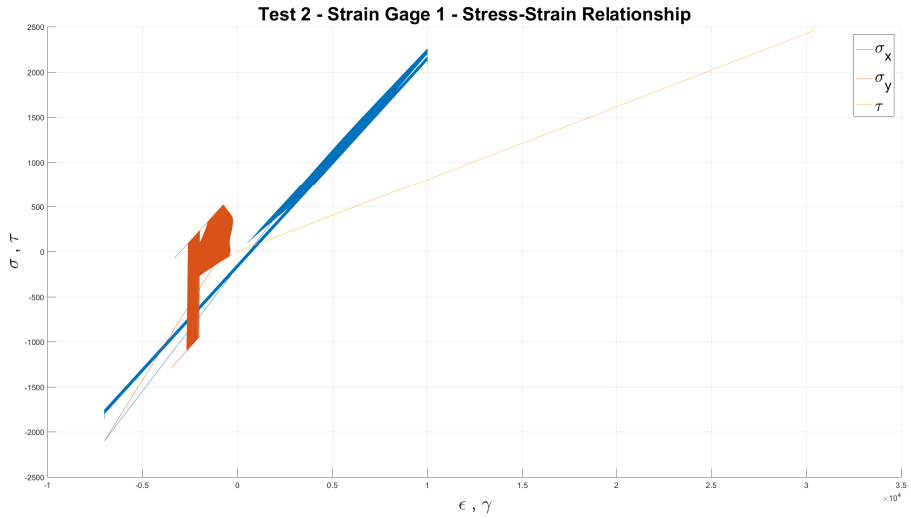

Figure 5.31: Stress-Strain Relationship at Gage 1 from Test 2

The increasing stress in this figure is also due to the gradually increasing stress calculated from the gage strain. This increasing stress is due to the linear stress theory, and is invalid for the plastic effects observed for many of the gages. Future stress calculation should use other methods than the linear relationship if the stresses from the gage is of interest.

5.2 Experiment Comments

There are several things that is worth mentioning about the fatigue tests done during this thesis, and this section is dedicated for that. The following irregularities happened:

Test 1:

The gage factor was set to 2.0 instead of 2.1 during the test. This is considered when plotting the values from the gage.

Test 2:

The strain gages along the dent were attached in reverse order. This is not considered when referring to gage values, meaning that gage 5 should be thought of as gage 1 and gage 4 as gage 2 to coincide with the other tests. Strain gage 3 slipped during the test, giving uncertain values for this gage. The crack initiated over gage 2, making the gage fail before the pipe did. The values from gage 1 seem to coincide more with the leak of the pipe.

Test 3 and 4:

Nothing out of the ordinary.

Test 5:

The material used for this test was from an older batch of steel, which means that the material behavior could be different from the other values. The pipe failed in the weld on the endcap in the static pressure part at 21 bar, going up with increments to 70 bar. This gave a displacement of 0.002 mm. This meant that the endcap needed rewelding, making this test one of the last to be completed. The next pipe test was selected at 70 bar, so the dynamic pressure was changed to 80 bar to give more spread out values in the SN-curve. Gage 5 was put on an angle by mistake, which means that the stress/strain referring to axial and hoop direction will be at an angle. The principle stresses should therefore be used instead. The gage in question is seen in figure 5.32.

Figure 5.32: Misplacement of Gage 5 in Test 5

The wire for the hoop strain of gage 2 accidentally snapped when placed, giving no reading for this direction, and messing up the stress calculations from the gage.

Test 6:

The placement of gage 5 deviated from the correct position by mistake, and at an angle. This certainly affects the measurements for this gage. The gage can be seen in figure 5.33.

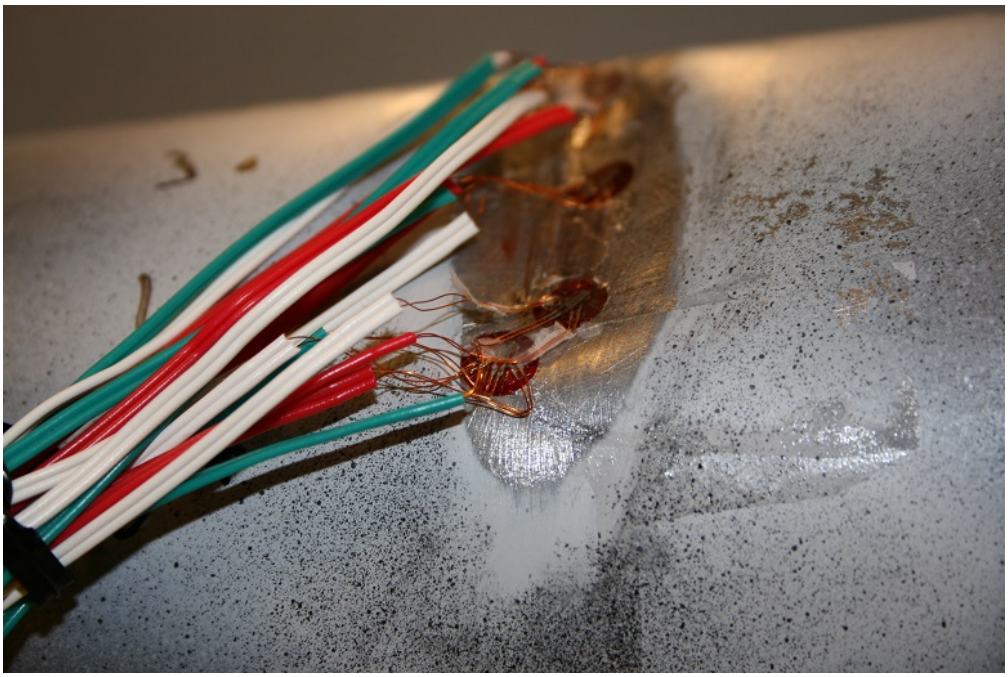

Figure 5.33: Misplacement of Gage 5 in Test 6

The LVDT-device slipped during the test, which could have affected the measurements of gage 3, 4 and 5 when the device fell over the wires. It was also observed that the wires of gage 1 and 2 was glued to the pipe and moved with the dent during the pressure-cycles. This could affect the values from the gages.

Test 7:

Gage 3 used wrong gage factor. The test was done with a gage factor of 2.11, while the gage actually read 1: 2.06, 2: 2.05, 3: 2.03. This has been considered in the plots and values. The point of failure was difficult to determine, since nobody was present when the leak appeared and the leak was difficult to spot from the cylinder position. The number of cycles used here can therefore be viewed as conservative.

Test 8:

This test failed in the weld on one side during the pressure cycles. After taking down the

test and rewelding it, it failed again on the other side. The test needed to be rewelded again. This process probably influenced the strain measurements from the gages. The hoop direction wire of gage 2 snapped from the gage during one of these resets.

Test 9:

The LVDT-device moved in the axial direction during the test and might have initiated the crack.

Test 10:

This test used a larger static pressure than the other tests to have a larger rerounding effect before the pressure cycles. This gave a much larger number of cycles than the other tests. Unfortunately, the pump supplying pressure to the pipe failed before the pipe itself. The lower limit for the pump cylinder was not enabled during the last part of the test, making the pump continue to work even though the hydraulic liquid was slowly leaking out. Many of the last cycles have therefore probably been on a lower pressure than the one intended. This would be fine if all the cycles and pressure where registered by the computer program. But unfortunately, also the computer program failed during the last part of the test. So, the log stopped approximately 100 000 cycles before the number seen in table 5.1. Using linear regression on the internal leak gives the number 588 500 cycles. The total number of cycles are much larger, but with a gradually reducing pressure, without any record to tell how fast it happened. The computer controlling the pump did not fail, and registered the total number of cycles to be 704 738. This test was certainly the longest, but it had only around 588 500 cycles at full pressure range. Any larger number would be uncertain, but this value is conservative

General Remarks:

The gage size changed during the test phase. Table 5.5 shows the gage radius for each gage in each test.

Table 5.5: Gage Size

Test	Gage 1 [mm]	Gage 2 [mm]	Gage 3 [mm]	Gage 4 [mm]	Gage 5 [mm]
1	3	3	3	3	3
2	3	3	3	3	3
3	3	3	3	3	3
4	3	3	3	3	3
5	2	2	2	2	2
6	3	3	3	3	3
7	3	3	2	3	3
8	6	6	6	6	6
9	2	2	2	2	2
10	2	2	2	2	2

Different gage size affects the measurements. The gage takes an average over the area it is placed, so a large gage will get a smeared-out result compared to a small gage. Given the large local peaks observed during the numerical tests a small gage could hit one of these local peaks, and therefore get results that are not necessarily so comparable with the other tests. The results from the two last tests gives no indication that this has happened, and these are the only two tests using only small gages.

5.3 Material Tests

Here the results from the material tests are presented. Material was collected from four of the fatigue tests. The tests in question were two high-pressure tests, test 1 and 2, and two low-pressure tests, test 8 and 9. Material strips were cut out in hoop direction for all tests. The geometry of these tests can be seen in table 5.6.

Table 5.6: Material Strip Geometry

Test:	Orientation:	Width:	Thickness:
Pipe 1	Top	10.00	1.81
	Center	10.02	1.86
	Bottom	10.00	1.81
Pipe 2	Top	10.10	1.84
	Center	10.11	1.87
	Bottom	10.08	1.86
Pipe 3	Top	9.89	1.78
	Center	9.89	1.86
	Bottom	9.85	1.82
Pipe 4	Top	10.04	1.79
	Center	10.10	1.84
	Bottom	10.12	1.81

The tests were run on a 0.2 mm/min rate until it reached 0.6 mm, and continued with a rate of 1.0 mm/min until it reached 10.6 mm. The stress-strain plot for these tests can be seen in figure 5.34. A more detailed view can be seen in figure 5.35 together with the curve from *ABAQUS*.

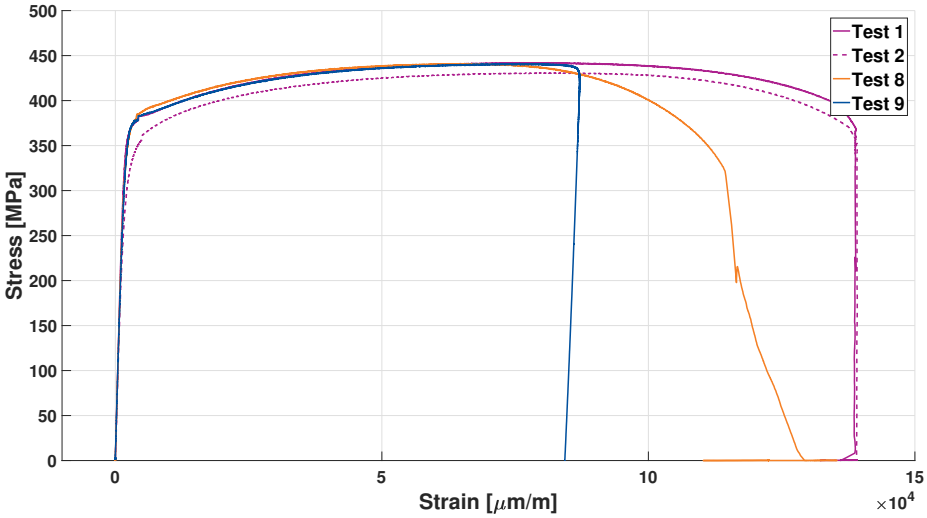

Figure 5.34: Stress-Strain Plot for Material Tests

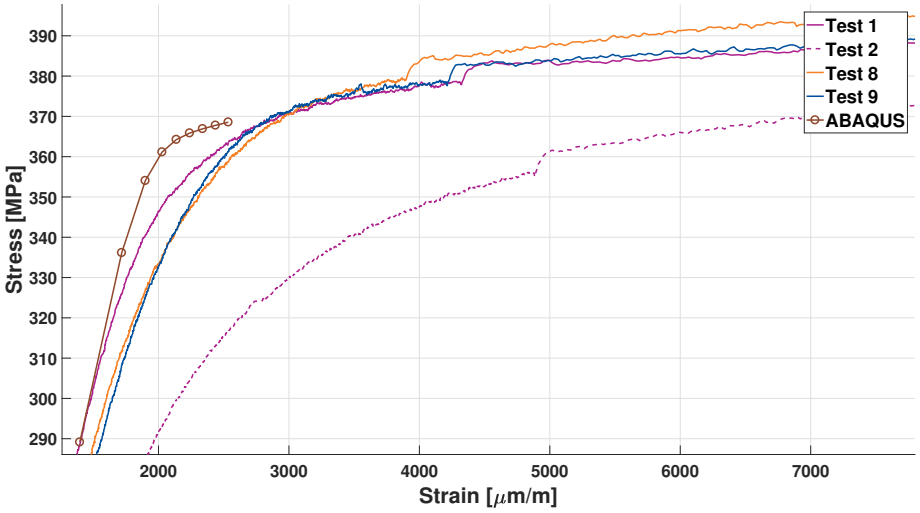

Figure 5.35: Stress-Strain Plot for Material Tests, with Values used in *ABAQUS*

The material tests show that the material have different properties for the different tests. The material properties can be found in table 5.7. The Young's modulus is taken as the slope of the linear fit of the elastic part of the graph. The yield strength is the 0.2 % strain value intersection, and the ultimate tensile strength is the largest value in the graph. The values used in *ABAQUS* does not match the values from the material tests.

Table 5.7: Material Properties

Test:	Pressure [bar]	E [GPa]	σ_y [MPa]	σ_u [MPa]
Pipe 1	10-100	221.6	330.9	442.2
Pipe 2	10-100	181.6	278.8	430.9
Pipe 8	6-60	211.3	315.7	441.2
Pipe 9	5-50	196.2	312.7	441.4
ABAQUS	-	207	289.15	399.49

There are notable differences in the Young's modulus and the yield strength for the tests. Test 2 is strange compared to the other tests, which are more similar to each other. All values are considerably lower than for the other tests. These differences will affect the results. This also gives some uncertainty for the other tests performed during the project, which do not have material tests performed on them.

It was observed during the cutting of the material strips that there was curvature of the test piece due to residual stress in the pipe. The strain measurement was difficult due to the strips not being completely straight. This complicates the resulting measurements.

5.4 Numerical Results

5.4.1 Measured Path

Different parameters are extracted from the program and used to create plots. Figure 5.36 shows the nodes selected when measuring along the symmetry cross-section at the location of the dent. The indenter have moved from right to left in this figure.

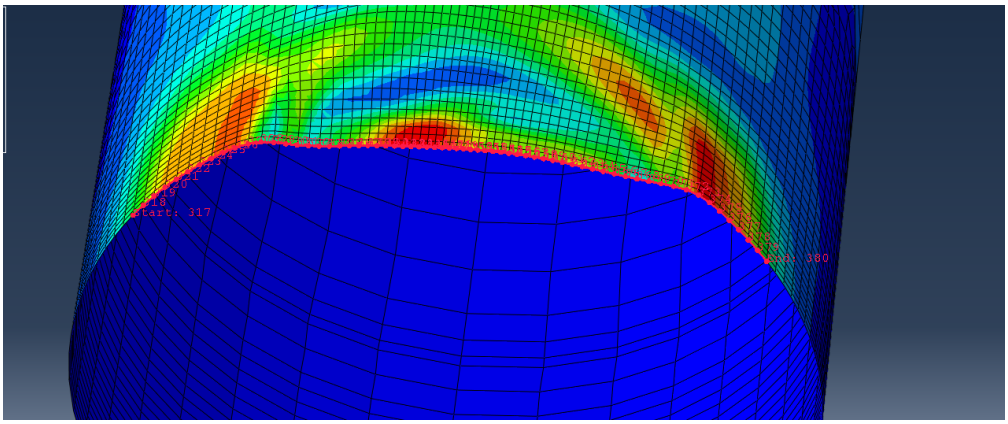

Figure 5.36: Symmetry Path used in *ABAQUS*

Figure 5.37 shows the path measured orthogonal out of the dent from the fine mesh in the center of the dent towards the beginning of the transitional area of the mesh.

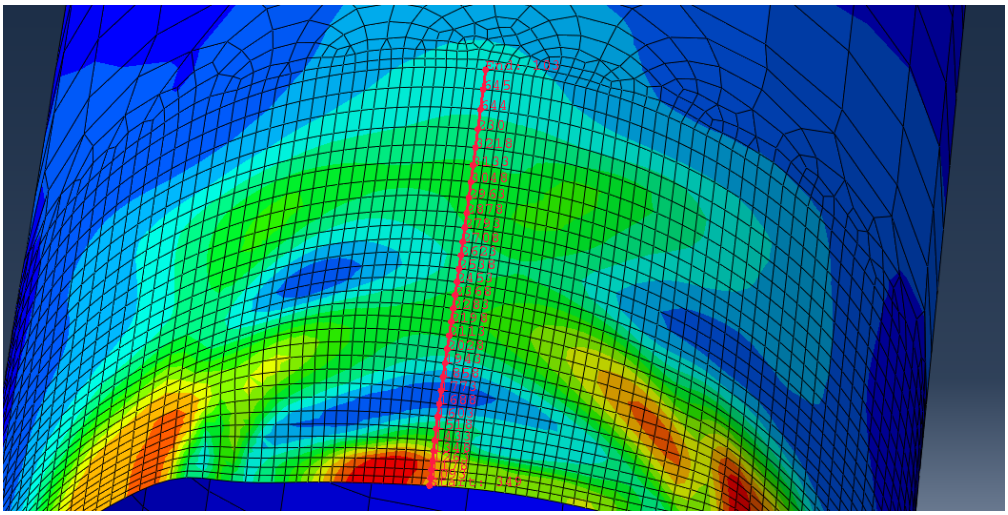

Figure 5.37: Orthogonal Path used in *ABAQUS*

Figure 5.38a and 5.38b shows the measurement path on the top and bottom of the pipe. These are taken from the end of the transitional mesh area to the endcap.

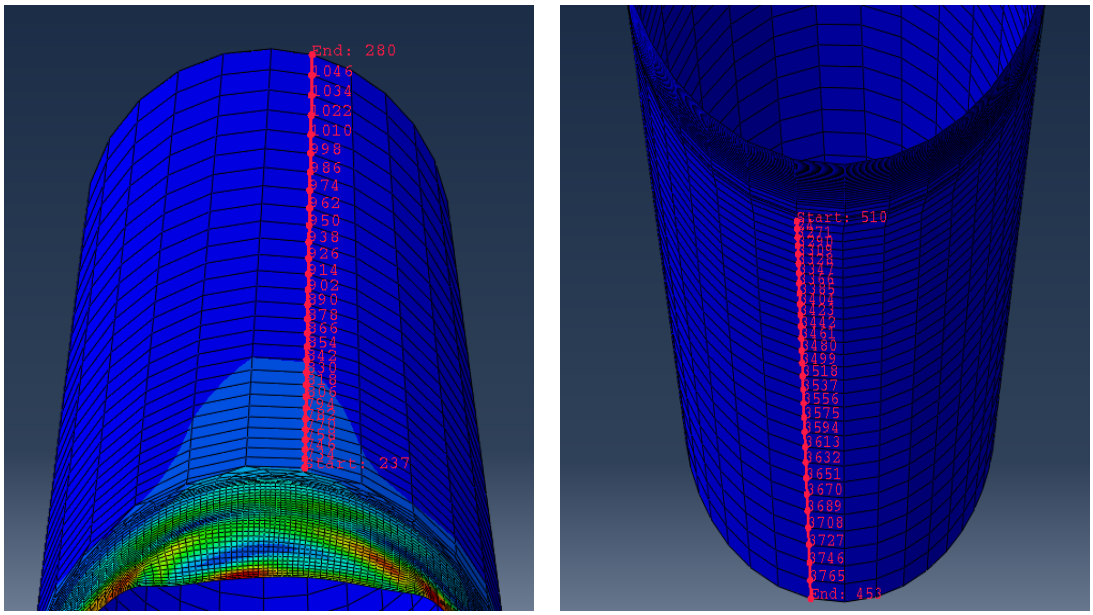

(a) Top Path (b) Bottom Path

Figure 5.38: Pipe Paths used in *ABAQUS*

5.4.2 Indenter Type

There were two indenter types used in this project, one with a sharp- and one with a blunt shape, as seen in figure 4.15. The indenter that leaves the smoothest dent with the least local stress concentrations and geometry-changes would be the best one for fatigue purposes, since it will minimize the complexity of the dent. The von Mises stress for the two indenter types along the whole dent cross-section can be seen in figure 5.39. These measurements clockwise and are taken at an internal pressure of 100 bar.

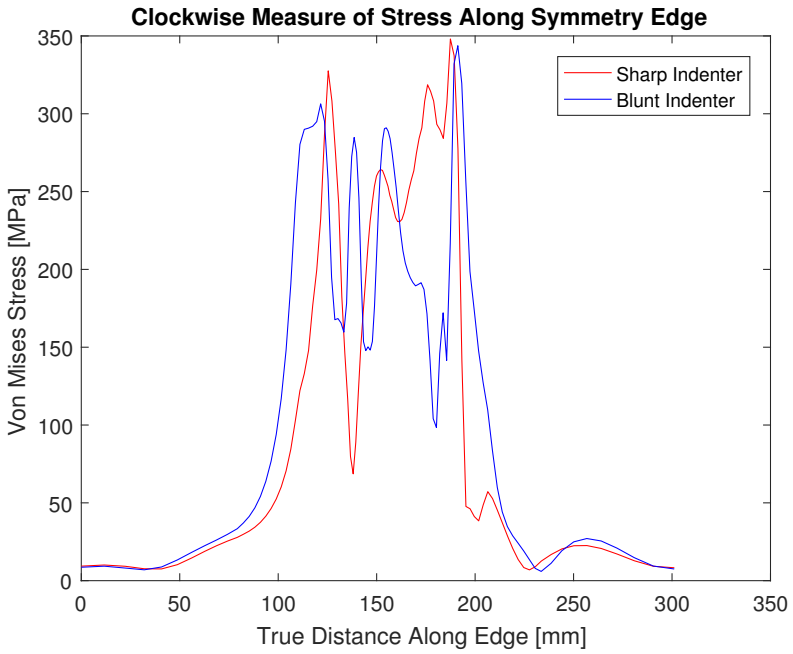

Figure 5.39: Comparison of von Mises Stress for Two Indenter Types

The stresses are similar outside the dent, but are different and have large peak values within the dent, especially around the dent entrance/exit. The stresses vary a lot within the dent with the sharp-indenter type having the largest values around the peaks at the entrance/exit, which are seen as the two stress-towers on either side of the high-stress area. The pipe subjected to the blunt indenter have increased stress levels on a larger area of the cross-section.

The radial and hoop relative deformation can be seen in figure 5.40a and 5.40b.

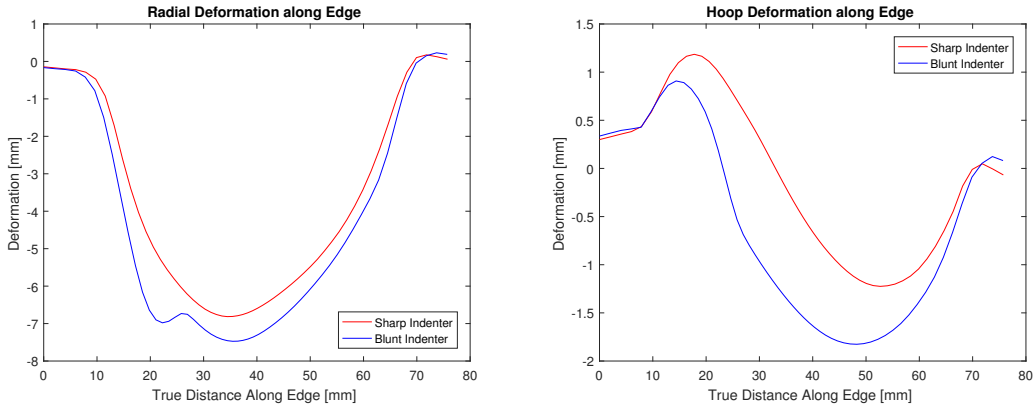

(a) Relative Radial Deformation (b) Relative Hoop Deformation

Figure 5.40: Relative Deformation in Radial and Hoop Direction

The deformation is smoother for the dent made by the sharp indenter than the blunt indenter, and the dent depth is also smaller. The dent made by the blunt indenter also have a small extra dent at the left in the radial figure, which can further complicate the behavior. The geometry made by the two indenters can be seen in figure 5.41. The dent made by the blunt indenter is blue, sharp indenter is red while black is the pipe before indentation. Each cross represents a node.

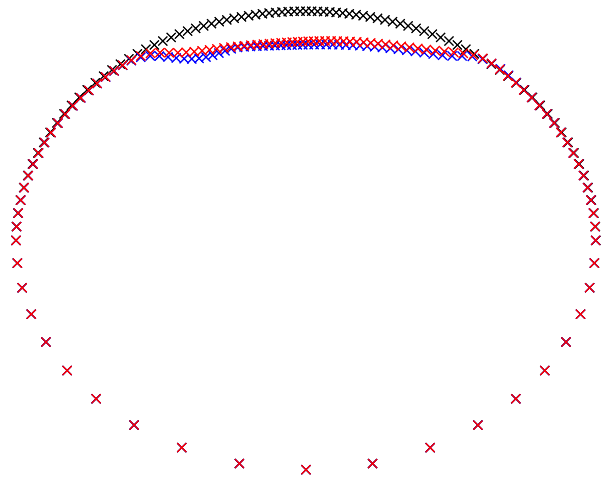

Figure 5.41: Comparison of Dent Geometry for Two Indenter Types

As for the deformation values, the dent made by a blunt indenter type has a more irregular shape than the dent made by a sharp indenter, which appears smoother and straighter.

5.4.3 Element Type and Mesh Size

Some values in the plots have steep stress values, where as little as one node determines peak values. It could therefore be of interest to reduce the mesh size. Also, to see how a more accurate element type influence the result. A short analysis was made to compare two different mesh sizes and two different element sizes to see how these changes affect the numerical results. The two different element types are $S4R$ and $S8R$, where the first element type was tested for different mesh size. Figure 5.42 shows the von Mises stress along the dent cross-section for two different mesh sizes. The mesh is changed so that twice as many elements are used in the most critical parts of the dent, the middle of the dent, and the mesh size increase to the same value as the previous mesh in the other parts of the circumference. The rest of the model have decreased mesh size to get a smoother mesh transition in the transitional area.

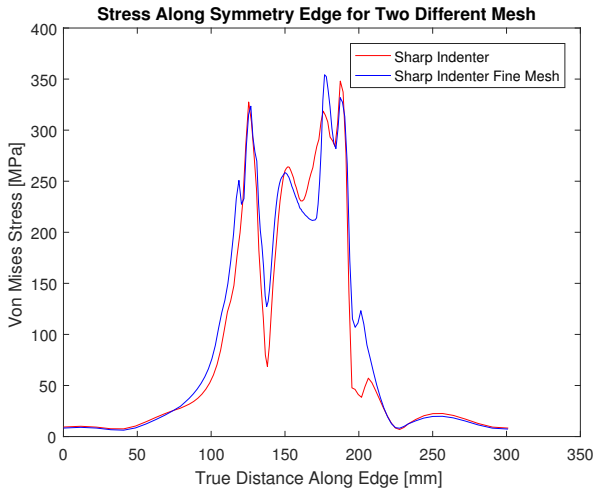

Figure 5.42: Comparison of von Mises Stress for Two Mesh Sizes

The general behavior of the stress is similar, while the size and shape of the stress peaks have small differences. Figure 5.43 shows the pipe geometry for the two mesh sizes.

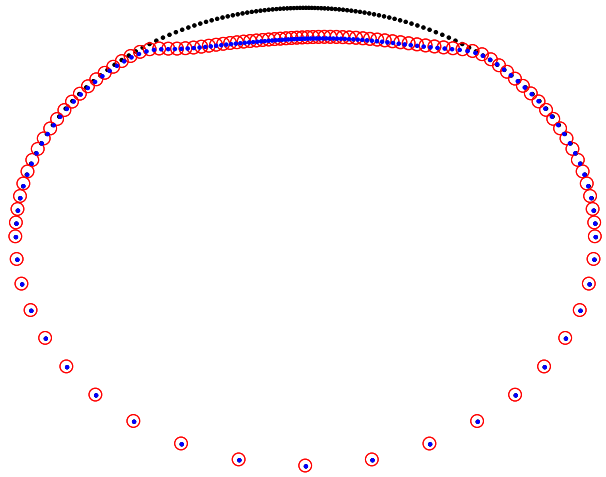

Figure 5.43: Comparison of Dent Geometry for Two Mesh Sizes

Each point is a node in the fine mesh and circle is a node in the coarse mesh, so this figure also shows the compared mesh sizes. The geometries are identical.

The coarse mesh is used to compare the stress and geometry for two element types. Figure 5.44 shows the von Mises stress for the two element types at 100 bar for the sharp indenter.

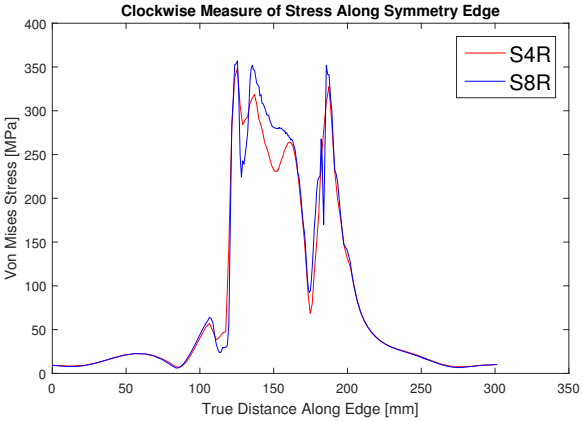

Figure 5.44: Comparison of von Mises Stress for Two Element Types

As the other plots, the behavior is similar, with some difference in the peak values. The $S8R$ element should be more accurate than the $S4R$ element, but it is more expensive in terms of computational cost. The geometry difference in the cross section can be seen in figure 5.45.

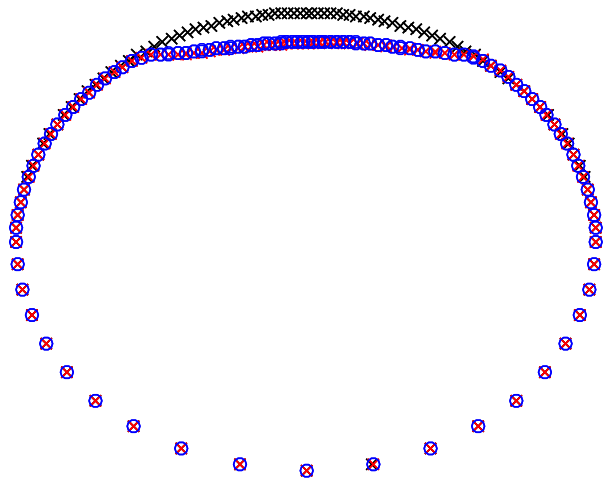

Figure 5.45: Comparison of Dent Geometry for Two Element Types

This figure shows that the geometry for the two element types are very similar. For the rest of the numerical results the coarse mesh will be used together with the $S8R$ element type. This combination is chosen to give good accuracy, but still be fast enough to be effective.

5.4.4 Strain Measurements

The axial and hoop strain is measured along the paths mentioned in section 5.4.1. Figure 5.46a and 5.46b shows the strain measurements along the dent cross-section. These measurements are made in the top of the element. This is done to be more comparable with the x-ray measurements and the strain gages.

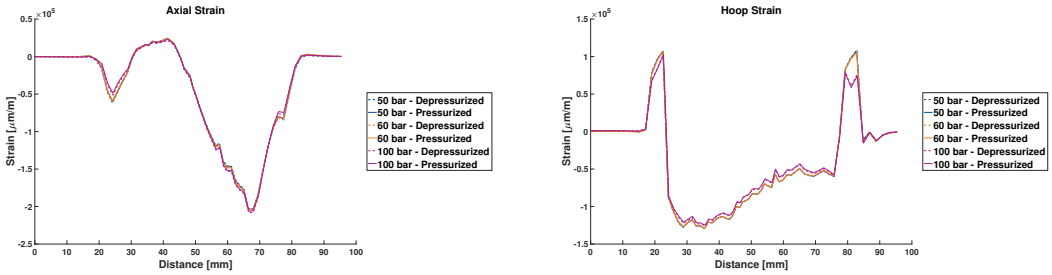

(a) Axial Strain (b) Hoop Strain

Figure 5.46: Strain in Symmetry Cross-Section

The main thing to notice in these figures is the large values that occur by the peaks in the graph. There are strain values of above 100 000 μm/m in absolute value. There is also an apparently small difference between the pressurized and depressurized state for each test and between the different pressures. These measurements consider the strain that occurs during the indentation, which are very large relative to the ones that occur during the pressurization. The strain gage measurements done in section 5.1 does not take these strains into account, since they are put on the pipe after the indentation. Figure 5.47a and 5.47b shows the relative difference between the pressure-states for the axial and hoop strains, which have values more consistent with the values from the strain gages.

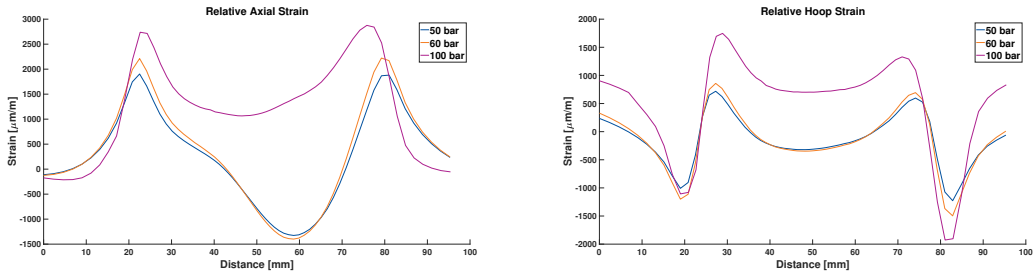

(a) Relative Axial Strain (b) Relative Hoop Strain

Figure 5.47: Relative Strain in Symmetry Cross-Section

The major strain components are situated around some peak values, which are the entrance and exit of the dent. The same high strain from indentation can be seen in figure 5.48a and 5.48b representing the strain orthogonal out from the dent center.

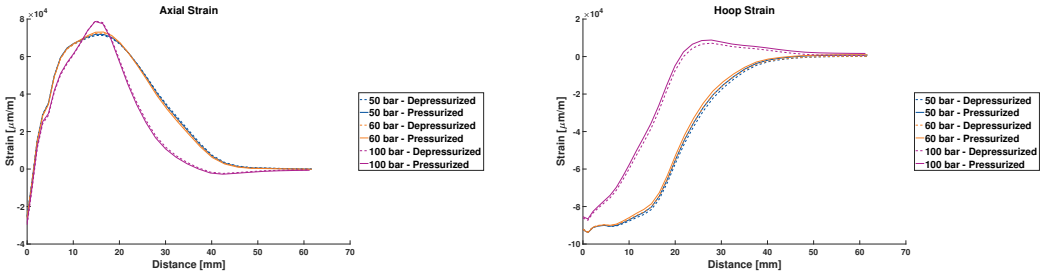

(a) Axial Strain (b) Hoop Strain

Figure 5.48: Strain measured Orthogonal out of the Dent

And again, the relative strain can be seen in figure 5.49a and 5.49b.

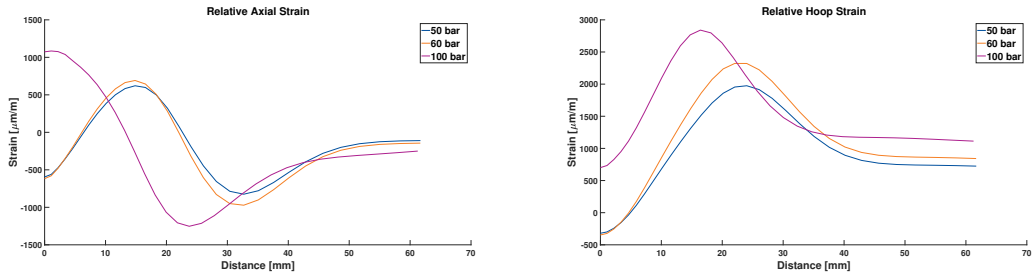

(a) Relative Axial Strain (b) Relative Hoop Strain

Figure 5.49: Relative Strain measured Orthogonal out of the Dent

An interesting observation from the relative strain values is the fact that the high-pressure test in blue have a positive value at the dent center, while the two low-pressure tests have negative values. All tests have positive and negative values going out of the dent, both for relative and actual values.

Figure 5.50a and 5.50b show the strain along the bottom path, while figure 5.51a and 5.51b shows the strain along the top path.

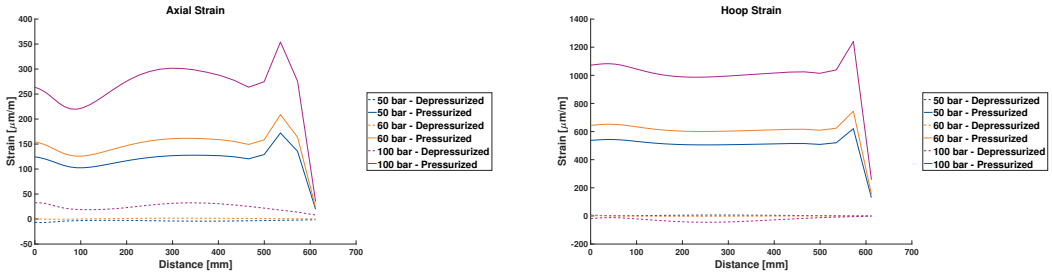

(a) Axial Strain (b) Hoop Strain

Figure 5.50: Strain measured along the Bottom Path out of the Dent

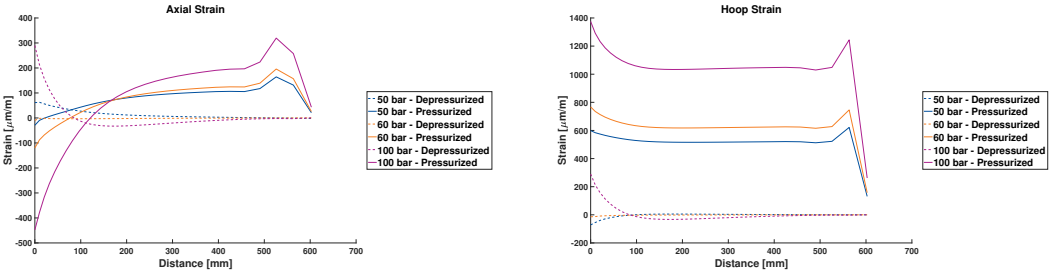

(a) Axial Strain (b) Hoop Strain

Figure 5.51: Strain measured along the Top Path out of the Dent

The hoop strain quickly reaches a state where the value remains stable with values that coincides with the reference strain gages measuring at the same pressures. The axial strain does not behave in the same way. For the pressurized states the axial strain tends to increase along the pipe, especially for the 100 bar test and along the top path. This makes it challenging to know where to place reference strain gages for the axial direction. At the end of the path the endcap starts to influence the values for the strain. For the depressurized states the strain quickly approaches values close to zero.

5.4.5 Stress Measurements

Stress measurements are also done for the different paths in axial and hoop direction. First, the stresses from the symmetry cross-section can be seen in figure 5.52 and 5.53.

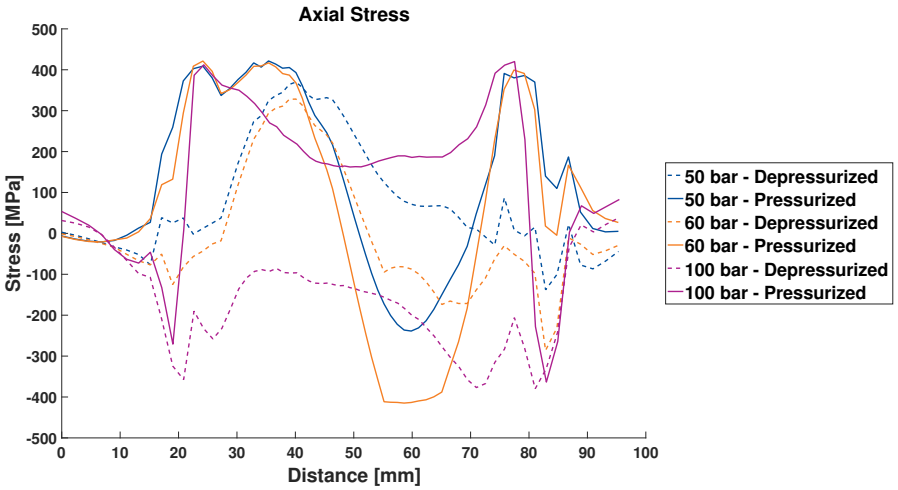

Figure 5.52: Axial Stress in Symmetry Cross-Section

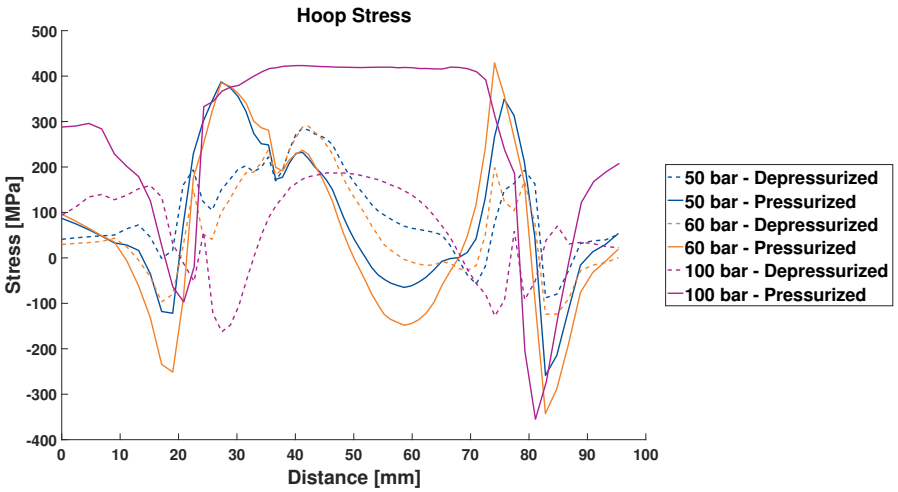

Figure 5.53: Hoop Stress in Symmetry Cross-Section

Both stress directions experience large compressive stress spikes around the dent entrance/exit. Within the dent itself the stresses are varying a lot for both states. For the 100 bar case the pressurized state is generally larger than the depressurized within the dent, while for the other two cases this varies. Both tests have higher stress values at the dent entrance (right peak) for the depressurized in both directions, where pressurizing the pipe pushes the stresses into or towards compression.

Another interesting thing would be to look at relative stress difference in the dent, which gives a better indication of how the stress range changes throughout the dent. Figure

5.54a and 5.54b shows the relative stress in axial and hoop direction.

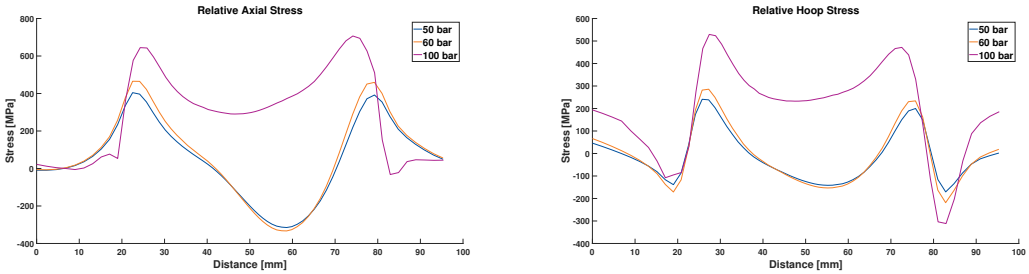

(a) Relative Axial Stress (b) Relative Hoop Stress

Figure 5.54: Relative Stress in Symmetry Cross-Section

This shows that the stress range behavior is similar for all test, with the low-pressure test having similar values and similar behavior as the high-pressure test.

Figure 5.55 and 5.56 shows the stresses going orthogonal out of the dent over the dent shoulder.

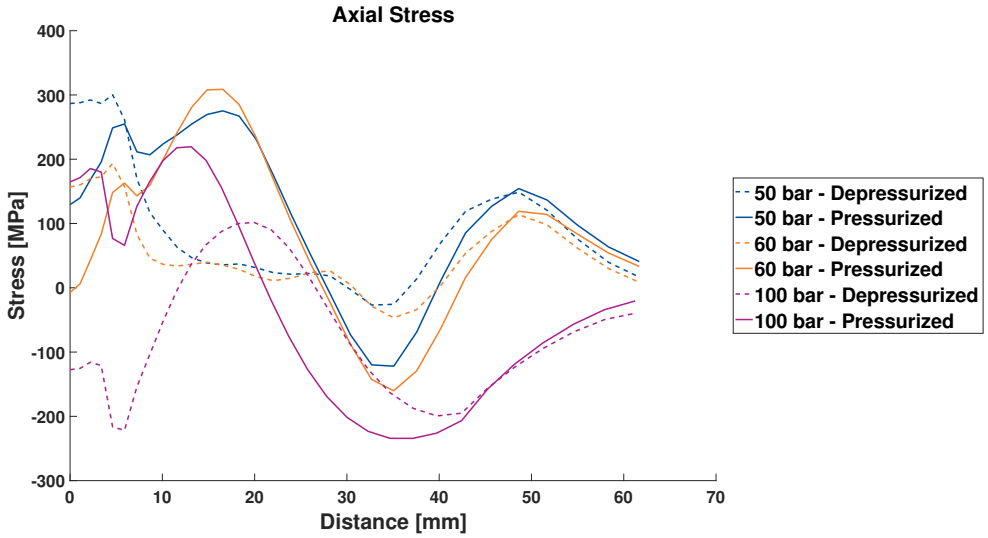

Figure 5.55: Axial Stress measured Orthogonal out of the Dent

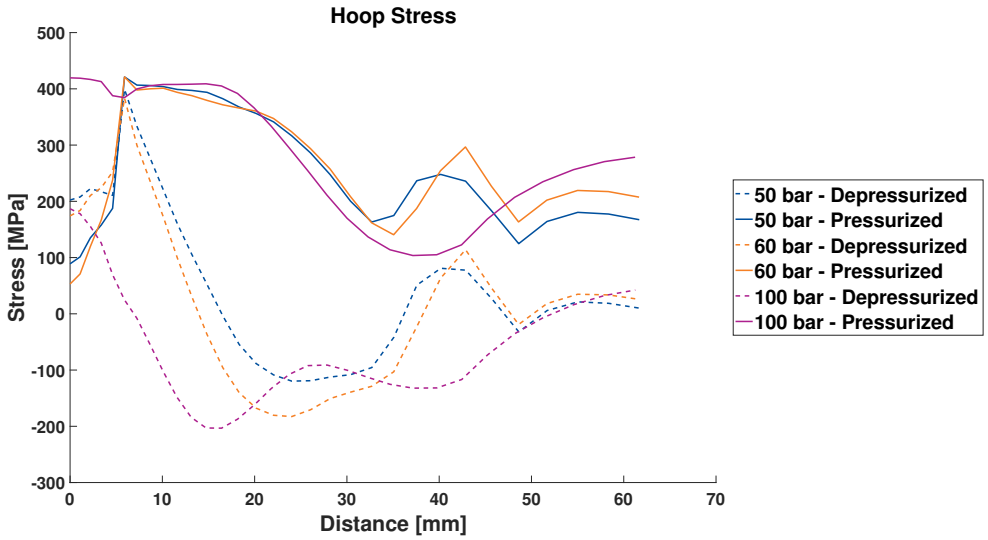

Figure 5.56: Hoop Stress measured Orthogonal out of the Dent

Although they have different values the stresses in the pressurized state behaves similarly for all the tests. The axial stress increases in tension before going into compression on the other side of the shoulder before increasing again. The hoop stress behaves similarly, but does not go into compression. The depressurized state is different for the high-pressure test and the low-pressure tests. The stresses for the low-pressure tests are larger approaching the dent shoulder and have a high hoop stress spike on the shoulder. This is probably because of the increased rerounding effect of the high pressure, and might explain why some of the low-pressure tests initiated cracks axially on the dent shoulder instead of at the dent entrance/exit. The high-pressure test does not experience such a hoop stress spike in the depressurized state.

As for the stress along the dent, figure 5.57a and 5.57b shows the relative stress going out of the dent.

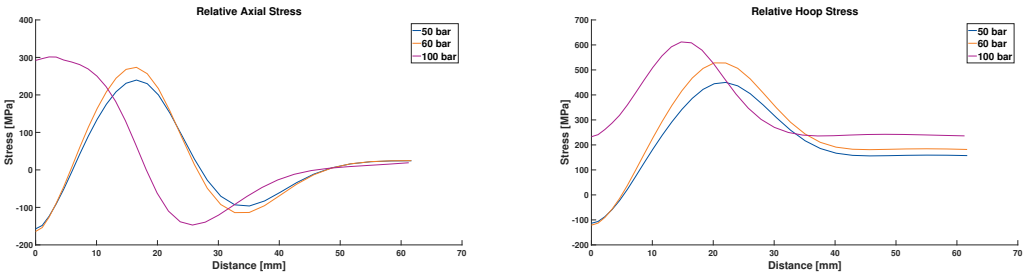

(a) Relative Axial Stress (b) Relative Hoop Stress

Figure 5.57: Relative Stress measured Orthogonal out of the Dent

Again, different values but similar behavior. The high-pressure test has its peak value closer to the dent center than the low-pressure tests.

Figure 5.58a and 5.58b shows the stress along the bottom path, while figure 5.59a and 5.59b shows the stress along the top path.

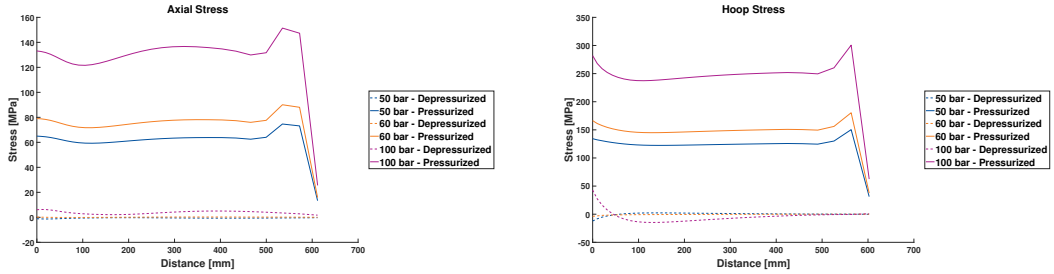

(a) Axial Stress (b) Hoop Stress

Figure 5.58: Stress measured along the Bottom Path out of the Dent

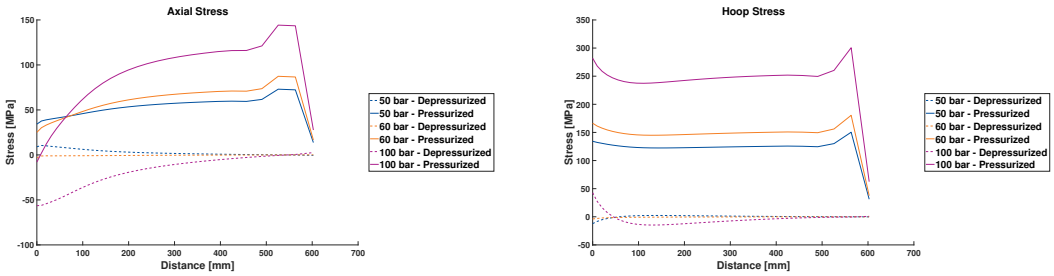

(a) Axial Stress (b) Hoop Stress

Figure 5.59: Stress measured along the Top Path out of the Dent

The bottom path shows that both stresses behave quite ordinary, with small interaction from the dent on the left and from the endcap on the right. The pressurized state gives stresses close to what is expected from analytic calculations, and the depressurized stresses are close to zero. The top path also behaves ordinary for the hoop stress, but have increasing axial stress longer down the path. For the high-pressure test the depressurized axial stress is compressive for the top path and in tension for the bottom path, while the low-pressure tests are close to zero. This indicates that there is a stress skewness for the high-pressure test.

5.4.6 Design without Endcap

A suggestion was made to design the fatigue test without the welded endcaps, but rather a removable elastic cap that could be a part of the rig itself instead of a part of the pipe.

The axial stress in the pipe would then be different from the values described in section 2.4. The effects of removing the endcap were investigated in *ABAQUS*. The analysis was made with an internal pressure of 100 bar. Figure 5.60a and 5.60b shows the strain along the bottom path, while figure 5.61a and 5.61b shows the strain along the top path.

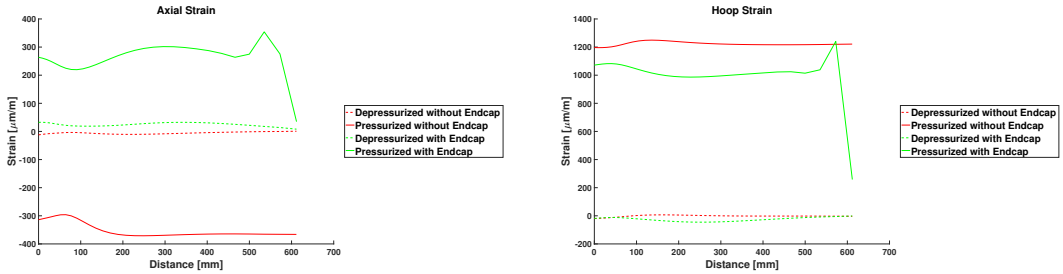

(a) Axial Strain (b) Hoop Strain

Figure 5.60: Strain measured along the Bottom Path out of the Dent without Endcap

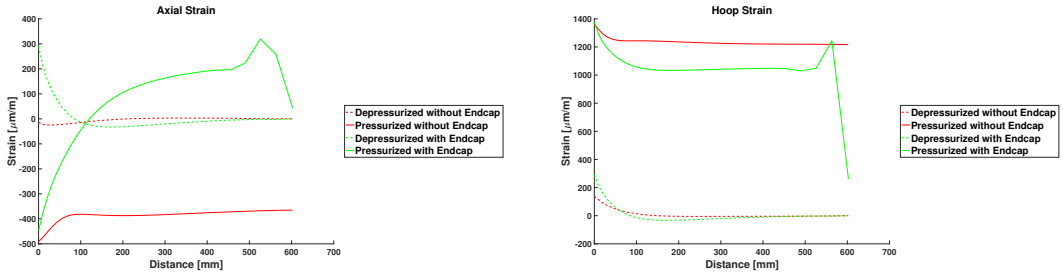

(a) Axial Strain (b) Hoop Strain

Figure 5.61: Strain measured along the Top Path out of the Dent without Endcap

Here, hoop strain is larger for the model without the endcap, and has strain increasing effects near the end of the pipe. The axial strain has a compressive value when pressurized. Both the pressurized and depressurized values approach a stable value more quickly than for a model with an endcap.

Figure 5.62a and 5.62b shows the stress along the bottom path, while figure 5.63a and 5.63b shows the stress along the top path.

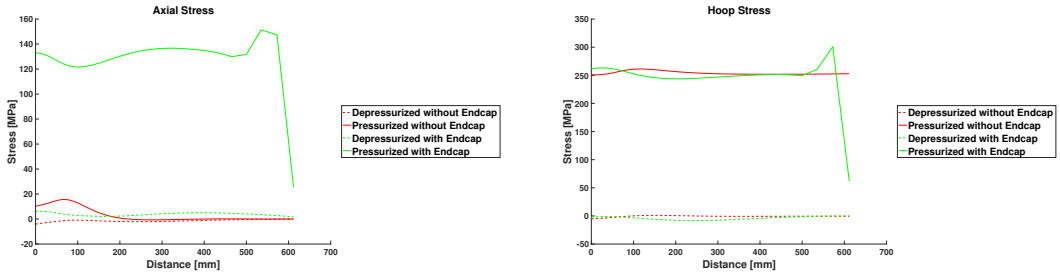

(a) Axial Stress (b) Hoop Stress

Figure 5.62: Stress measured along the Bottom Path out of the Dent without Endcap

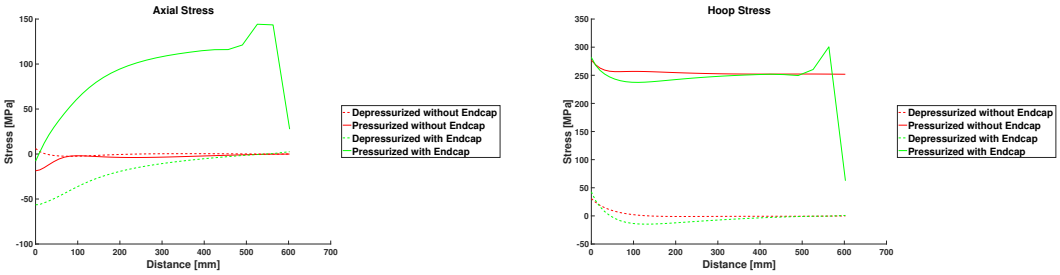

(a) Axial Stress (b) Hoop Stress

Figure 5.63: Stress measured along the Top Path out of the Dent without Endcap

The model without an endcap have no effects at the end of the pipe. The axial stress approaches zero stress for both states, while the hoop stress is close to the value with endcap. There will probably be some axial contribution from the elastic claps that replace the welded endcap, but these will most likely be small in comparison. The values level out faster for the model without the endcap.

Having no endcap contributions, and having the values stabilize quicker, means that the pipe could be made shorter for future tests. The only factor to consider would be the effects from the dent itself which have some contribution at the left of the plots for the model without endcap. The pipe length could be at least reduced by a 50 % value, which will save material cost and weight (a pipe full of oil weighs a lot!). The new model with removable elastic claps also have the potential to save time, since the previous method have tedious rigging work.

5.4.7 Dent Geometry

There is also interesting to see how the pressure influences the pipe geometry. This will also give the numerical values for the rerounding effect caused by the pressure. Figure 5.64 shows the effect of the pressure along the dent.

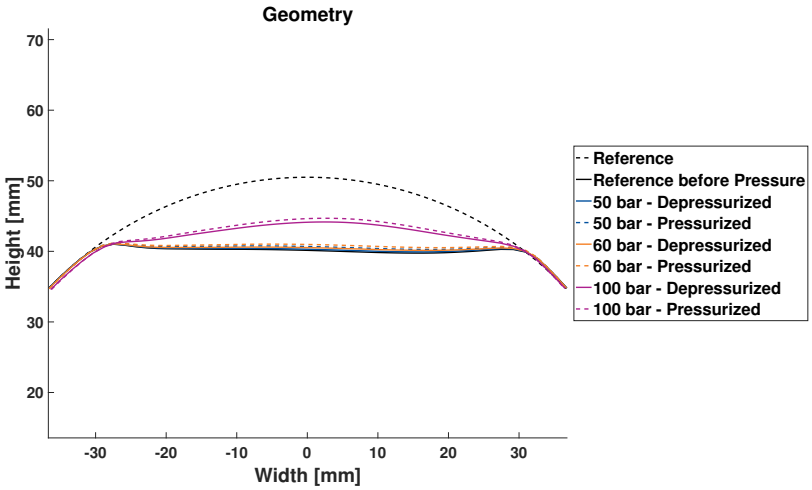

Figure 5.64: Geometry Change due to Pressure in the Symmetry Cross-Section

This figure shows that there is a significant rerounding effect from the pressure, seen when the pressure is removed again. The interesting part is that the two low-pressure tests are very similar, while the high-pressure test has a much larger effect. It is clear, also seen from the other pressure plots, that the high-pressure test has severe plastic effects during the pressurization. Figure 5.65 shows the geometry going out of the dent.

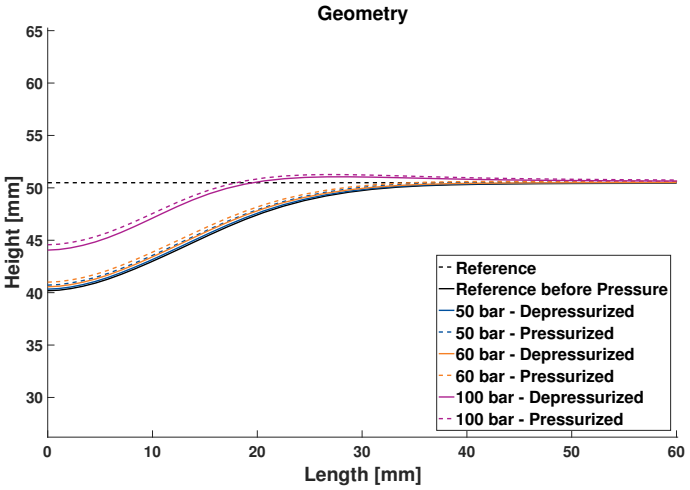

Figure 5.65: Geometry Change due to Pressure out of the Dent

This plot shows the same tendencies as the one from the cross-section. The high-pressure test rerounds the dent more than the two low-pressure tests. This gives dent geometry as in table 5.8. The geometry is for the pipe before pressure, and the geometry for the pipe

after the pressure is removed. The values are taken from the point where the orthogonal path meats the symmetry cross-section path.

Table 5.8: Dent Geometry from *ABAQUS*

Pressure [bar]	Depth [mm]	Length [mm]	Width [mm]
None	10.31	45.8	56.7
50	10.15	42.0	56.7
60	9.93	38.1	56.6
100	6.43	26.1	56.2

This makes the rerounding value 0.16 mm, 0.38 mm an 3.88 mm for increasing pressure. There is a large jump from the low-pressure tests to the high-pressure test, which is due to the increased plastic effects. The half-length is found for when the low-pressure tests are 0.1 mm from the unaffected pipe, since they never actually intersects with the original pipe line for this path. The width was determined the same way as for the 3D-model, and changes very little for different pressure. The high-pressure test has a more curved profile than the others, so the width was harder to determine for that test.

5.5 Results from X-Ray Scan

The x-ray stress scanner was used to take measurements on some specific tests. The tests chosen were test 1, 2, 8 and 9; one high-pressure and one low-pressure with and without a gouge. There are ten points chosen for each test to coincide with the strained gages and the measured paths from *ABAQUS*. The ten points can be seen in figure 5.66.

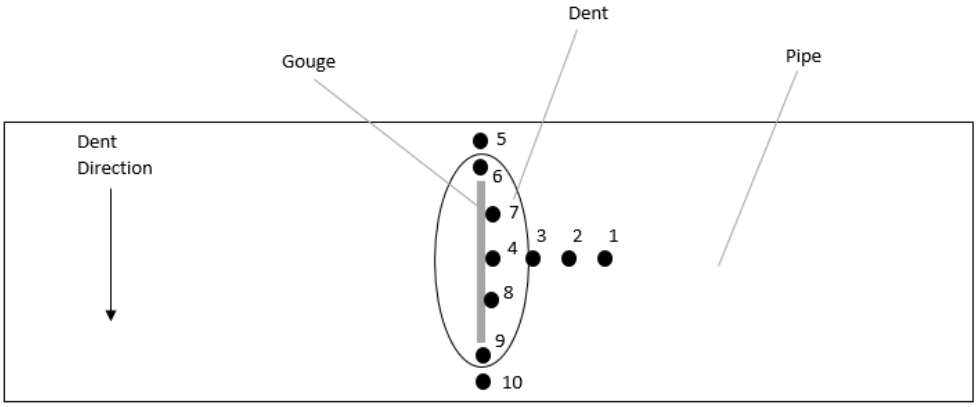

Figure 5.66: Points for X-Ray Measurements

Figure 5.67a and 5.67b shows the axial and hoop stress for test 1 and 8 going out of the dent (points 4, 3, 2, 1), and figure 5.68a and 5.68b shows the results for test 2 and 9.

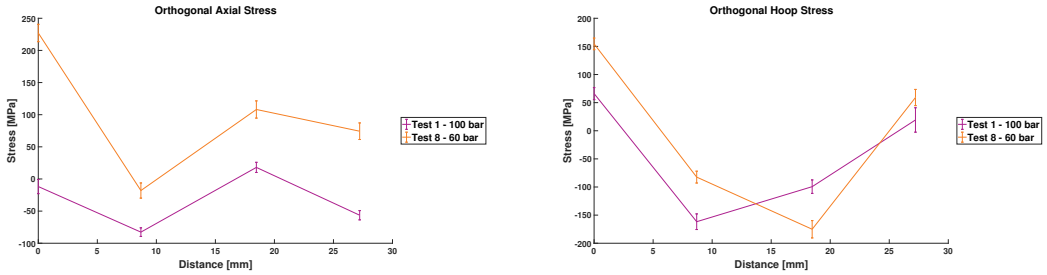

(a) Axial Stress (b) Hoop Stress

Figure 5.67: Stress from X-Ray measured out of the Dent for Test 1 and 8

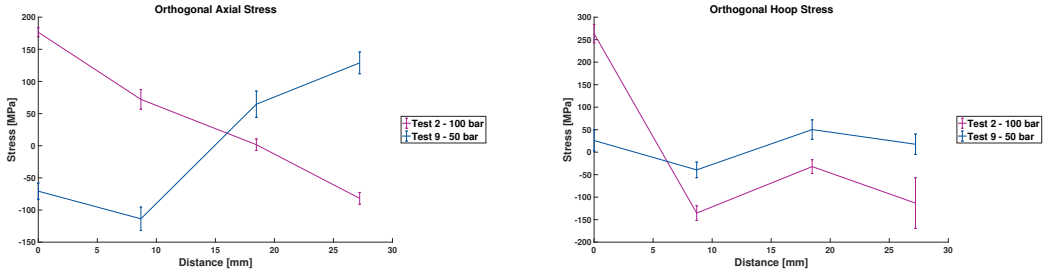

(a) Axial Stress (b) Hoop Stress

Figure 5.68: Stress from X-Ray measured out of the Dent for Test 2 and 9

The data from the test 1 and 8 without gouge shows that the residual stress is generally larger for the low-pressure test than for the high-pressure test. This is not the case for the measurement in hoop at point 2, but both test have similar behavior in both stress directions. The result is also consistent with the stress in the depressurized state from *ABAQUS*, where the low-pressure tests had larger stress values than the high-pressure test measuring out of the dent. The curves from test 2 and 9 follow the same general behavior as for test 1 and 8 except for the axial stress for test 2. This stress has a very large value compared with the other tests at the bottom of the dent, and decreases away from the dent, while the data from test 9 increases. For the hoop stress the tests generally have the same behavior, but the hoop stress is also very large for test 2.

The axial and hoop stress measured along the dent can be seen in figure 5.69a and 5.69b for test 1 and 8, and figure 5.70a and 5.70b for test 2 and 9.

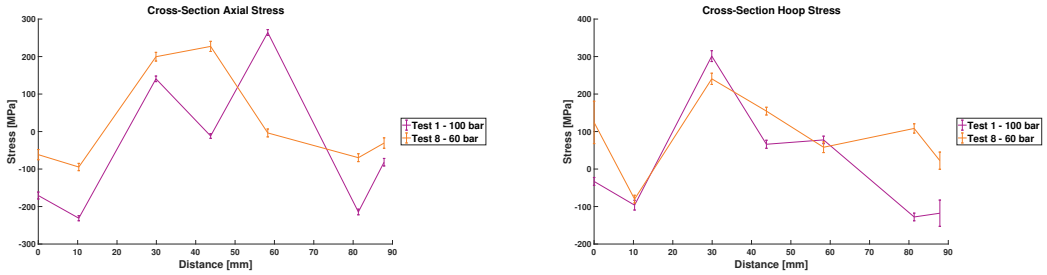

(a) Axial Stress (b) Hoop Stress

Figure 5.69: Stress from X-Ray measured along the Dent for Test 1 and 8

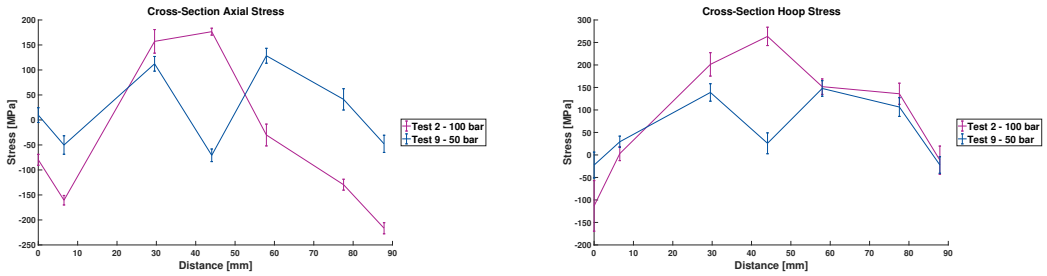

(a) Axial Stress (b) Hoop Stress

Figure 5.70: Stress from X-Ray measured along the Dent for Test 2 and 9

The behavior is generally similar for test 1 and 8 with compressive stress around the entrance/exit of the dent and large tension values in the middle, with some difference in the stress values. There is a larger difference between the results from test 2 and 9, especially near the middle of the dent.

5.6 Compared Results

The following section seeks to compare some of the results found above in figures and tables for easier reference.

5.6.1 Strain Comparison

First, the strain measurements from the strain gages are compared with the values found from the numerical analysis. Table 5.9 and 5.10 shows the relative strain values for test 1, 2 and 3 for all gages. These tests were run at a maximum pressure of 100 bar. The table shows the strain as the strain value at maximum pressure minus the value at minimum

pressure. The *ABAQUS* data was plotted in section 5.4, while the strain gage values can be implicitly found from the figures in the appendix. All values are given in $\mu m/m$.

Table 5.9: Axial Strain Comparison between Numerical and Experimental Results, 100 bar.

Test	Gage 1	Gage 2	Gage 3	Gage 4	Gage 5
1	2100-2250	3050-3300	750-1200	500-1600	4000-5000
2	2700-3500	3700-Broken	770-820	3000-Broken	1280-1370
3	1200-1300	3300-3500	750-950	3200-4400	1950-2500
ABAQUS	1400-2700	1850-2700	1000-1100	2400-2700	1900-2700

Table 5.10: Hoop Strain Comparison between Numerical and Experimental Results, 100 bar.

Test	Gage 1	Gage 2	Gage 3	Gage 4	Gage 5
1	-1900-2000	1500-1600	1150-1350	Broken	250-600
2	-500-2100	1200-Broken	1950-2150	650-800	-1500-2000
3	-1600-1800	480-530	1350-1550	1280-1340	-500-2200
ABAQUS	-700-1100	1300-1700	700-950	1000-1300	-300-2000

Both the *ABAQUS* and the gage results are given in a range. The *ABAQUS'* result range are due comparison issues, because of the uncertainty in the exact placement of the gage. The areas in question have large differences in stress and strain in small areas. The range of the gage is due to the actual change in relative strain during the test. Especially the high-pressure tests have strain values that explode as the pipe goes to failure. Some of the values have very strange behavior, and are therefore set as broken. The *ABAQUS* relative strain use values from a completely depressurized state, while the minimum strain for the strain gages are at 10 bar, which will make a difference. The values from the numerical tests and the experimental tests are generally similar, but have strange values for some gages. The ranges are also very large in some cases.

Similar tables can be seen for test 7 and 8 at 60 bar seen in table 5.11 and 5.12.

Table 5.11: Axial Strain Comparison between Numerical and Experimental Results, 60 bar.

Test	Gage 1	Gage 2	Gage 3	Gage 4	Gage 5
7	1220-1650	2350-Broken	370-460	1900-2450	2250-2300
8	1600-1650	1490-1560	540-580	1640-1710	1150-1170
ABAQUS	1500-2000	1600-2000	-400-600	1500-2000	1700-2200

Table 5.12: Hoop Strain Comparison between Numerical and Experimental Results, 60 bar.

Test	Gage 1	Gage 2	Gage 3	Gage 4	Gage 5
7	-710-980	720-920	590-630	700-750	-810-890
8	-1040-1120	935-940	1530-1650	850-930	-1160-1300
ABAQUS	-600-900	300-700	-300-400	600-800	-700-1400

The ranges become smaller for these tests with lower pressure, since most of the gages have stable values during the entire life, with some exceptions. There are still some change in the strain-range during the test. The range in *ABAQUS* still needs to be large, since there are large differences in only small steps along the dent. The values generally lie close to or within the data from the numerical tests. One large difference is the fact that the numerical solver gets negative values for the low-pressure tests in the middle of the dent, while the strain gages gets positive values. There is also a difference between the two tests, where test 8 has larger values of hoop strain for all gages, while having smaller axial strain for some of the gages.

The strains for test 9 can be seen in table 5.13 and 5.14.

Table 5.13: Axial Strain Comparison between Numerical and Experimental Results, 50 bar.

Test	Gage 1	Gage 2	Gage 3	Gage 4	Gage 5
9	570-610	1500-1600	380-440	1900-1960	850-870
ABAQUS	900-1400	1100-1400	-400-600	1200-1600	1100-1400

Table 5.14: Hoop Strain Comparison between Numerical and Experimental Results, 50 bar.

Test	Gage 1	Gage 2	Gage 3	Gage 4	Gage 5
9	-680-700	720-730	810-830	280-310	-710-720
ABAQUS	-500-800	300-600	-250-350	500-700	-550-1200

The ranges for the strain gage is even smaller for this test. Strain gage 3 is still in compression in the *ABAQUS* result compared with the strain gage result. It is difficult to determine how well these two data sets compare. They seem to be generally close, but almost never the same.

The values for the gages in all tables are close to the numerical values, but rarely within the range itself. There are several difference from the real dent to the numerical dent,

and a direct comparison between them is difficult. This in comparison with differences in the gages and small changes that occurred, makes comparison more difficult.

5.6.2 Geometry

Here, the dent geometry is compared for the values from the 3D-models and the numerical model. The dent geometry is compared in table 5.15.

Table 5.15: Comparison of Dent Geometry between 3D-Model and Numerical Model

Test:	Scan:	Depth [mm]	Length [mm]	Width [mm]
3	First	7.73	36.97	49.06
	Second	5.19	24.82	48.69
ABAQUS, 100 bar	First	10.31	45.8	56.7
	Second	6.43	26.1	56.2
8	First	7.67	35.73	50.30
	Second	6.36	27.87	45.79
ABAQUS, 60 bar	First	10.31	45.8	56.7
	Second	9.93	38.1	56.6

The main thing to see here is the fact that the initial depth of the numerical simulation is deeper than that of the 3D-model. There could be several reasons for that. First, it is the accuracy of the 3D-model, as mentioned in section 5.1.3. The path of the indenter is not completely straight when creating the dent for the experiments. The opening is larger than the indenter, so the indenter follows the curvature of the pipe when it passes through, which could cause this difference, since the numerical indenter path is straight. It could also be that the numerical model is conservative in the response of the pipe when interacting with the indenter, causing a more severe response.

The differences in half-length and width are probably due to the same reasons.

5.6.3 Rerounding

Here, the LVDT-data for the tests are compared with the permanent change in the depressurized state from *ABAQUS*. Note that only the initial static pressure test is used from the experimental tests, since the continued rerounding of the dent from the dynamic pressure part is substantial, especially for the high-pressure tests. The tables are numbered as table 5.16 and 5.17 and all displacements are in mm.

Table 5.16: Comparison of Static Rerounding between Numerical and Experimental Results, 100 bar

Test:	2	3	*ABAQUS*, 100 bar
Displacement	0.575	0.605	3.877

Table 5.17: Comparison of Static Rerounding between Numerical and Experimental Results, 60 bar and 50 bar.

Test:	7	8	*ABAQUS*, 60 bar	9	*ABAQUS*, 50 bar
Displacement	0.446	0.424	0.377	0.388	0.153

For the two low-pressure tests the numerical values underestimates the actual rerounding caused by the pressure. The rerounding is similar for the tests with the same pressure. Another striking thing is that the numerical calculation horribly overestimates the rerounding at high pressure, seen here as the difference between test 2 and 3 compared to the 100 bar result. The total rerounding of test 2, as an example, is 2.499 mm after almost 20 000 cycles at a $10 - 100$ bar cyclic internal pressure. Even this value is far from the numerical value. This indicates that the material properties used in *ABAQUS* does not reflect the real behavior correctly. The rerounding from the 3D-model is 2.54 mm for test 3 (100 bar), and 1.31 mm for test 8. These values are neither close to the LVDT-values nor the *ABAQUS* values. The elastic strength is probably overestimated in *ABAQUS*, while the plastic strength and hardening effects are probably underestimated. This can be seen in the values used in *ABAQUS* in table 4.2, compared to the ones found from the pipes after the fatigue tests in table 5.7. *ABAQUS* use a slightly larger Young's modulus with 207 GPa compared to an average of 202.7 GPa for the tests. The yield strength is lower with 289.15 MPa compared to an average of 309.5 MPa. Finally, the ultimate tensile strength is also lower with 399.49 MPa compared to an average of 439.4 MPa.

From figure 5.64, it should be noted that the rerounding value for the numerical simulation changes for where the measurement is made. Especially for the high-pressure test, which varies a lot. It could vary around 0.15 mm around the area where the LVDT was placed. The LVDT placement could also vary for each test.

5.6.4 Nominal Strain and Stress Comparison

Here, the nominal strain and stress for the tests which had a reference gage are compared with the values from *ABAQUS*. The strains can be seen in table 5.18 and 5.19, and the stress in table 5.20 and 5.21.

Table 5.18: Comparison of Reference Axial Strain between Numerical and Experimental Results

Test:	1	2	*ABAQUS,* 100 bar	9	*ABAQUS,* 50 bar
Reference, Strain:	240	232	184	Broken	91

Table 5.19: Comparison of Reference Hoop Strain between Numerical and Experimental Results

Test:	1	2	*ABAQUS,* 100 bar	9	*ABAQUS,* 50 bar
Reference, Strain:	980	975	1062	488	514

Table 5.20: Comparison of Reference Axial Stress between Numerical and Experimental Results

Test:	1	2	*ABAQUS,* 100 bar	9	*ABAQUS,* 50 bar
Reference, Stress:	122	121	119	Broken	55

Table 5.21: Comparison of Reference Hoop Stress between Numerical and Experimental Results

Test:	1	2	*ABAQUS,* 100 bar	9	*ABAQUS,* 50 bar
Reference, Stress:	244	241	255	Broken	123

For some reason, the axial strain gage measurement for test 9 corrupted somewhere, and did not register any values, so both strain and stress are invalid. The strains and stresses for the two high-pressure tests are similar for all values. The numerical axial values are lower while the hoop values are higher. This is also the case for the low-pressure test in hoop. The stresses for test 1 and 2 have twice as large hoop stress as axial stress, as expected from section 2.4.

5.6.5 Stress Comparison

Due to difficulties in the stress calculation from the strain gages, the numerical stress values are primarily compared with the x-ray data. The points in the tables are the same as for figure 5.66. Table 5.22 and 5.24 shows the axial and hoop stress for test 1 and 2, while table 5.23 and 5.25 shows them for test 8 and 9. All stresses have units in *MPa*.

Table 5.22: Axial Stress Comparison between Numerical Result and X-Ray Scan, 100 bar.

Test/ Point	1	2	*ABAQUS,* 100 bar
1	-56.4±7.2	-81.9±9.2	-15
2	18±7.9	1.6±9	100
3	-82.7±6.7	72.1±15.3	-102
4	-11.8±11	176.6±6.9	-128
5	-170.6±9.2	-216.6±11.1	-221
6	-231.1±6.8	-129.5±10.9	-230
7	140.6±7.4	-30.1±21.8	-94
8	264.1±7.8	157.2±23.6	-164
9	-214.5±7.5	-160.5±9.5	-368
10	-81.7±10	-79.7±10.9	-230

Table 5.23: Axial Stress Comparison between Numerical Result and X-Ray Scan, 60 bar and 50 bar.

Test/ Point	8	*ABAQUS,* 60 bar	9	*ABAQUS,* 50 bar
1	74.3±12.9	25	128.9±16.8	20
2	108.1±13.4	28	64.6±20.4	37
3	-18±11.8	46	-113.7±18.2	116
4	227.1±13.5	183	-70.7±12.6	303
5	-61.6±13.6	-58	9.7±14.8	37
6	-94.6±9.7	-43	-50.1±18.5	12
7	199.6±11.6	311	112.3±14.7	345
8	-3.7±10.5	-85	128.4±14.9	104
9	-69.7±10.5	-110	41.2±21.3	-8
10	-30.7±13.9	-57	-47.8±17.2	3

Table 5.24: Hoop Stress Comparison between Numerical Result and X-Ray Scan, 100 bar.

Test/ Point	1	2	*ABAQUS,* 100 bar
1	19.2±21.7	-113.2±56.2	-91
2	-99.4±12	-32.1±15.3	-183
3	-161.7±13.9	-135.4±16.3	-55
4	66.1±10.7	263.5±20.4	187
5	-33±10.5	-11.6±31.3	123
6	-96.3±13	136±23.5	52
7	301.2±14.5	151.8±17.2	132
8	77.7±10	201.3±26	160
9	-127.8±10.2	3±15.6	-80
10	-117.8±35	-113.2±56.2	7

Table 5.25: Hoop Stress Comparison between Numerical Result and X-Ray Scan, 60 bar and 50 bar.

Test/ Point	8	*ABAQUS,* 60 bar	9	*ABAQUS,* 50 bar
1	59.1±14.4	-160	17.6±22.6	-115
2	-175.1±15.4	-142	50.2±21.7	-57
3	-82.4±10.5	231	-39.4±17.3	274
4	154.5±10.3	195	25.9±23.2	221
5	124.4±56.5	-96	-22.5±28.8	1
6	-80.2±10.3	52	29.3±12.5	124
7	240.6±15	196	138.9±19.4	192
8	58.1±14.2	16	147.8±17.3	84
9	108.3±12.4	50	106.5±20.8	-19
10	22.3±22.9	128	-22.3±18.4	174

It can be seen that the x-ray values are somewhat close to the *ABAQUS* values, with differences between the tests with the same pressure. To easier see the comparison the values are put in figures similar to the ones in section 5.4 and 5.5. The axial and hoop stress along the dent can be seen in figure 5.71 and 5.72, while the stress out of the dent can be seen in figure 5.73 and 5.74. The tests with the same pressure have the same color.

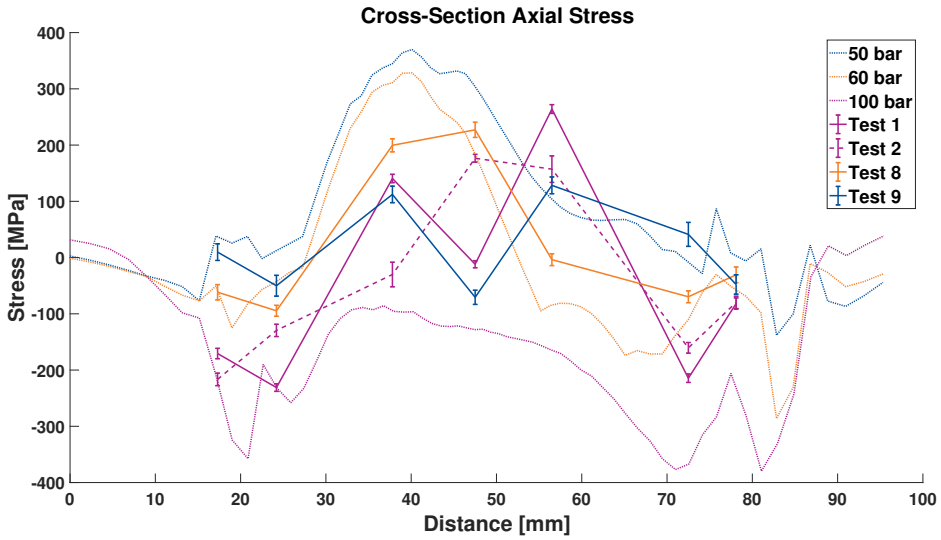

Figure 5.71: Axial Stress along the Dent from Numerical Results and X-Ray Scan

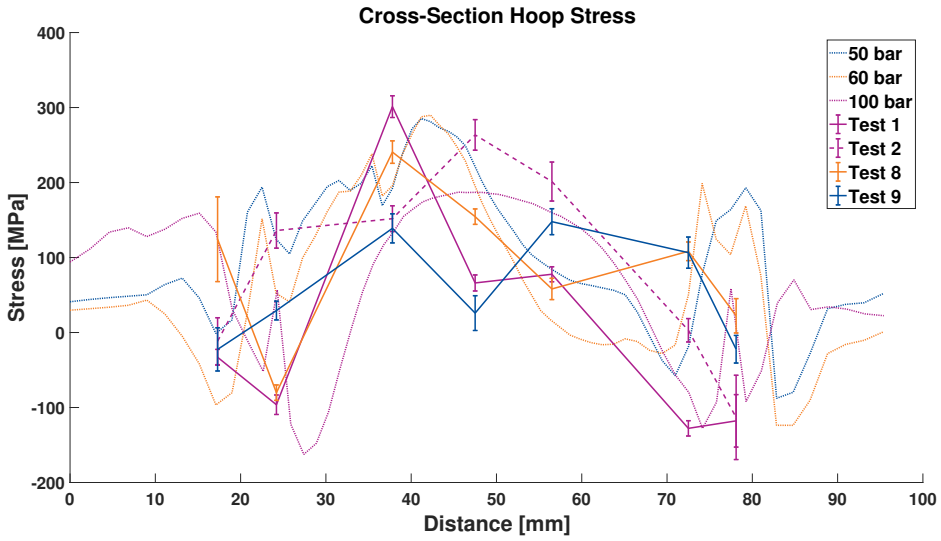

Figure 5.72: Hoop Stress along the Dent from Numerical Results and X-Ray Scan

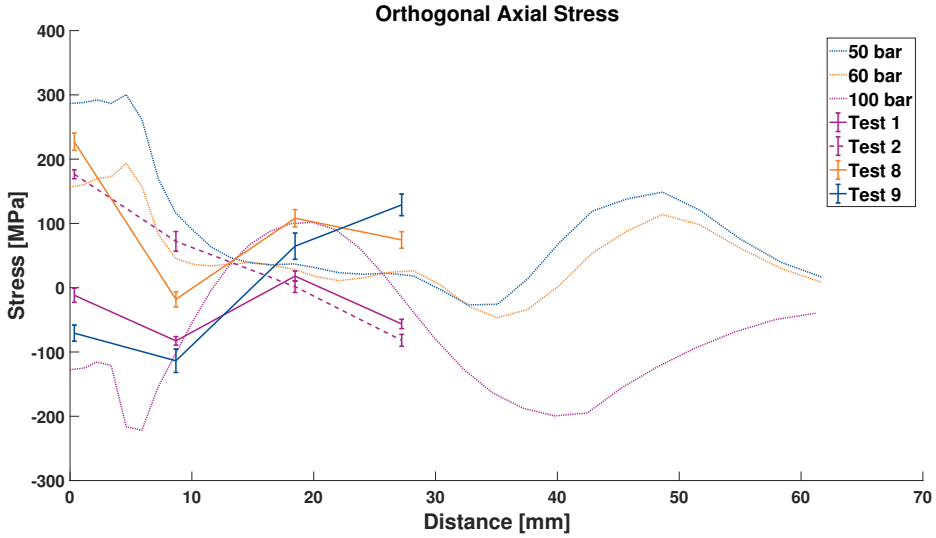

Figure 5.73: Axial Stress out of the Dent from Numerical Results and X-Ray Scan

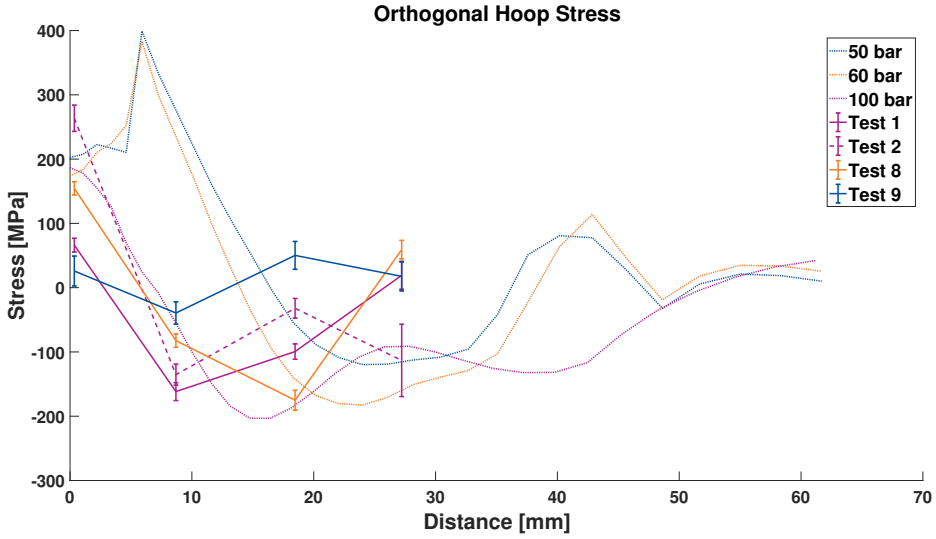

Figure 5.74: Hoop Stress along the Dent from Numerical Results and X-Ray Scan

There are both similarities and differences in the results. The differences could be due to slight variations in where the x-ray scan was performed in the dent. The points are placed on the same grid for all tests, but the dent geometry could be slightly different for the tests. The rerounding is different for the tests, which could affect the diffraction angles for some of the scans compared with the others. The rerounding of the high-pressure test is much larger than in reality, so this will give differences in these results.

The two low-pressure tests have similar geometry as the numerical result, and should have a better fit. The 60 bar test follows the x-ray test well, while the 50 bar test are more different.

Chapter 6

Discussion

There are a lot of things worth discussing in this thesis. Many experimental and numerical tests were performed, and many different methods were used to study and assess the tests. There are a difference in geometry and material properties from numerical to experimental results, as well as variations between the tests themselves.

6.1 Indentation

The dent in figure 4.4a and 4.4b seems to become wider at the indenter exit compared to the entrance. The indenter is a little bit smaller than the hole it passes through, so upon first contact the indenter will be pressed upwards and follow the pipe curvature somewhat. The indenter is then pushed down as it passes the midpoint of the pipe, seen as the widening of the dent at the exit. The numerical analysis uses an indenter that follows a completely straight path, so there will be a difference in the geometry from this. Some contraption installed to the rig could force the indenter to move completely straight, but this requires some redesign and were therefore neglected from this thesis.

At the exit, there is also remnants of excess material that has been dragged by the indenter, due to friction forces from contact between the steel. The excess material can be seen in figure 6.1a and 6.1b for sharp and blunt indenter. The blunt indenter type had worse material dragging than the sharp indenter.

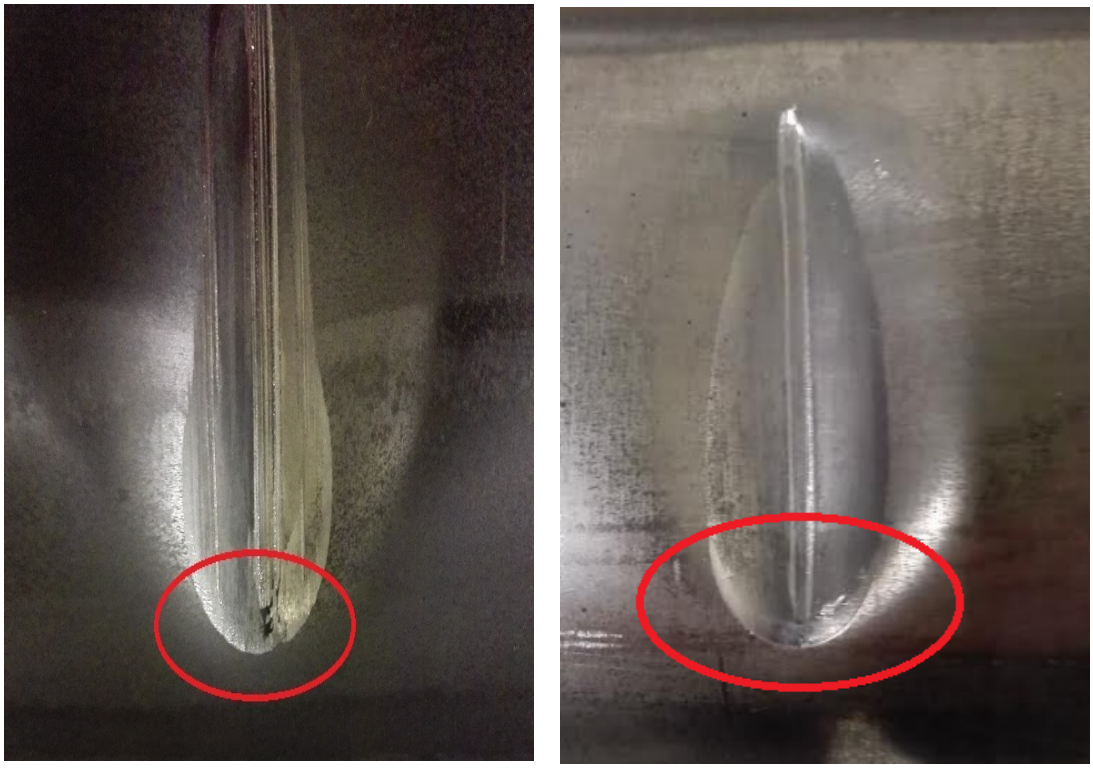

(a)
Sharp Indenter

(b)
Blunt Indenter

Figure 6.1: Excess Material Comparison

This edge will surely have an effect in this region of the dent, changing the material behavior and strength. Grease was added on all tests after test 2 to reduce the friction, and the material dragging was reduced as a result of that. A concern when adding grease was that the indenter could rotate during indentation due to reduced friction, but this was not observed in any tests.

There are small imperfections in the gouged dent along the sides from where the indenter was in contact with the pipe. This could be due to the fact that the same indenter model was used for both experiments, wearing and tearing and introducing small imperfections in the indenter when rotating it for different analysis. The importance of these imperfections is uncertain, but preferably two different indenters of the same type could be used. One creating a plain dent, and one creating a gouged dent.

6.2 Pipe Failure and Crack Location

As mentioned in section 5.1, there were several challenges connected to finding out the actual moment the crack broke through the pipe thickness, and finding the crack itself afterwards. The best way of detecting the crack was to actually be present when the crack appears. The leak from the pipe could be violent in some cases, spilling a lot of oil in a short amount of time. Other times it was more subtle and hidden, but was still visible as a slow pour out of the crack. Most times, however, the pipe failed during the afternoon or when nobody was present. The pump supplying pressure had a limit of how low it could move before it would automatically stop. This meant that soon after the leak appeared, enough liquid had left the pipe for this limit to be triggered. This gave the total number of cycles before failure. This number did not represent the number of cycles before through-crack appeared, however. That moment was found by looking at the development of the internal leak from the pump, and looking for the moment this leak accelerated rapidly. But not all tests failed rapidly, some had small leaks which were harder to find using this method. This means that the values in table 5.1 are approximate, but are chosen conservatively when in doubt.

Another problem is to find the actual crack after it appeared. The simplest way to find the general location is to look for the location of leaking oil, but if the leak had been pouring for a while, the oil spill would often be severe. It was still relatively easy to spot the crack when the strain gages were removed. A method tried in this thesis was to spot the leaking crack using a UV-light with some fluorescent liquid in the oil. This proved very effective in spotting the leaking oil. It was only tried for one test, but could be a nice addition to a future rig. Another method was to use a microscope to determine the size, shape and location of the crack. If the general location was known, the crack would be easily visible in the microscope. For the cracks coming out of the gouge, the microscope images were essential for finding them. Unfortunately, the microscope sessions take a long time and are expensive, since it in this case require a technician to operate. It could not be used in larger scale than for verifying one or two tests.

6.3 Pipe Geometry

The pipe geometry used for both numerical and experimental tests was initially as the values in table 4.1, with a diameter of 100 mm and thickness of 2 mm. On closer inspection, the thickness was measured as seen in section 5.3 in table 5.6, with a decreased thickness. These values were measured after the pressure tests. If the changing thickness is different from the numerical to the experimental results it would lead to different values. As an example, if the equation for hoop stress for a thin walled pipe from section 2.4 is used with an internal pressure of 100 bar and no external pressure, the result with original geometry will give a stress of 250 MPa. With new geometry the answer becomes 268.8 MPa for a thickness of 1.83 mm and outer diameter of 100.2 mm. This is

an increase of 7.5 %. It was to time-consuming to check the wall-thinning behavior of the numerical results, since it was discovered at a late stage. Future experimental tests should measure the geometry of the pipe before and after testing to look at the wall-thinning behavior. It is not absolutely certain that the pipes actually had a thickness of 2 mm at the beginning, but the batch was measured prior to pipe manufacture, and afterwards, so it should be correct. The wall-thinning could also be the reason for larger observed nominal values than what is expected from analytical calculations.

6.4 Stress Concentration Factor

Values of the SCF are found from the theoretical equation in section 2.6 (equation 2.26), based on values found using the numerical results. In table 6.1 the numerical SCF are compared to the ones found using the method developed by PETROBRAS. This empirical method has the largest relevance for this project, since it had the best correlation, works for tests up to and above 10^5 cycles, and can be used on pressurized pipes. The calculations used by PETROBRAS uses von Mises stress, so the nominal stress in the numerical results need to be calculated as in section 2.4, with von Mises stress for a thin walled pipe. The nominal stress is calculated using the original pipe geometry. The depth in equation 3.9 is taken as the depth after pressurization from the numerical analysis, while the coefficients are the ones for a transverse dent. Table 6.1 shows the stress values together with the SCF for the different pressures and corresponding depths.

Table 6.1: Stress Concentration Factors

Test [bar]:	Nominal Stress [MPa]:	Maximum Top [MPa]:	Maximum Bottom [MPa]:	Max SCF:	PETROBRAS SCF:
100	216.5	618.3	734.5	3.4	6.9
60	129.9	599.2	499.0	4.6	9.4
50	108.3	518.0	399.2	4.8	9.6

There are several interesting things to discuss in this table. All the maximum values found in the top of the element are found on the dent shoulder, while the bottom values are found around the entrance and exit of the dent. This gives the high-pressure test its largest SCF at the exit/entrance, while the low-pressure tests have it on the shoulder of the dent. This is consistent with the location of failure for both test types found from the experiments.

The SCF is increasing with decreasing pressure. This is because the dent depth is decreasing with increasing rerounding behavior. This shows that it could be a good idea to use pressured rerounding as a way of decreasing the severity of dents in pipelines. As the final test indicates, the fatigue life greatly increased when the initial pressure

was increased. This decreased the dent depth, which have decreased the critical stress concentrations. More tests should be done to find more details about the effect. The one test done was merely to get an idea of the effect. Tests should also include the gouge, which could affect the rerounding behavior.

As seen in the table, the SCF are much larger for PETROBRAS than those found by the numerical values. Almost consistently twice as large for all depths. There could be several reasons for this. The thin walled pipe used in this project is expected to be more impacted by the dent according to PETROBRAS, than it actually is. The method used by PETROBRAS, and other similar methods, are used because it is easy to find the geometry of interest, and therefore easy to get an assessment. This might not be applicable for a geometry like the one in this project. There are often safety factors involved in these methods, which makes them more conservative.

6.5 Difference in Result

There are several differences in the results between the different methods of observation, but also within the same type of observation. There are, for instance, large variation in the results from the strain gages from test to test, where the difference can seem inconsistent. There are several things that could lead to this unwanted difference in result, with some reasons mentioned in section 5.1 and 5.2. The gage size used, and the location of the gage, could differ from test to test. The placement of the gage was determined from the relative shape of the dent and placed accordingly. When the larger gage sizes was used, gage placement 1/2 and 4/5 were too close to each other, and had to be placed a little further apart than for the smaller gage sizes. Even for the gages of the same size the placements would not be identical to each other. The gage also calculates an average over its area, so a larger gage would get smoother strain values than a smaller gage. Seeing the sharp stress peaks from the numerical analysis, the smaller gage would be more influenced by the peak than the larger gage. The different tests failed in different areas and the gages were affected by the growing crack, especially if the crack grew right beneath the gage. It was worse for the tests with higher pressure, where more gage values suddenly exploded violently. According to [MM08] plastic effects in the area of the gage will affect the measurements, and these effects are stronger for the high-pressure tests.

The gouge geometry changed during the testing, becoming wider and shallower. This indicates that the indenter has had wear during the tests. Another possible explanation is that the difference in rerounding between the two tests created this difference. Then the gouge of test 2 should be wider, since this was pushed out the most. Table 5.4 shows that it is the low-pressure test that has the widest gouge. Ideally, the gouge geometry should stay unchanged during the tests to reduce uncertainty of its impact on the result.

The rerounding result shows that there is a difference between the numerical result and

the experimental result. The numerical result indicates that the elastic strength is too high, while the plastic strength and hardening is too low. This is because the rerounding for the high-pressure test is higher than the observed value, while the low-pressure test is lower. The difference in material properties is an obvious reason for difference between the numerical analysis and the experimental results. In retrospect, the material should have been tested prior to the numerical analysis. This was not done in this case because of time-constraints. Both the numerical analysis and the stress-conversion from the strain gages used standard steel values. Knowing the exact material properties will hopefully make the two methods more comparable.

The material properties found in this thesis have uncertainty. The samples curved after they were taken out because of the residual stress, and testing was difficult since the samples were not completely straight. The work done on the strips before the test likely altered the properties somewhat. The material would have had some hardening effects from the fatigue tests which affect the resulting properties. Ideally, one test of the material patch should be tested before the fatigue test and one afterwards. There are severe plastic effects around the dent. The stress-conversion used in the project assumes elastic conditions. This makes the resulting stress essentially incorrect. Future tests should use other methods for stress calculation in the fatigue part, like Neuber's equation discussed briefly in section 2.11.

The x-ray data produced difference in the result between tests that had similar conditions. There are possible reasons for this difference. It was difficult to remove all the glue and tape rests from the gages when the measurements were made. According to [Fit+05], a layer of glue, tape, coating or similar could change the x-ray diffraction. Test 2 had a layer of spray-paint on some of the points going out of the dent, which could have an influence on the measurements. The problem with coating is primarily if it has any material properties itself, so this should not be a huge problem, but it could obscure the diffraction. The removal of the strain gages provides some work to the material which could change the residual stress in the top layer of the material. This could also lead to unnecessary errors. It could explain the sudden change in some values in the figures, where most of the points follow the numerical solution and suddenly one point falls way off. The points measured could also be at different locations in the dent. Even though the placement was measured, it used the local geometry as reference, and this could vary between the tests due to rerounding.

6.6 Design without Endcap

The numerical simulation indicates that a design without a welded endcap will reduce the axial contribution in the stresses. This will allow a design with a shorter pipe, saving material costs. This design will feature some elastic claps instead of the welded endcap, so it will also be quicker to install. The elastic clamps will most likely give some axial contribution, but they will be much smaller than the current rig produces. As seen from

the numerical simulations, the axial stress along the top path changes along the whole length with a welded endcap, which makes the placement of the nominal reference strain gages non-arbitrary.

6.7 Endurance Limit

From section 5.1.1, the endurance limit is seen to decrease by 18.2 % from stress cycles of $4.4 - 44$ bar to $3.6 - 36$ bar with the inclusion of a gouge. As seen in section 2.9 and 2.6, there are many factors affecting the endurance limit of the pipe. Material quality, surface finish and load type are mentioned in the sections. The load in the dent is highly complex when going through a pressure cycle, as seen in section 5.4. There are regions alternating between tension and compression with large relative stress values. Going into compression in each cycle will give a longer fatigue life compared to an area with cycles only in tension. The load type is a combination of all the load types mentioned in the section. The quality of the steel will also affect the endurance limit. A high-quality steel will be more affected by notches, scratches or gouges than a low-quality steel. Low-quality steel already have imperfections in the material, so the damage will not be as critical. If higher-quality steel was used, it is expected that the difference between the fatigue life of the pipes with and without gouge would be greater, where the gouge would have a bigger impact. Stress concentration factor is important for the fatigue life, and it is mainly governed by the dent geometry. It was observed that the factor increased for decreasing pressure due to rerounding effects. The location of the largest SCF also changed, consistent with the changing location of the crack. So, the SCF is important because it can predict where the crack should appear, while the gouge is dangerous because it leads to crack-initiation in the hoop direction along the gouge base. More fatigue tests would make the impact of the gouge clearer compared to the effect of dent depth.

Chapter 7

Conclusion

The objective of this thesis was to look at how gouges introduced into smooth dents affect the fatigue life of the pipe compared to a smooth dent, and how the results from a numerical simulation compared to values measured around the dent. It proved challenging to get a correct representation of the numerical results compared with the actual measurements. Both geometry and material properties were different, making comparison hard. However, both methods exhibited similar behavior, so the numerical simulations give a good notion on how the dented pipe behaves. The x-ray measurement gave residual stresses that were close to the stresses from the numerical results, with only some values being off.

There are several factors creating differences in the results. The material properties originally used in *ABAQUS* do not match the material properties found from the pipes. The diameter and thickness also changes during the fatigue tests, which affect the stresses in the material compared to the numerical results. The strain gages do not behave ideally in the area where they are placed, with values exploding as the strain gage fails. This is especially a problem for the tests with high internal pressure. Since there are considerable plastic effects, the conversion from strain to stress is not correct in these regions. Without material properties covering plastic- and hardening behavior, and a stress method considering plastic effects, the stress values from the strain gages are incorrect.

A smooth dent containing a gouge is a severe form of mechanical damage. The fatigue tests show that the gouge reduces the fatigue life compared to a smooth dent. In [CH04], previous fatigue tests suggest that the fatigue life of a pipe with gouge is a factor of one hundred shorter than without the gouge. For the experiments in this thesis, the factor increases for decreasing internal pressure, but a factor of one hundred is not observed. The maximum pressure for the endurance limit is reduced by a factor of 18.2 % when introducing a gouge. The gouges used here are introduced at the same time as the dent, with a gouge depth relatively large compared to the pipe thickness, making them realistic.

Using microscope, it is clear that the cracks in the tests with gouge are initiated from the gouge itself. This makes a gouge in a dent a more severe form of damage than a smooth dent by itself. The largest stresses occur around the areas where the indenter enters and exits the pipe, and this is especially true for tests with high internal pressure. The gouge initiates a crack that propagate over this sharp geometry change. For test with lower pressure, the stress concentration is larger on the side of the dent, at the dent shoulder, where the cracks appear for these tests. This is consistent with the numerical stress result.

One of the tests were subjected to a large static pressure to reduce the dent depth before subjecting it to dynamic pressure. This pipe did not fail after more than twice the cycles a pipe without this initial pressure had. This suggests that it could be a good idea to use this initial pressure to increase the lifetime of a dented pipeline. More tests should be performed.

The tests made in this thesis only use pipes with one diameter and thickness, and only creates dents with one depth. More tests with varying geometry should be performed to get a better picture of how initial rerounding can help repair the dent, and how gouges affect dented pipes subjected to cyclic internal pressure. The numerical simulation did not include a gouge in the dent, which also limit the ability to compare with the dents with gouge in the experiments. The fatigue tests and numerical analysis should serve as a good starting point for future fatigue analysis.

7.1 Further Work

There are several things that could be worth looking at for future projects.

Thoughts were given on a new improved test rig for the fatigue tests. This would feature some elastic claps as a part of the rig itself, instead of the welded endcaps used in this project. Attaching the endcaps is a tedious process, and some tests also failed in the weld before they failed around the dent. The pipe without endcaps were modeled in section 5.4. The new rig would probably transfer some axial forces to the pipe, but not as much as the welded endcaps do. This will also create an opportunity to use shorter pipes, since the endcap interaction will be smaller. This reduces the time and cost of future fatigue tests.

For future numerical simulations, the gouge could be modeled in *ABAQUS*, either directly in the dent, or by itself taking input stress and strain from the dent model and returning response. This would give a notion of how the stresses in the dent are affected by the gouge, and ability to look on how the gouge depth affects the result.

Several fatigue tests should be done to give better statistical significance to the gouge effect. The thickness and diameter of the pipe should be varied, as well as the dent depth. The effect of rerounding used to repair the pipe should be investigated further,

as well as looking at how a gouge affects this process. This could potentially be a smart way of repairing dented pipelines.

There were wall-thinning effects, and differences in material properties from test to test and between the numerical and experimental methods. For future tests, it is advantageous to do the material tests before the pipes are used in fatigue tests, and before defining the numerical material properties. The pipe length, thickness and diameter should also be measured before the tests, to compare them to the values after the fatigue tests are finished.

The stress calculation from strain gage should in the future use theory or methods which consider the plastic- and hardening effects. An iterative method, like the one discussed in section 2.11, could be used for this purpose.

Pipelines are usually coated with different substances. Denting and fatigue on coated pipelines could be interesting to investigate. The coating would no doubt affect the denting process, and the damage to the pipe from indentation. Also indenting at different angles would be interesting to investigate.

The x-ray diffraction measurements gave results close to the results found in the numerical simulations. The x-ray measurements could be used on the pipe when pressurized to get stress measurements and compare them with the ones from the strain gages and the numerical values. Other stress calculation methods need to be used to get correct stress values in the plastic areas.

The indenter rig should be modified to allow for a straight indenter path, to get results more comparable with the numerical indentation. This would remove some uncertainties. The trawling impact would not be a completely straight interaction, so it could be interesting to look on an indenter path that resemble this motion, and how this affects the result.

Bibliography

[AK99] CR Alexander and JF Kiefner. *Effects of Smooth and Rock Dents on Liquid Petroleum Pipelines*. 1999.

[ASM04] ASME. *Gas Transmission and Distribution Piping Systems*. New York: American Society of Mechanical Engineers, 2004.

[ASM93] ASME. *Liquid Transportation Systems for Hydrocarbons, Liquid Petroleum Gas, Anhydrous Ammonia, and Alcohols*. 1992 edition. New York: American Society of Mechanical Engineers, 1993.

[Ber06a] Stig Berge. *Fatigue and Fracture Design of Marine Structures I: Fracture Design of Welded Structures*. Trondheim: Institutt for Marine Teknikk, 2006.

[Ber06b] Stig Berge. *Fatigue and Fracture Design of Marine Structures II: Fatigue Design of Welded Structures*. Trondheim: Institutt for Marine Teknikk, 2006.

[CH01] Andrew Cosham and Phil Hopkins. *The Pipeline Defect Assessment Manual (PDAM)*. 2001.

[CH04] Andrew Cosham and Phil Hopkins. *The Effect of Dents in Pipelines — Guidance in the Pipeline Defect Assessment Manual*. Vol. 81. 2. 2004, pp. 127–139.

[DG10] DNV-GL. *DNV-RP-F111 Interference Between Trawl Gear and Pipelines*. Standard. 2010.

[Eli16] Agnes Karin Eliassen. *Assessment of Pipeline Integrity after Trawling Impact by Investigating Dent with Gouge*. 2016.

[Fit+05] ME Fitzpatrick et al. *Determination of Residual Stresses by X-Ray Diffraction*. 2005.

[HWB99] Weiping Hu, Chun Hui Wang, and S Barter. *Analysis of Cyclic Mean Stress Relaxation and Strain Ratchetting Behaviour of Aluminium 7050*. 1999.

[Joh12] Ingrid Berg Johnsen. *Clump-Weight Trawl Gear Interaction with Submarine Pipelines*. 2012.

[LJ63] Charles Lipson and Robert C. Juvinall. *Handbook of Stress and Strength Design and Material Applications*. New York: The Macmillan Company, 1963.

[MM08] Vishay Micro-Measurements. *Strain Gage Rosettes: Selection, Application and Data Reduction*. Vol. 515. 2008, pp. 151–161.

[Rac08] Dr.J.M. Race. *Integrity Assessment of Plain Dents Subject to Fatigue Loading*. School of Marine Science and Technology, Newcastle University, 2008.

[Ric+88] R.C. Rice et al. *Fatigue Design Handbook AE-10*. Warrendale, Pa.: Society of Automotive Engineers, Inc., 1988.

[Roo+00] P Roovers et al. *EPRG Methods for assessing the Tolerance and Resistance of Pipelines to External Damage*. Vol. 2. 2000, pp. 405–425.

[SIB14] B. Cunha Sérgio, P. Pasqualino Ilson, and C. Pinheiro Bianca. *Plain Dent Fatigue - A Comparison Of Assessment Methodologies*. Unpublished, 2014.

[SM00] Darrell F. Socie and Gary B. Marquis. *Multiaxial Fatigue*. Warrendale, Pa.: Society of Automotive Engineers, Inc., 2000.

[Sæ15] Svein Sævik. *Lecture Notes in Offshore Pipeline Technology*. Trondheim: Department of Marine Technology, NTNU, 2015.

[VJE07] JW Valdemarsen, T Jørgensen, and A Engås. *Options to mitigate Bottom Habitat Impact of Dragged Gears*. Institute of Marine Research Bergen, Norway, 2007.

Appendix A

Appendix

The appendix contains the strain measurements from the strain gages, and the dent radial displacement measurements from the LVDT-device. The strains are converted into principle stress and directional stress, and these are stated along with the angle between them. The stress-strain relationship is also included. The sections are numbered alphabetically, with each test having its own section. The LVDT-data also have its own section.

Strain Gage, Test 1

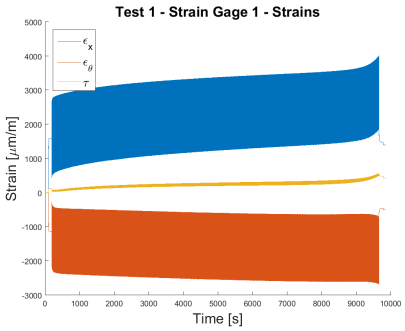

Figure A.1: Test 1, Gage 1 - Strain

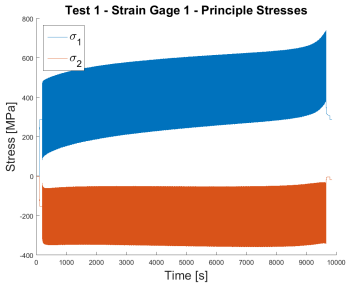

(a) Principle Stress

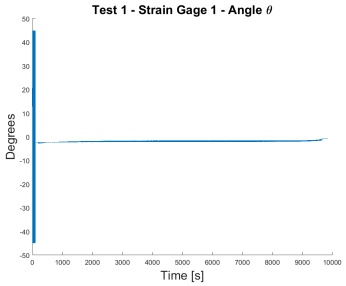

(b) Angle

Figure A.2: Test 1, Gage 1 - Principle Stress - Angle

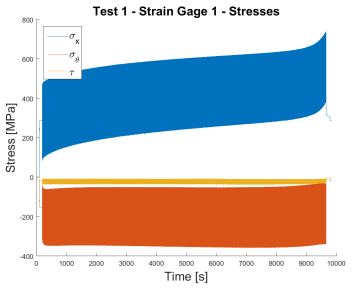

(a) Stress

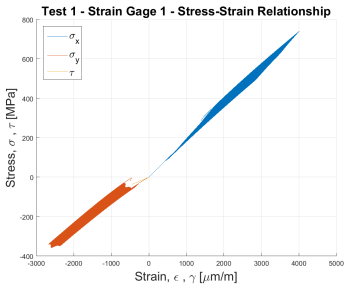

(b) Stress-Strain

Figure A.3: Test 1, Gage 1 - Stress - Stress-Strain

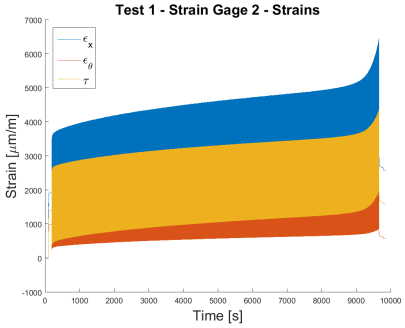

Figure A.4: Test 1, Gage 2 - Strain

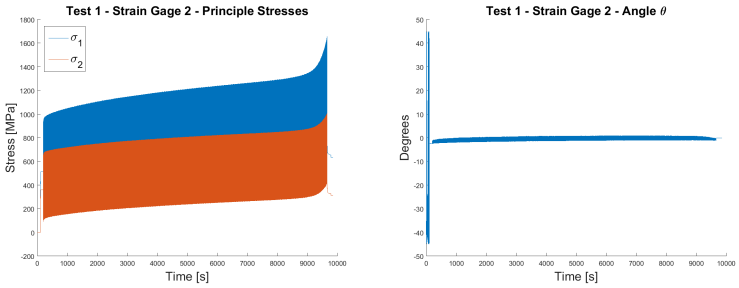

(a) Principle Stress (b) Angle

Figure A.5: Test 1, Gage 2 - Principle Stress - Angle

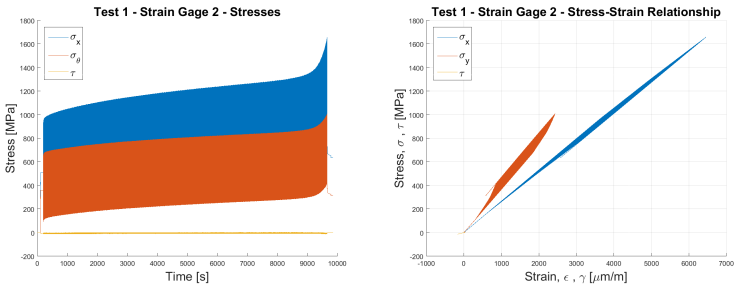

(a) Stress (b) Stress-Strain

Figure A.6: Test 1, Gage 2 - Stress - Stress-Strain

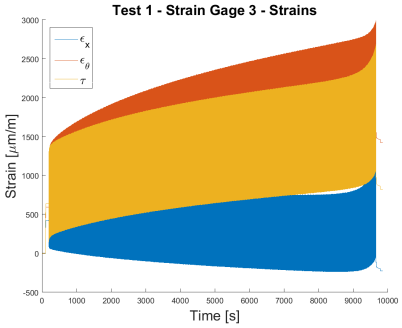

Figure A.7: Test 1, Gage 3 - Strain

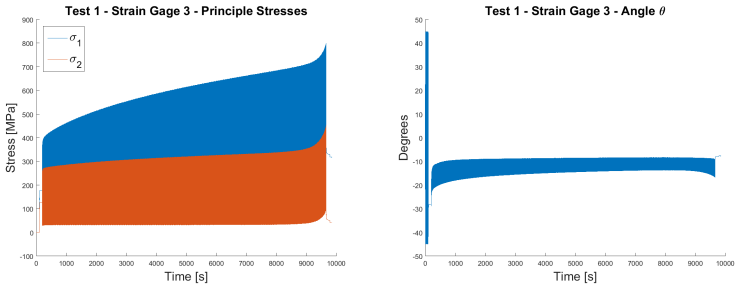

(a) Principle Stress (b) Angle

Figure A.8: Test 1, Gage 3 - Principle Stress - Angle

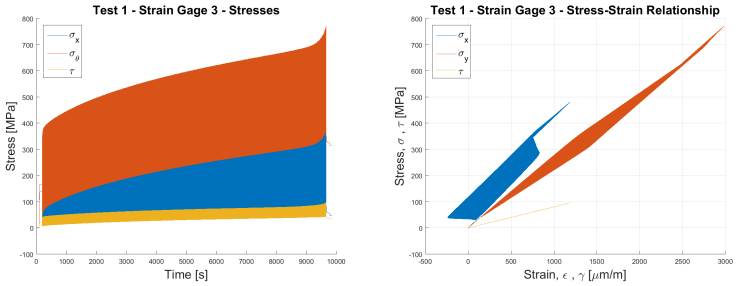

(a) Stress (b) Stress-Strain

Figure A.9: Test 1, Gage 3 - Stress - Stress-Strain

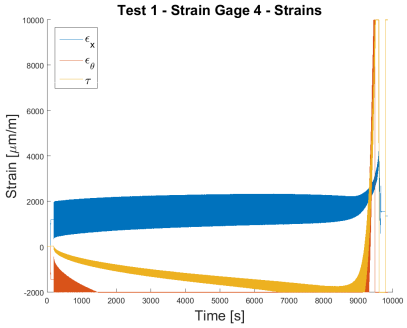

Figure A.10: Test 1, Gage 4 - Strain

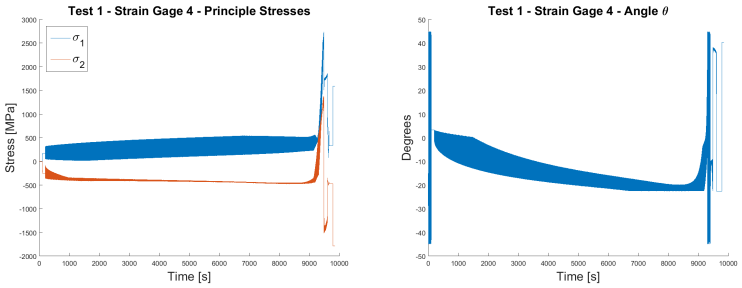

(a) Principle Stress (b) Angle

Figure A.11: Test 1, Gage 4 - Principle Stress - Angle

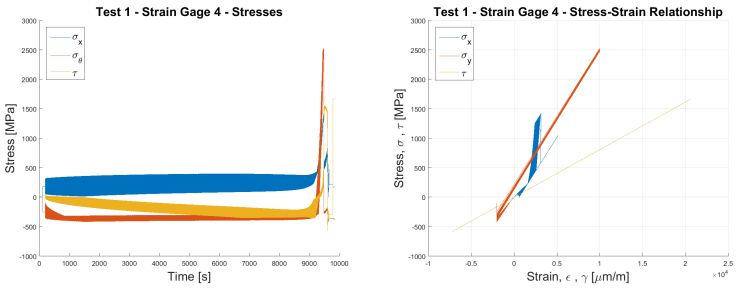

(a) Stress (b) Stress-Strain

Figure A.12: Test 1, Gage 4 - Stress - Stress-Strain

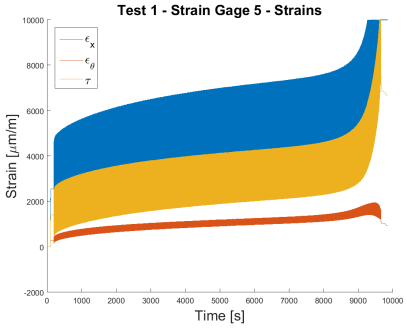

Figure A.13: Test 1, Gage 5 - Strain

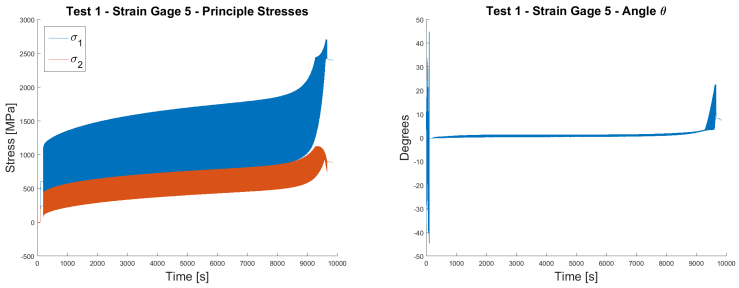

(a) Principle Stress (b) Angle

Figure A.14: Test 1, Gage 5 - Principle Stress - Angle

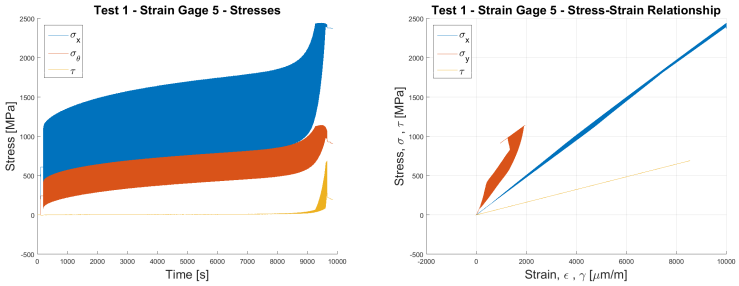

(a) Stress (b) Stress-Strain

Figure A.15: Test 1, Gage 5 - Stress - Stress-Strain

Strain Gage, Test 2

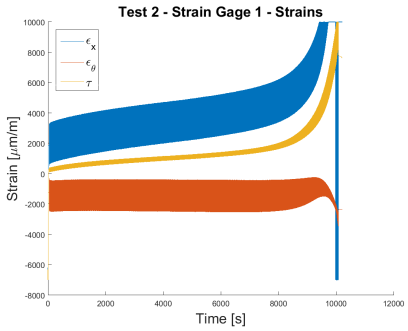

Figure A.16: Test 2, Gage 1 - Strain

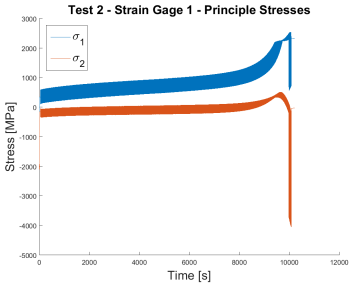

(a) Principle Stress

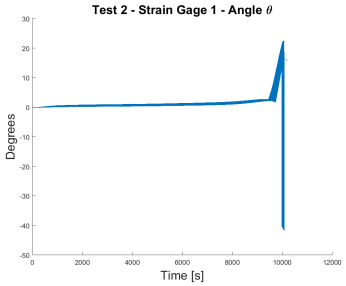

(b) Angle

Figure A.17: Test 2, Gage 1 - Principle Stress - Angle

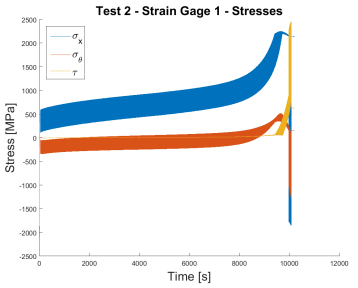

(a) Stress

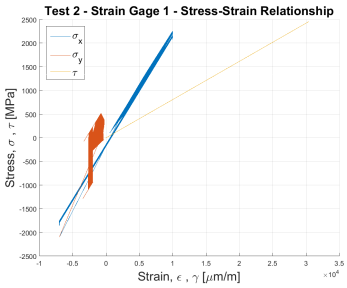

(b) Stress-Strain

Figure A.18: Test 2, Gage 1 - Stress - Stress-Strain

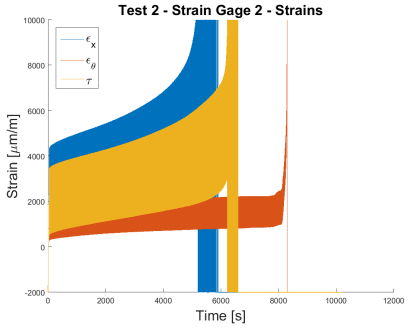

Figure A.19: Test 2, Gage 2 - Strain

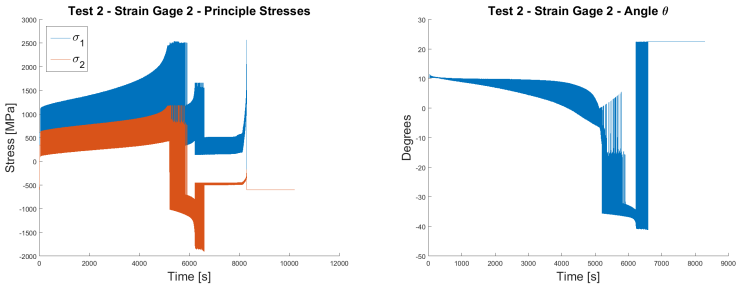

(a) Principle Stress (b) Angle

Figure A.20: Test 2, Gage 2 - Principle Stress - Angle

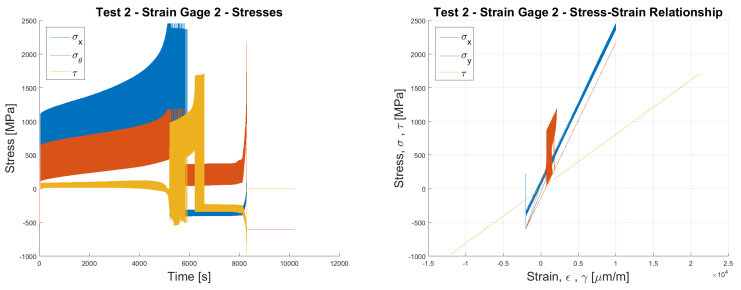

(a) Stress (b) Stress-Strain

Figure A.21: Test 2, Gage 2 - Stress - Stress-Strain

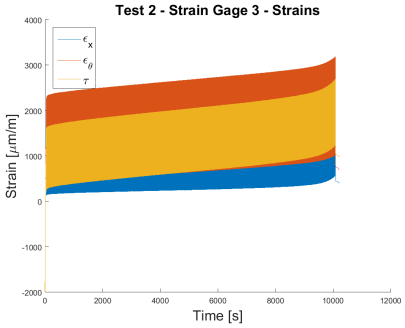

Figure A.22: Test 2, Gage 3 - Strain

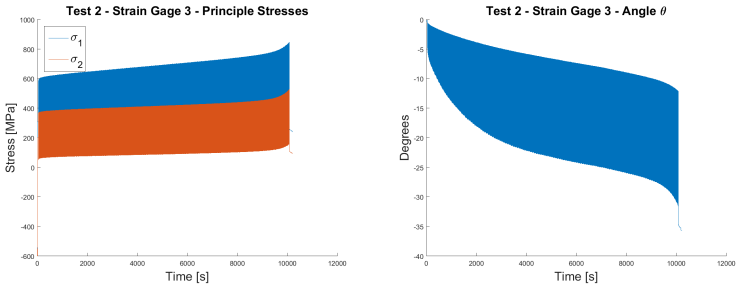

(a) Principle Stress (b) Angle

Figure A.23: Test 2, Gage 3 - Principle Stress - Angle

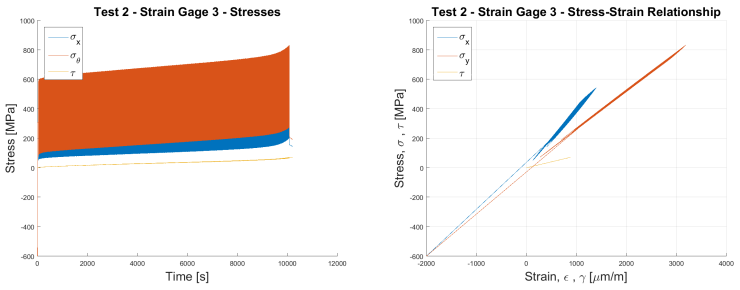

(a) Stress (b) Stress-Strain

Figure A.24: Test 2, Gage 3 - Stress - Stress-Strain

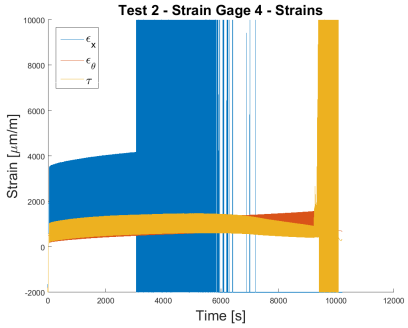

Figure A.25: Test 2, Gage 4 - Strain

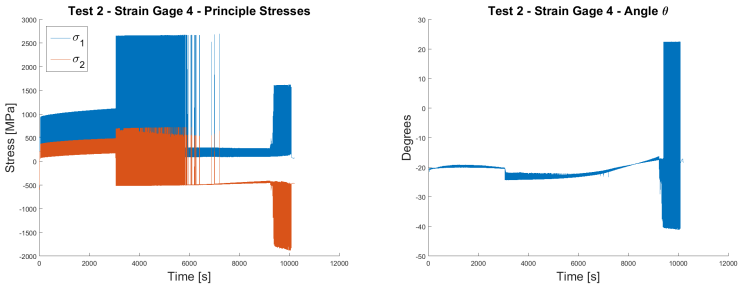

(a) Principle Stress (b) Angle

Figure A.26: Test 2, Gage 4 - Principle Stress - Angle

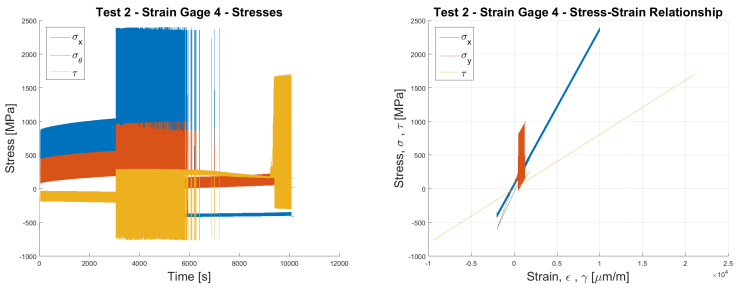

(a) Stress (b) Stress-Strain

Figure A.27: Test 2, Gage 4 - Stress - Stress-Strain

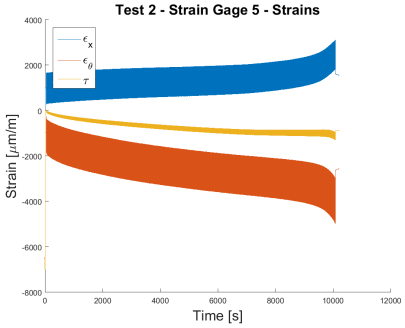

Figure A.28: Test 2, Gage 5 - Strain

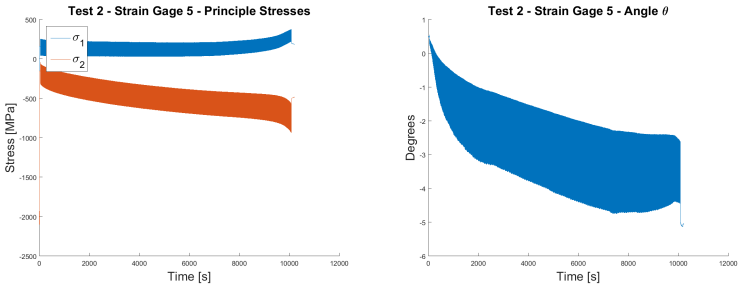

(a) Principle Stress (b) Angle

Figure A.29: Test 2, Gage 5 - Principle Stress - Angle

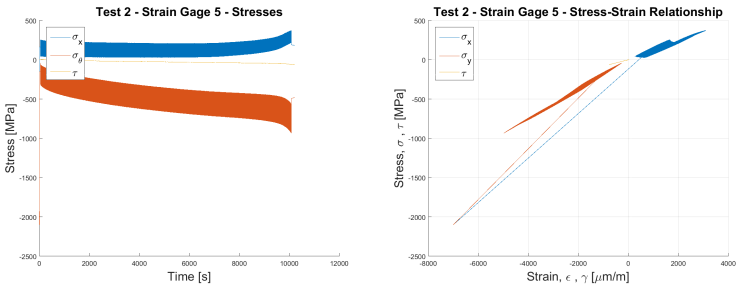

(a) Stress (b) Stress-Strain

Figure A.30: Test 2, Gage 5 - Stress - Stress-Strain

Strain Gage, Test 3

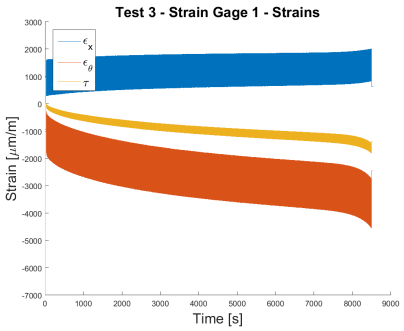

Figure A.31: Test 3, Gage 1 - Strain

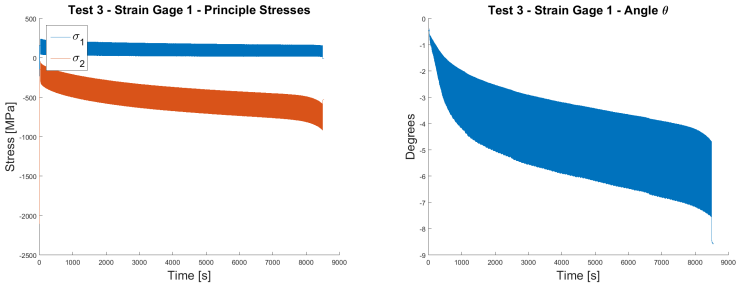

(a) Principle Stress (b) Angle

Figure A.32: Test 3, Gage 1 - Principle Stress - Angle

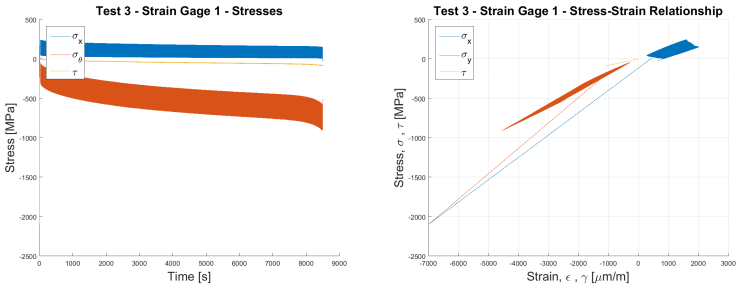

(a) Stress (b) Stress-Strain

Figure A.33: Test 3, Gage 1 - Stress - Stress-Strain

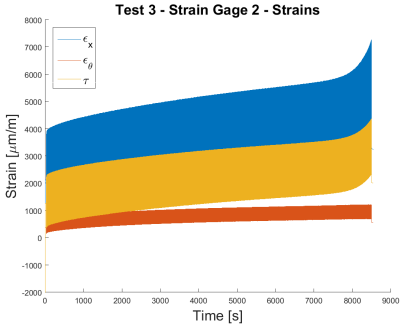

Figure A.34: Test 3, Gage 2 - Strain

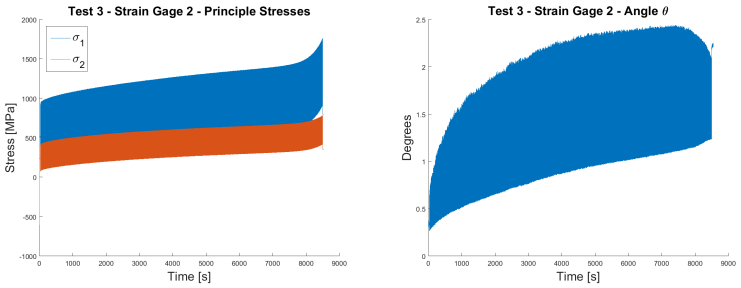

(a) Principle Stress (b) Angle

Figure A.35: Test 3, Gage 2 - Principle Stress - Angle

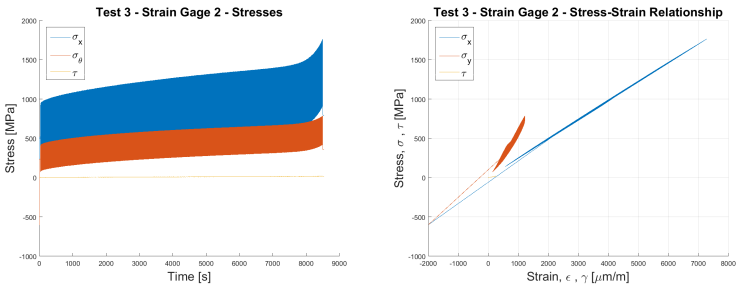

(a) Stress (b) Stress-Strain

Figure A.36: Test 3, Gage 2 - Stress - Stress-Strain

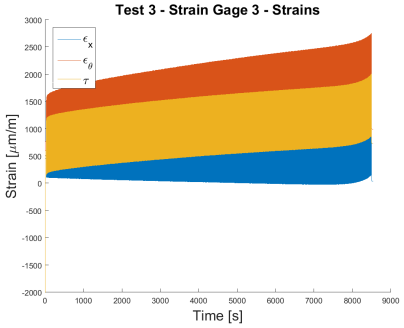

Figure A.37: Test 3, Gage 3 - Strain

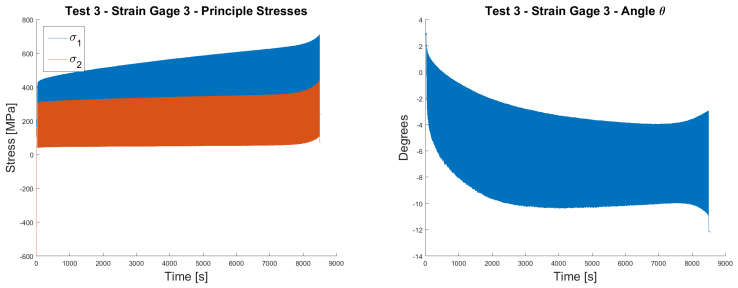

(a) Principle Stress (b) Angle

Figure A.38: Test 3, Gage 3 - Principle Stress - Angle

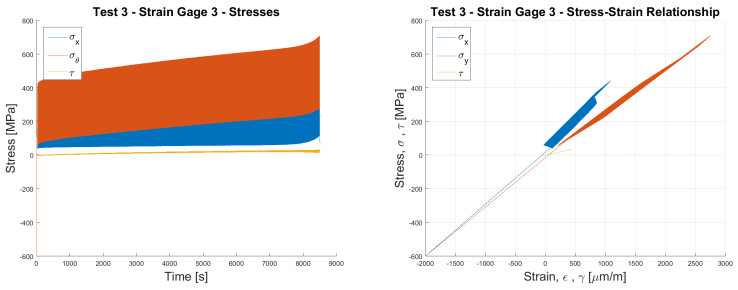

(a) Stress (b) Stress-Strain

Figure A.39: Test 3, Gage 3 - Stress - Stress-Strain

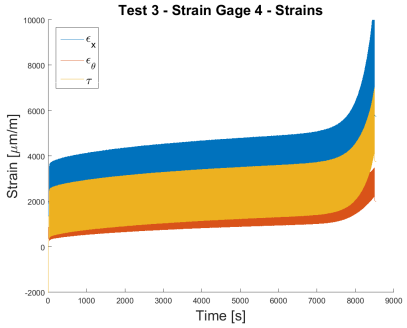

Figure A.40: Test 3, Gage 4 - Strain

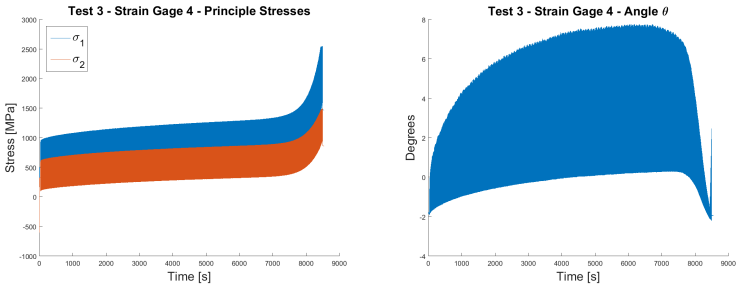

(a) Principle Stress (b) Angle

Figure A.41: Test 3, Gage 4 - Principle Stress - Angle

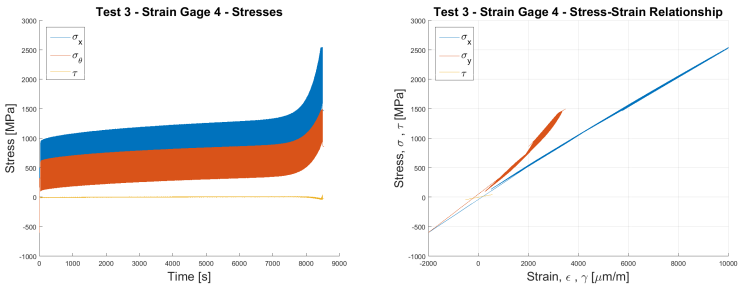

(a) Stress (b) Stress-Strain

Figure A.42: Test 3, Gage 4 - Stress - Stress-Strain

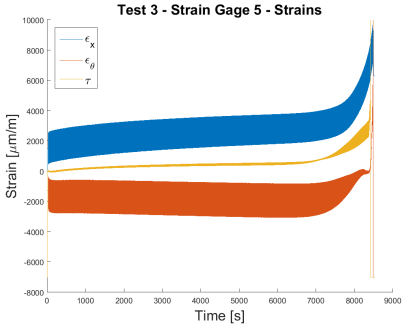

Figure A.43: Test 3, Gage 5 - Strain

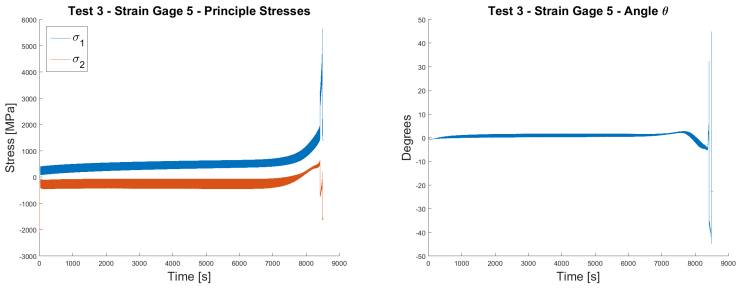

(a) Principle Stress (b) Angle

Figure A.44: Test 3, Gage 5 - Principle Stress - Angle

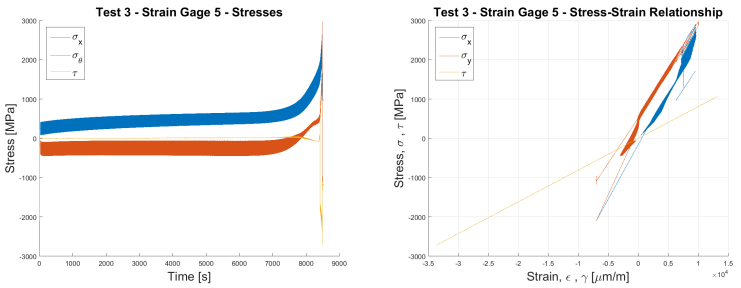

(a) Stress (b) Stress-Strain

Figure A.45: Test 3, Gage 5 - Stress - Stress-Strain

Strain Gage, Test 4

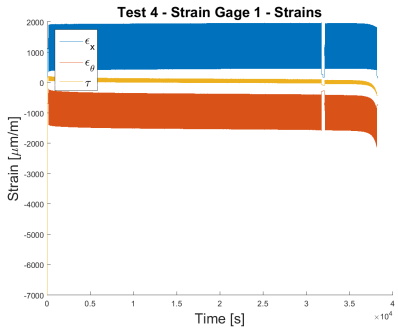

Figure A.46: Test 4, Gage 1 - Strain

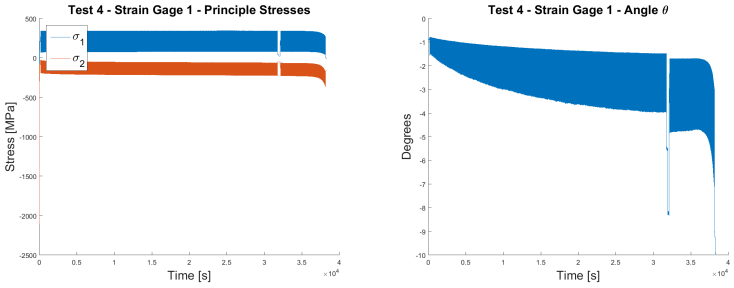

(a) Principle Stress (b) Angle

Figure A.47: Test 4, Gage 1 - Principle Stress - Angle

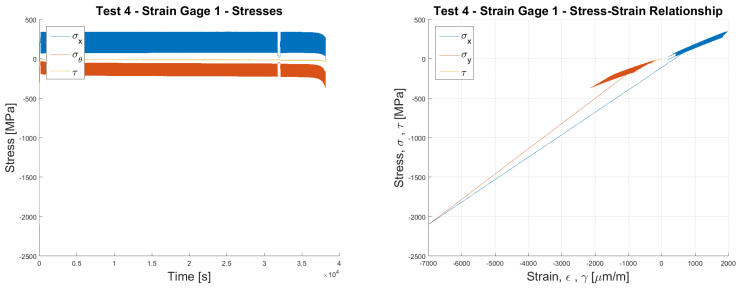

(a) Stress (b) Stress-Strain

Figure A.48: Test 4, Gage 1 - Stress - Stress-Strain

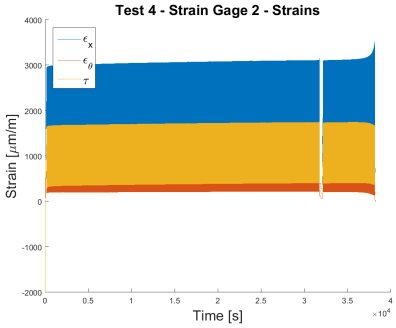

Figure A.49: Test 4, Gage 2 - Strain

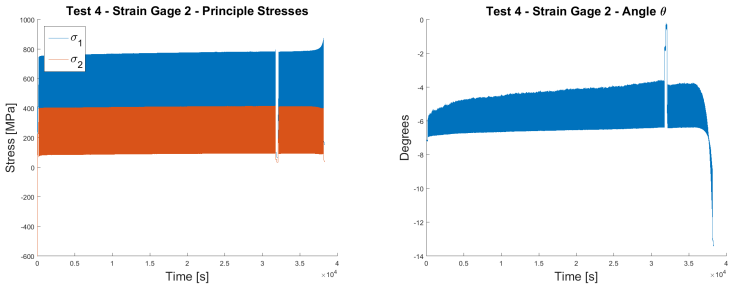

(a) Principle Stress (b) Angle

Figure A.50: Test 4, Gage 2 - Principle Stress - Angle

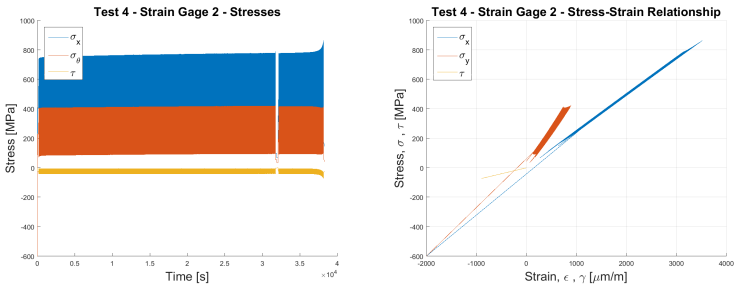

(a) Stress (b) Stress-Strain

Figure A.51: Test 4, Gage 2 - Stress - Stress-Strain

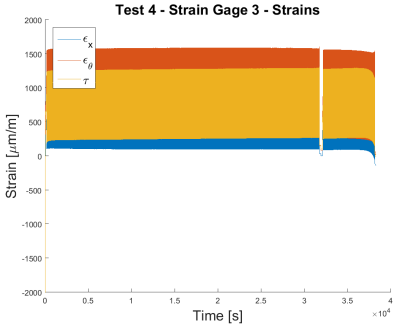

Figure A.52: Test 4, Gage 3 - Strain

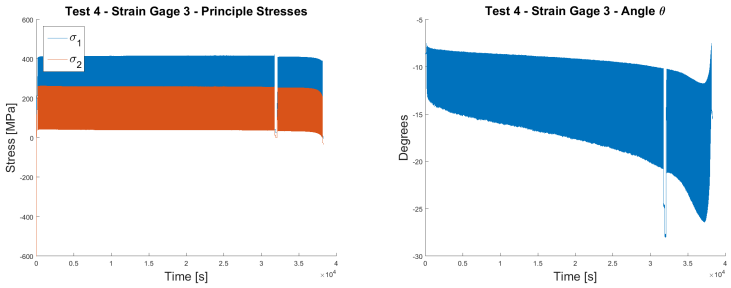

(a) Principle Stress (b) Angle

Figure A.53: Test 4, Gage 3 - Principle Stress - Angle

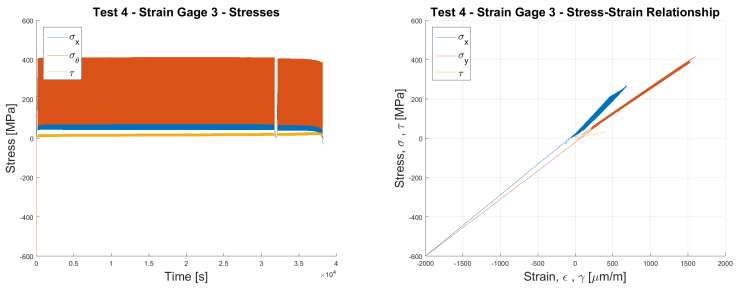

(a) Stress (b) Stress-Strain

Figure A.54: Test 4, Gage 3 - Stress - Stress-Strain

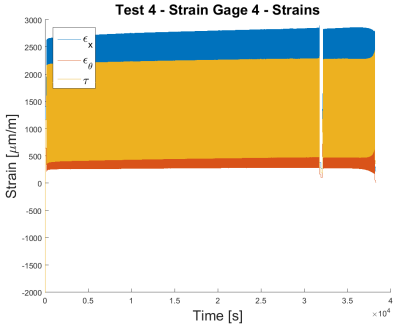

Figure A.55: Test 4, Gage 4 - Strain

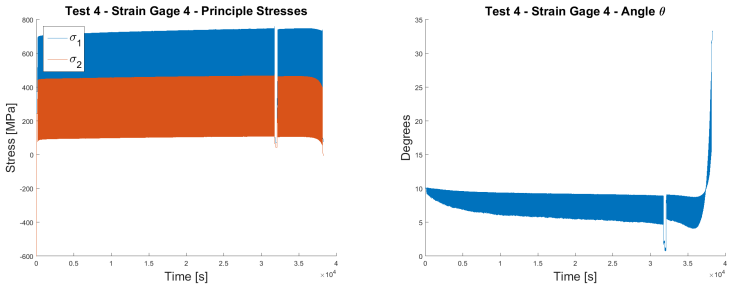

(a) Principle Stress (b) Angle

Figure A.56: Test 4, Gage 4 - Principle Stress - Angle

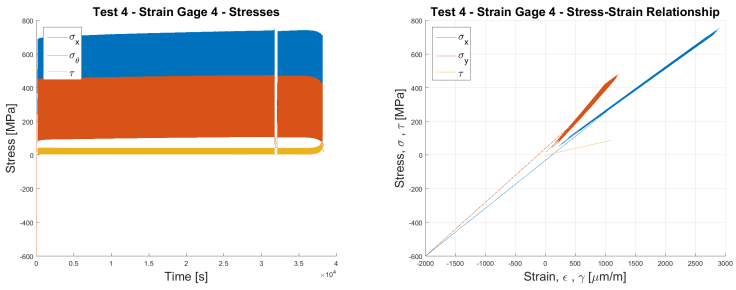

(a) Stress (b) Stress-Strain

Figure A.57: Test 4, Gage 4 - Stress - Stress-Strain

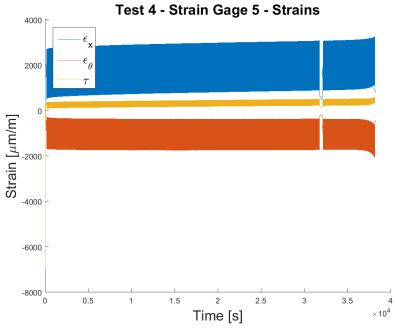

Figure A.58: Test 4, Gage 5 - Strain

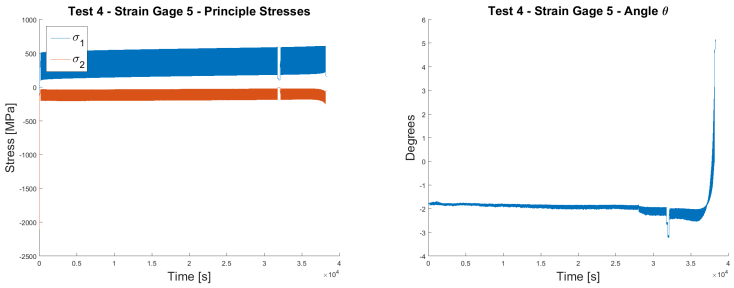

(a) Principle Stress (b) Angle

Figure A.59: Test 4, Gage 5 - Principle Stress - Angle

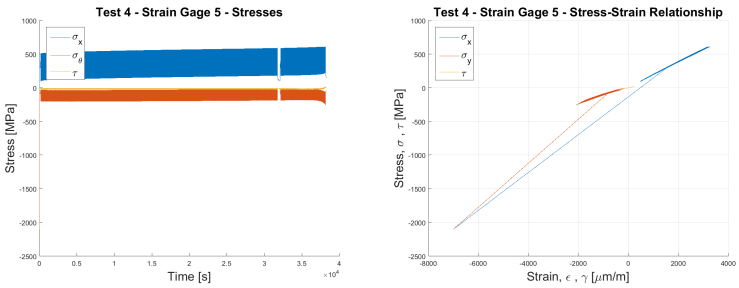

(a) Stress (b) Stress-Strain

Figure A.60: Test 4, Gage 5 - Stress - Stress-Strain

Strain Gage, Test 5

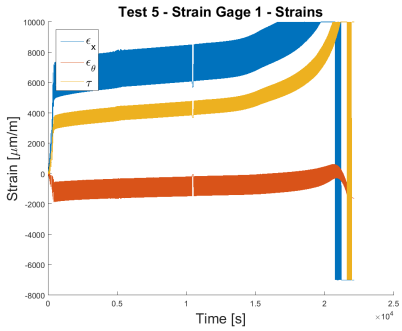

Figure A.61: Test 5, Gage 1 - Strain

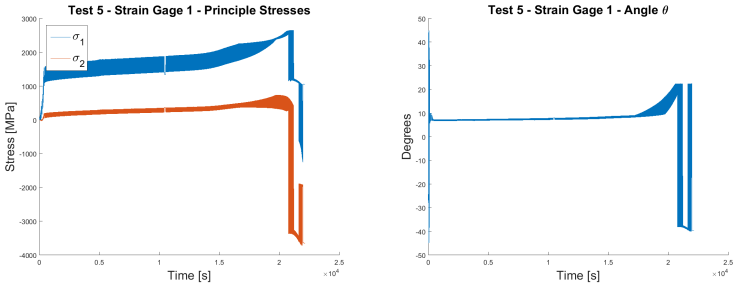

(a) Principle Stress (b) Angle

Figure A.62: Test 5, Gage 1 - Principle Stress - Angle

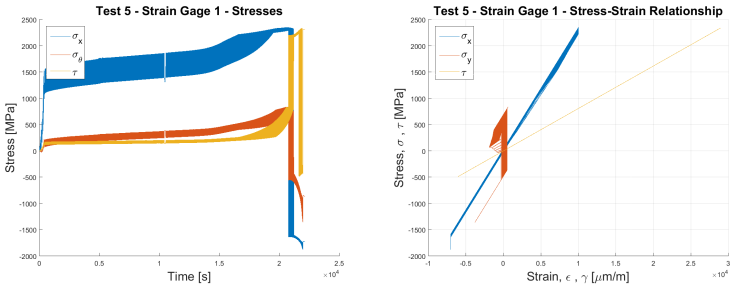

(a) Stress (b) Stress-Strain

Figure A.63: Test 5, Gage 1 - Stress - Stress-Strain

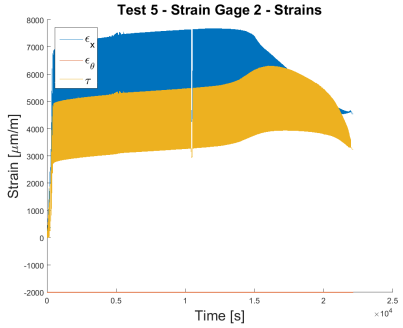

Figure A.64: Test 5, Gage 2 - Strain

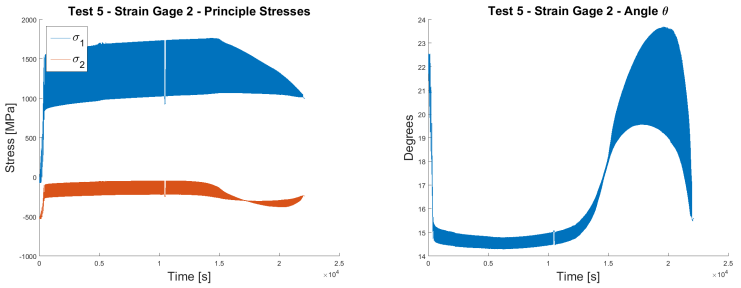

(a) Principle Stress (b) Angle

Figure A.65: Test 5, Gage 2 - Principle Stress - Angle

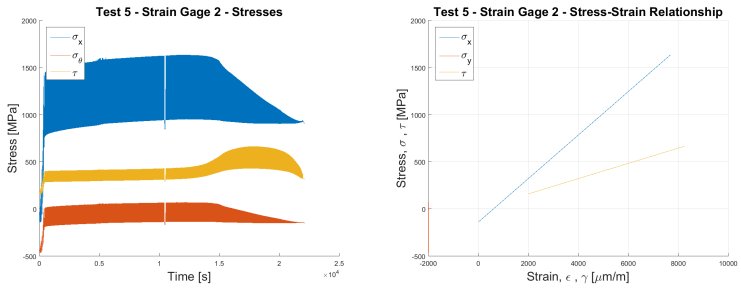

(a) Stress (b) Stress-Strain

Figure A.66: Test 5, Gage 2 - Stress - Stress-Strain

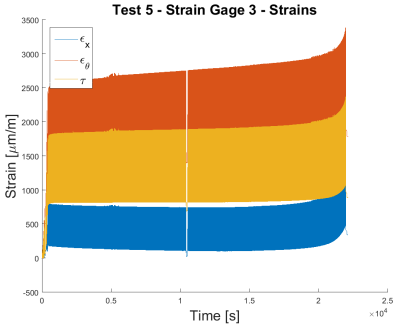

Figure A.67: Test 5, Gage 3 - Strain

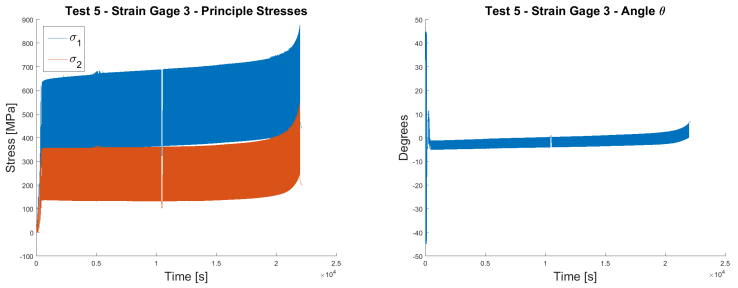

(a) Principle Stress (b) Angle

Figure A.68: Test 5, Gage 3 - Principle Stress - Angle

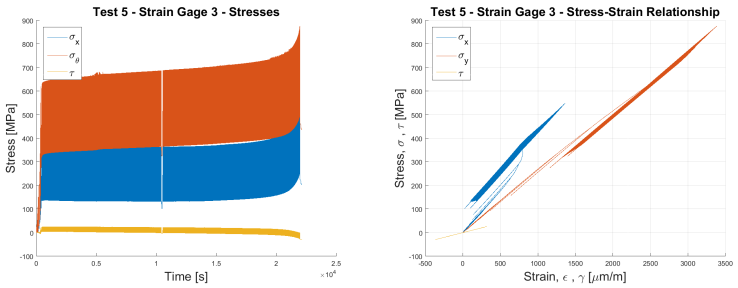

(a) Stress (b) Stress-Strain

Figure A.69: Test 5, Gage 3 - Stress - Stress-Strain

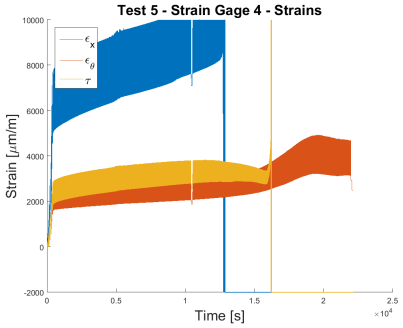

Figure A.70: Test 5, Gage 4 - Strain

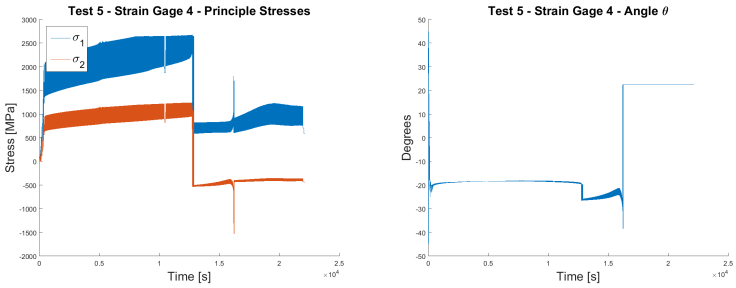

(a) Principle Stress (b) Angle

Figure A.71: Test 5, Gage 4 - Principle Stress - Angle

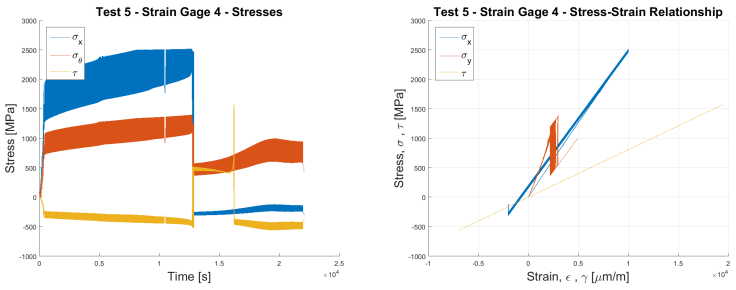

(a) Stress (b) Stress-Strain

Figure A.72: Test 5, Gage 4 - Stress - Stress-Strain

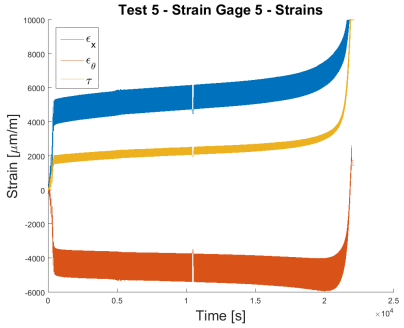

Figure A.73: Test 5, Gage 5 - Strain

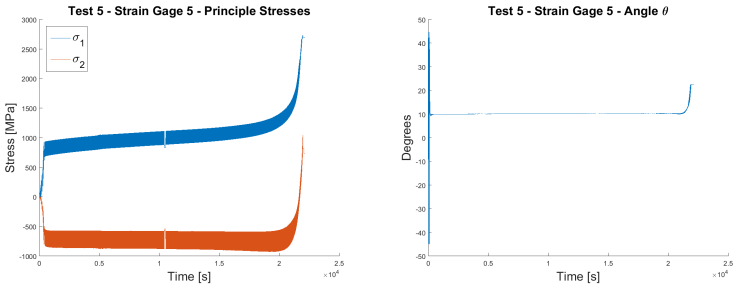

(a) Principle Stress (b) Angle

Figure A.74: Test 5, Gage 5 - Principle Stress - Angle

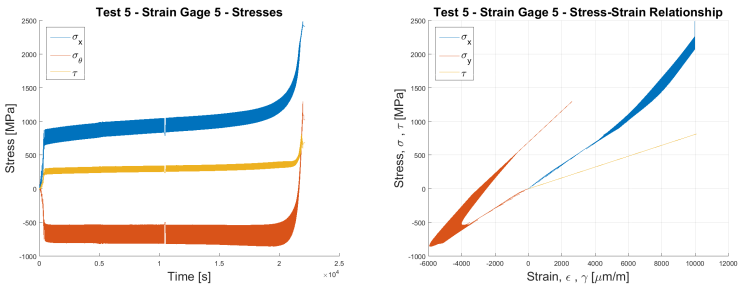

(a) Stress (b) Stress-Strain

Figure A.75: Test 5, Gage 5 - Stress - Stress-Strain

Strain Gage, Test 6

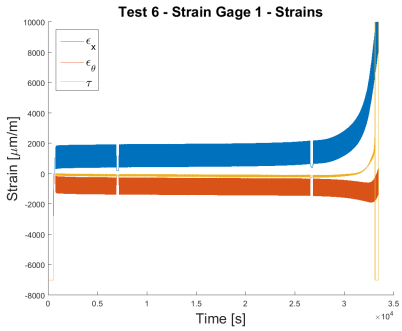

Figure A.76: Test 6, Gage 1 - Strain

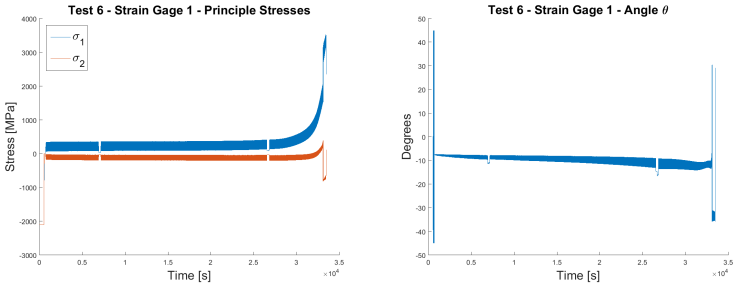

(a) Principle Stress (b) Angle

Figure A.77: Test 6, Gage 1 - Principle Stress - Angle

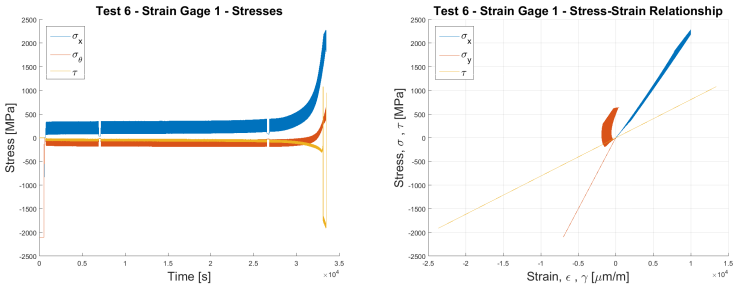

(a) Stress (b) Stress-Strain

Figure A.78: Test 6, Gage 1 - Stress - Stress-Strain

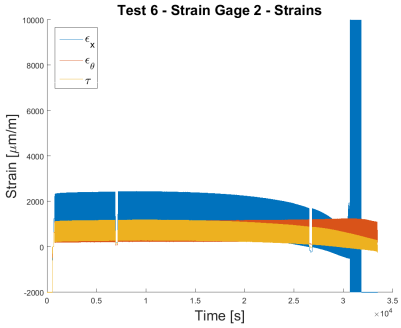

Figure A.79: Test 6, Gage 2 - Strain

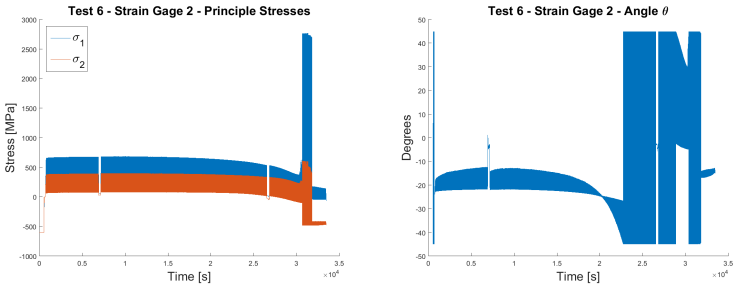

(a) Principle Stress (b) Angle

Figure A.80: Test 6, Gage 2 - Principle Stress - Angle

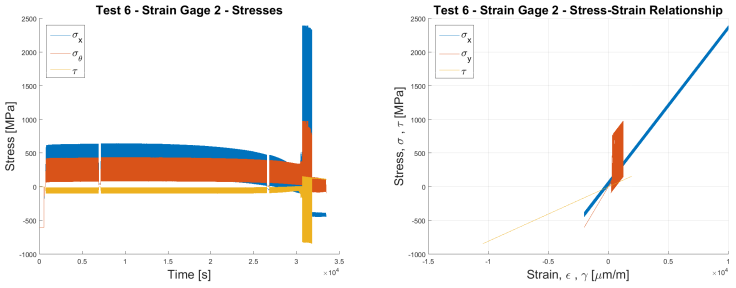

(a) Stress (b) Stress-Strain

Figure A.81: Test 6, Gage 2 - Stress - Stress-Strain

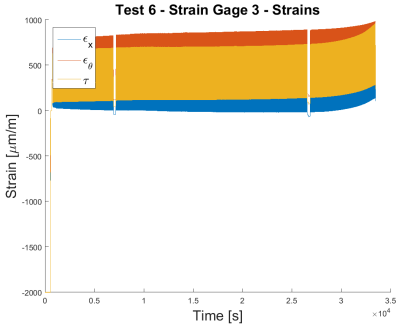

Figure A.82: Test 6, Gage 3 - Strain

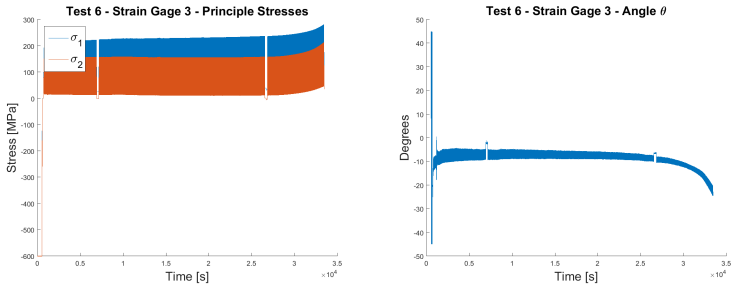

(a) Principle Stress (b) Angle

Figure A.83: Test 6, Gage 3 - Principle Stress - Angle

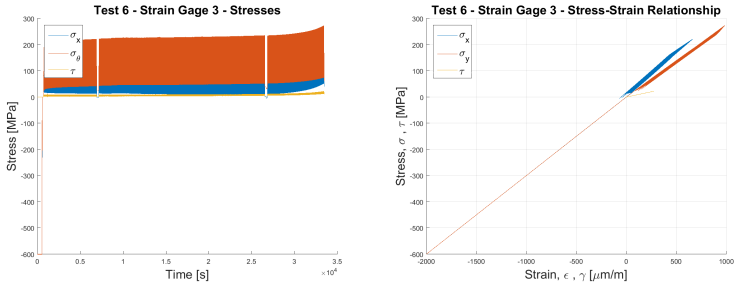

(a) Stress (b) Stress-Strain

Figure A.84: Test 6, Gage 3 - Stress - Stress-Strain

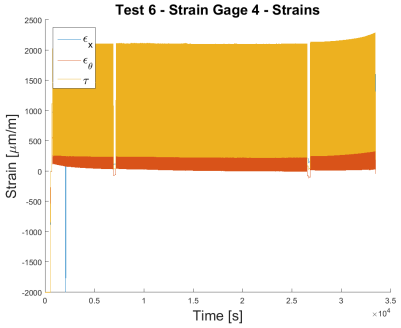

Figure A.85: Test 6, Gage 4 - Strain

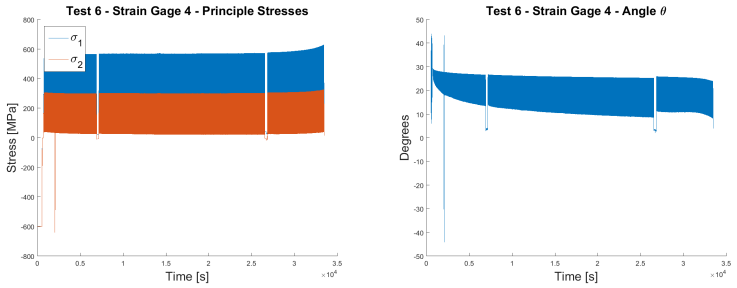

(a) Principle Stress (b) Angle

Figure A.86: Test 6, Gage 4 - Principle Stress - Angle

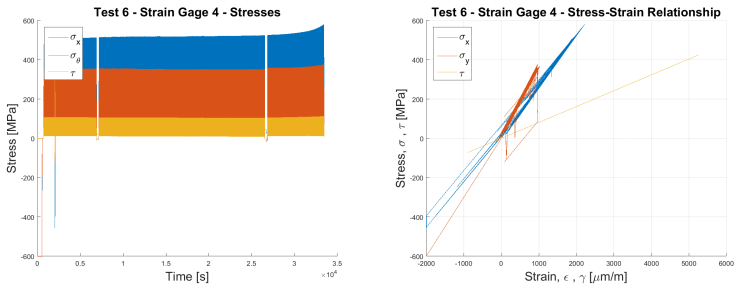

(a) Stress (b) Stress-Strain

Figure A.87: Test 6, Gage 4 - Stress - Stress-Strain

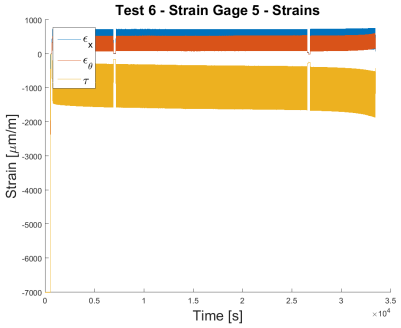

Figure A.88: Test 6, Gage 5 - Strain

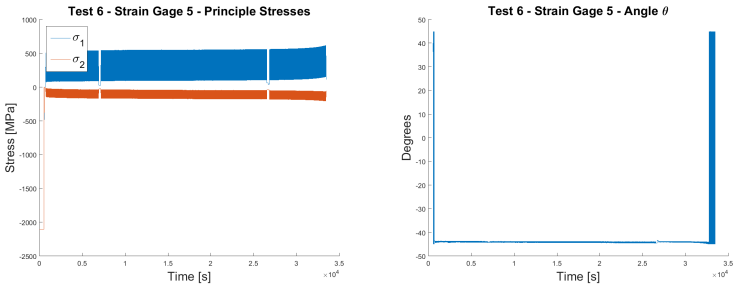

(a) Principle Stress (b) Angle

Figure A.89: Test 6, Gage 5 - Principle Stress - Angle

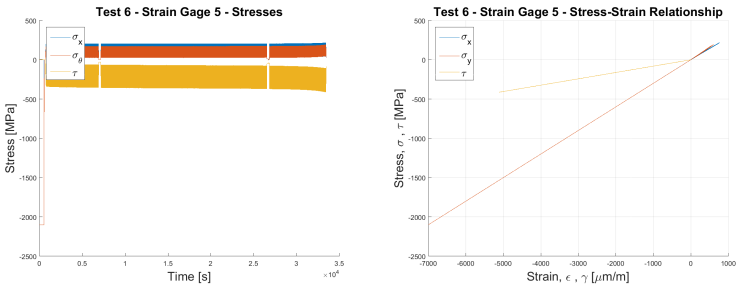

(a) Stress (b) Stress-Strain

Figure A.90: Test 6, Gage 5 - Stress - Stress-Strain

Strain Gage, Test 7

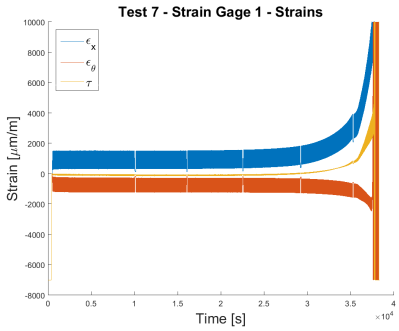

Figure A.91: Test 7, Gage 1 - Strain

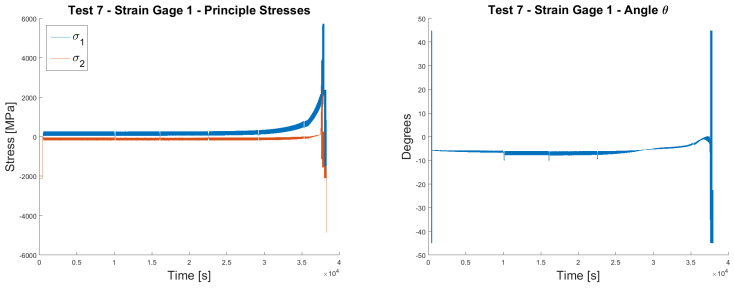

(a) Principle Stress (b) Angle

Figure A.92: Test 7, Gage 1 - Principle Stress - Angle

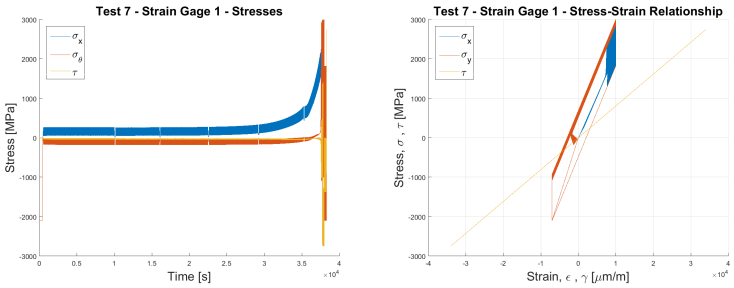

(a) Stress (b) Stress-Strain

Figure A.93: Test 7, Gage 1 - Stress - Stress-Strain

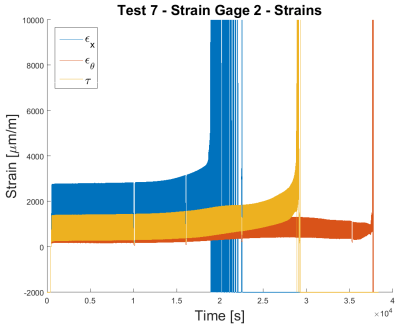

Figure A.94: Test 7, Gage 2 - Strain

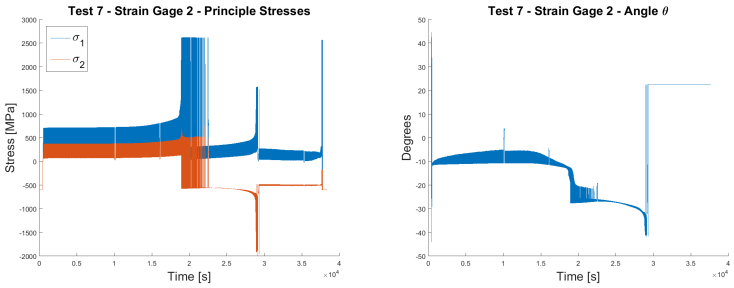

(a) Principle Stress (b) Angle

Figure A.95: Test 7, Gage 2 - Principle Stress - Angle

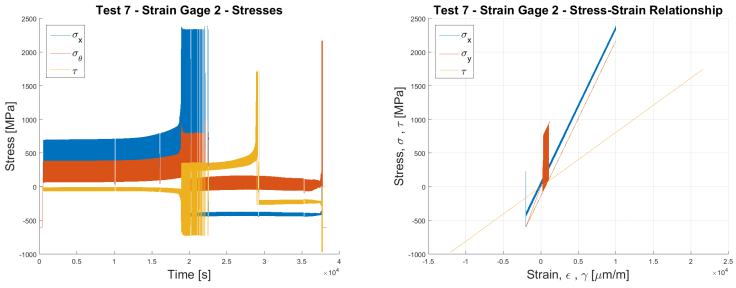

(a) Stress (b) Stress-Strain

Figure A.96: Test 7, Gage 2 - Stress - Stress-Strain

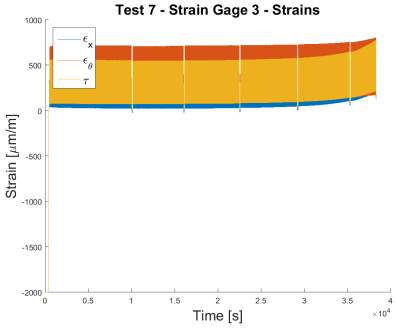

Figure A.97: Test 7, Gage 3 - Strain

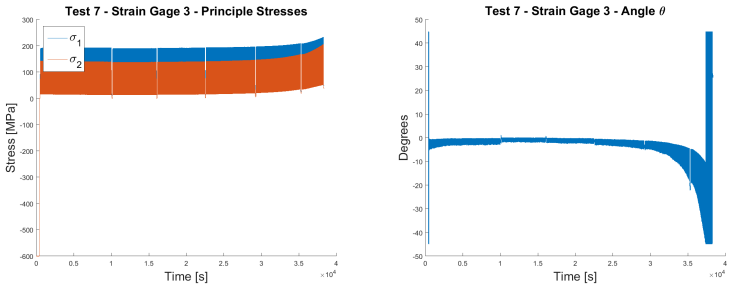

(a) Principle Stress (b) Angle

Figure A.98: Test 7, Gage 3 - Principle Stress - Angle

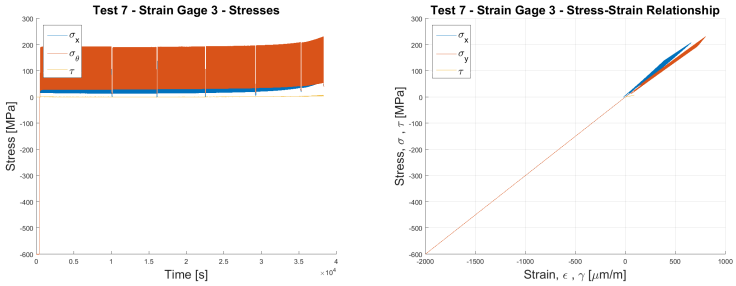

(a) Stress (b) Stress-Strain

Figure A.99: Test 7, Gage 3 - Stress - Stress-Strain

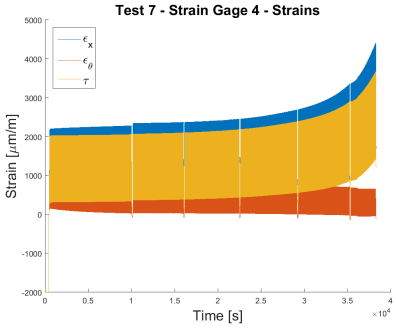

Figure A.100: Test 7, Gage 4 - Strain

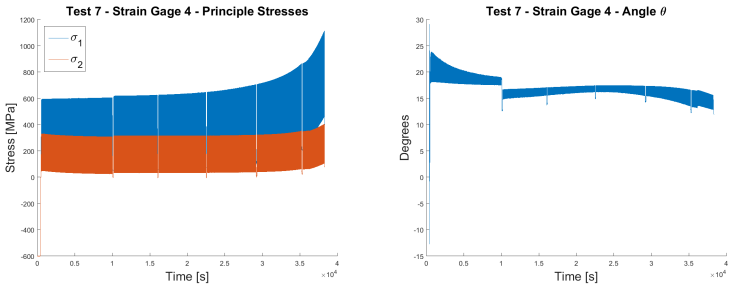

(a) Principle Stress (b) Angle

Figure A.101: Test 7, Gage 4 - Principle Stress - Angle

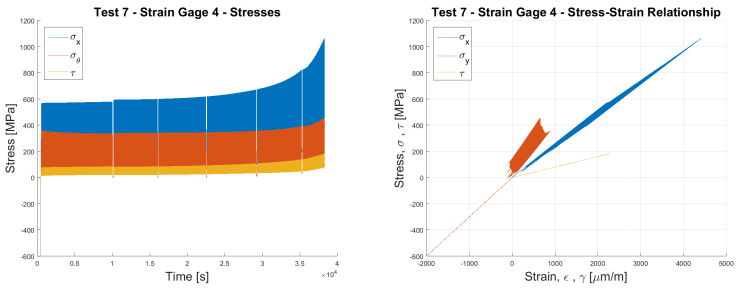

(a) Stress (b) Stress-Strain

Figure A.102: Test 7, Gage 4 - Stress - Stress-Strain

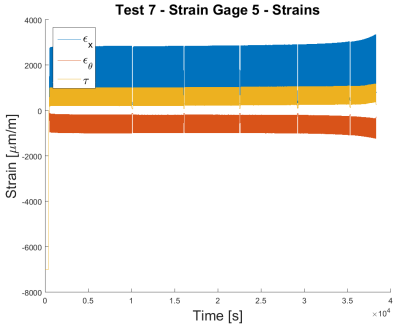

Figure A.103: Test 7, Gage 5 - Strain

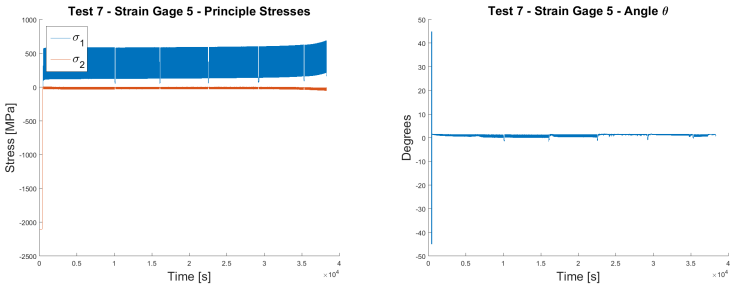

(a) Principle Stress (b) Angle

Figure A.104: Test 7, Gage 5 - Principle Stress - Angle

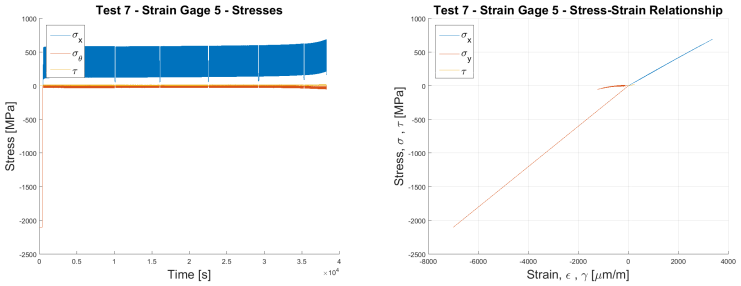

(a) Stress (b) Stress-Strain

Figure A.105: Test 7, Gage 5 - Stress - Stress-Strain

Strain Gage, Test 8

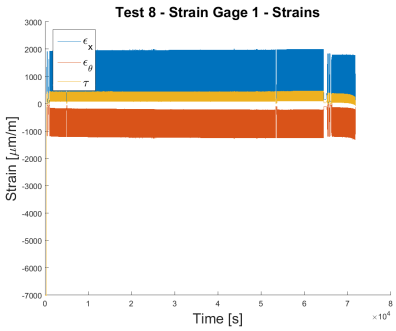

Figure A.106: Test 8, Gage 1 - Strain

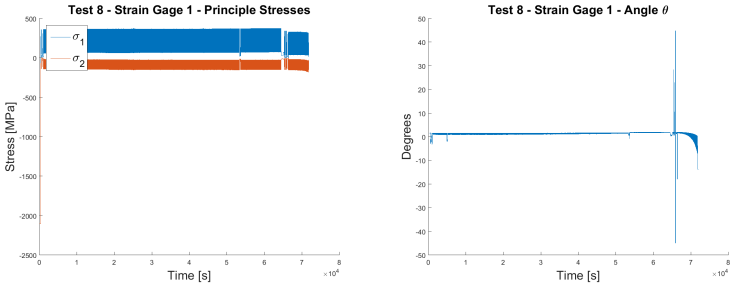

(a) Principle Stress (b) Angle

Figure A.107: Test 8, Gage 1 - Principle Stress - Angle

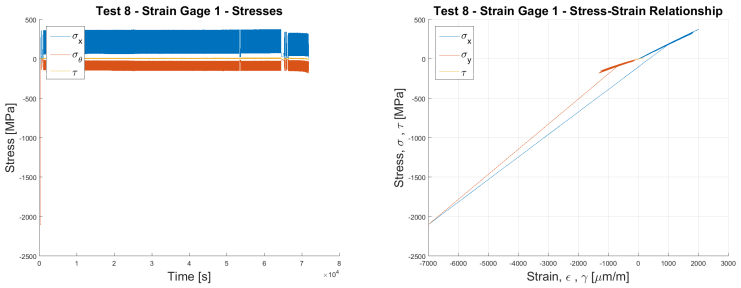

(a) Stress (b) Stress-Strain

Figure A.108: Test 8, Gage 1 - Stress - Stress-Strain

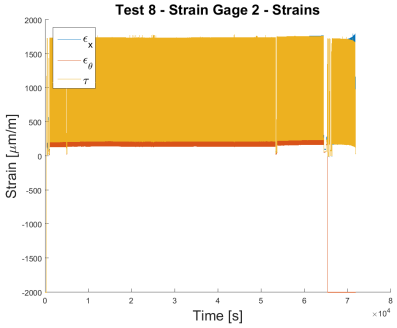

Figure A.109: Test 8, Gage 2 - Strain

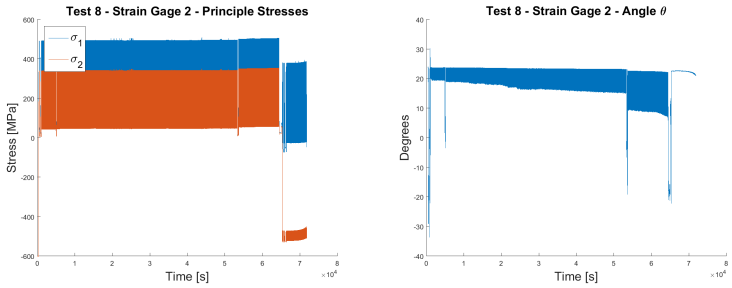

(a) Principle Stress (b) Angle

Figure A.110: Test 8, Gage 2 - Principle Stress - Angle

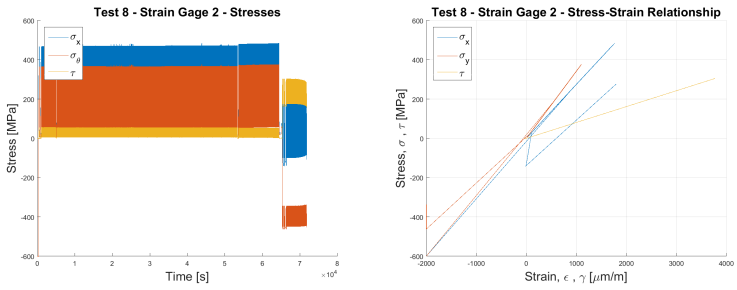

(a) Stress (b) Stress-Strain

Figure A.111: Test 8, Gage 2 - Stress - Stress-Strain

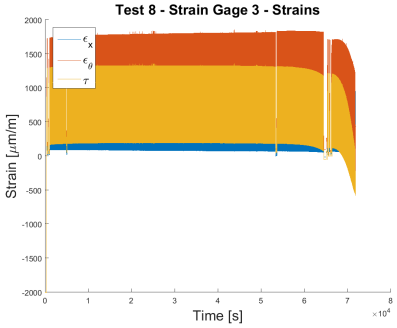

Figure A.112: Test 8, Gage 3 - Strain

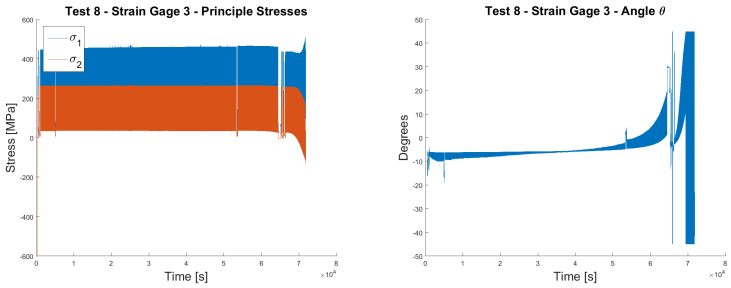

(a) Principle Stress (b) Angle

Figure A.113: Test 8, Gage 3 - Principle Stress - Angle

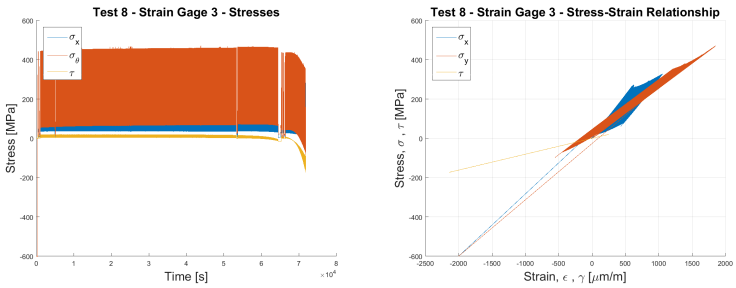

(a) Stress (b) Stress-Strain

Figure A.114: Test 8, Gage 3 - Stress - Stress-Strain

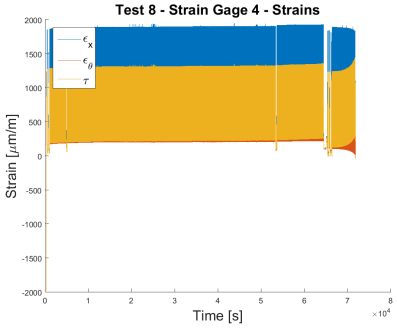

Figure A.115: Test 8, Gage 4 - Strain

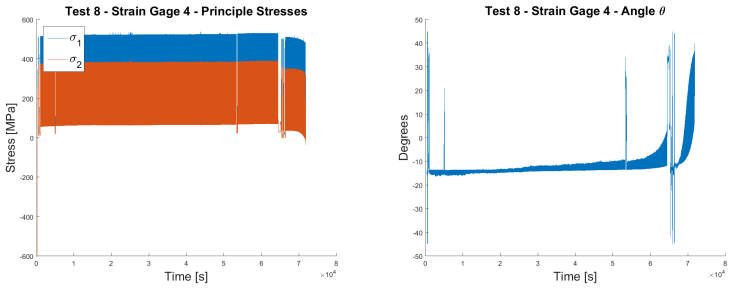

(a) Principle Stress (b) Angle

Figure A.116: Test 8, Gage 4 - Principle Stress - Angle

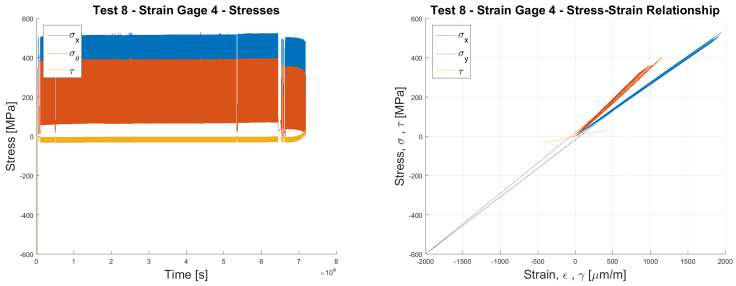

(a) Stress (b) Stress-Strain

Figure A.117: Test 8, Gage 4 - Stress - Stress-Strain

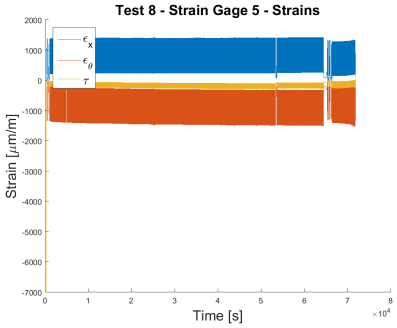

Figure A.118: Test 8, Gage 5 - Strain

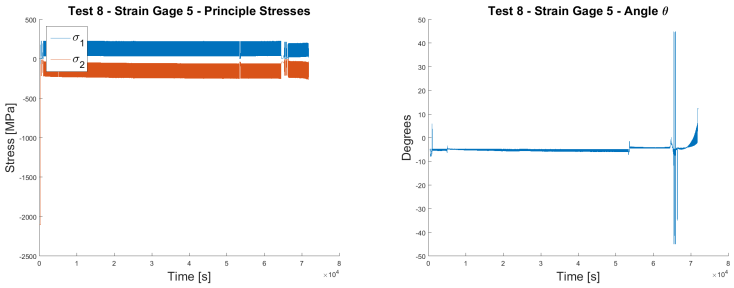

(a) Principle Stress (b) Angle

Figure A.119: Test 8, Gage 5 - Principle Stress - Angle

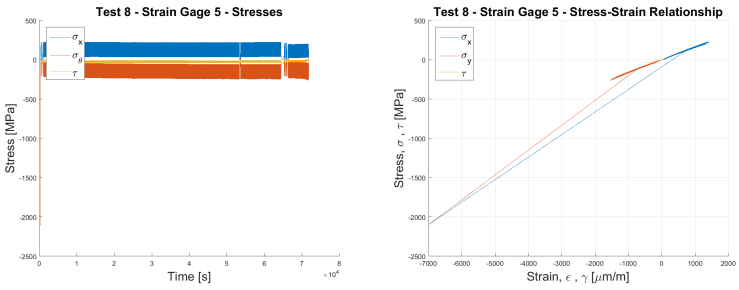

(a) Stress (b) Stress-Strain

Figure A.120: Test 8, Gage 5 - Stress - Stress-Strain

Strain Gage, Test 9

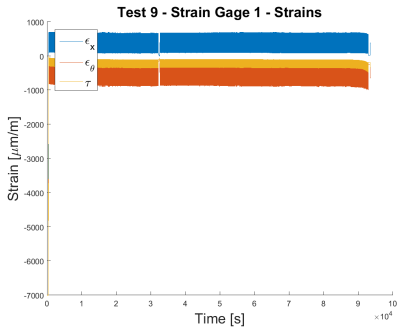

Figure A.121: Test 9, Gage 1 - Strain

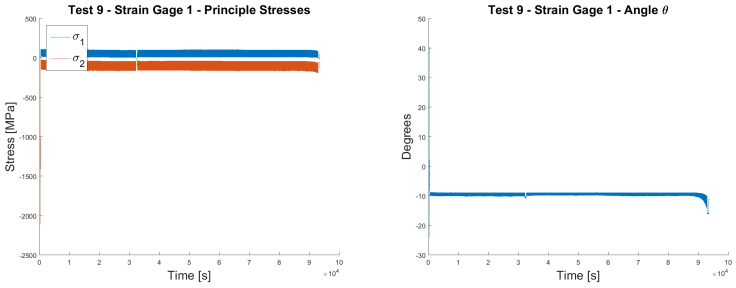

(a) Principle Stress (b) Angle

Figure A.122: Test 9, Gage 1 - Principle Stress - Angle

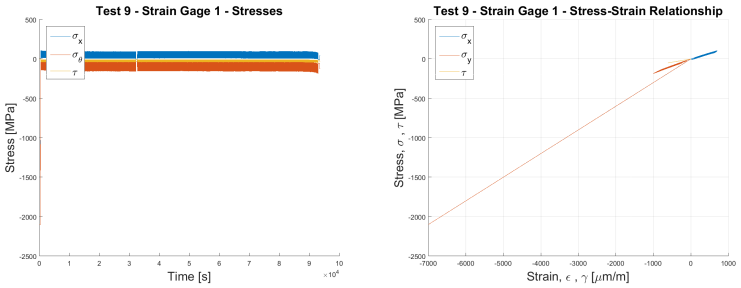

(a) Stress (b) Stress-Strain

Figure A.123: Test 9, Gage 1 - Stress - Stress-Strain

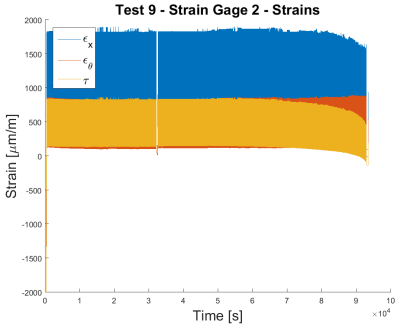

Figure A.124: Test 9, Gage 2 - Strain

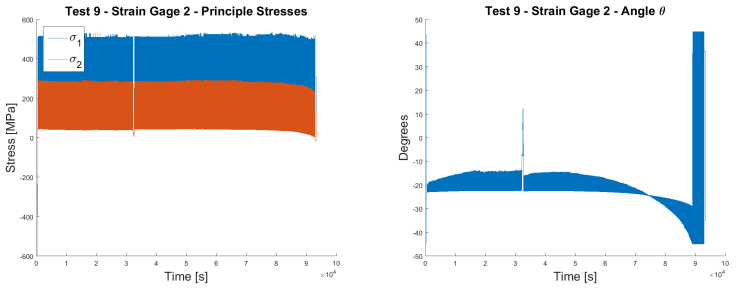

(a) Principle Stress (b) Angle

Figure A.125: Test 9, Gage 2 - Principle Stress - Angle

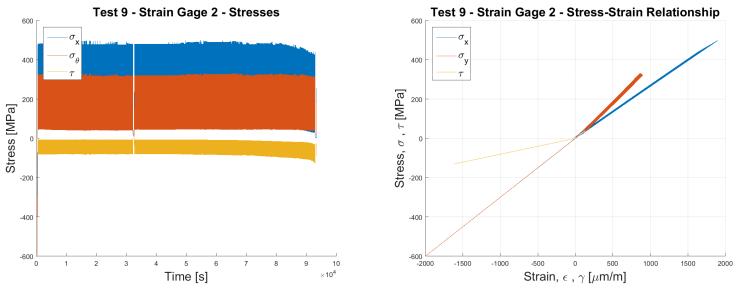

(a) Stress (b) Stress-Strain

Figure A.126: Test 9, Gage 2 - Stress - Stress-Strain

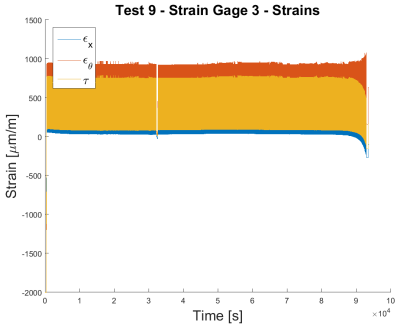

Figure A.127: Test 9, Gage 3 - Strain

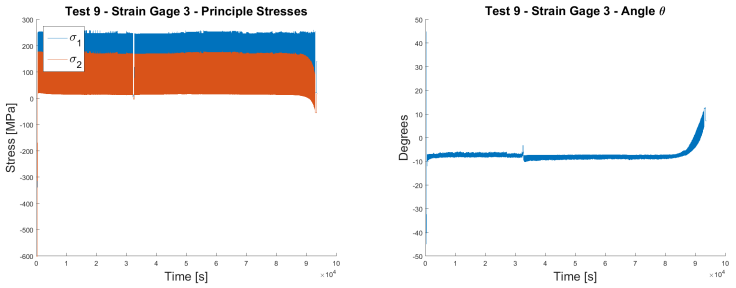

(a) Principle Stress (b) Angle

Figure A.128: Test 9, Gage 3 - Principle Stress - Angle

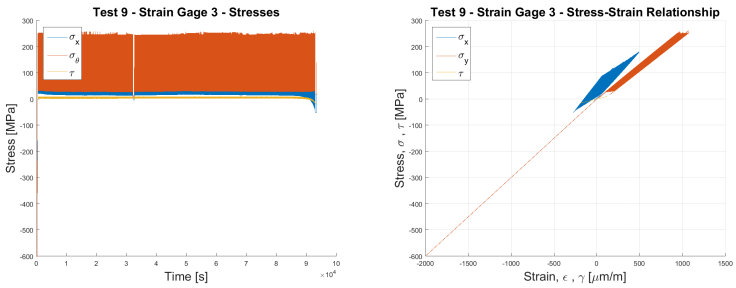

(a) Stress (b) Stress-Strain

Figure A.129: Test 9, Gage 3 - Stress - Stress-Strain

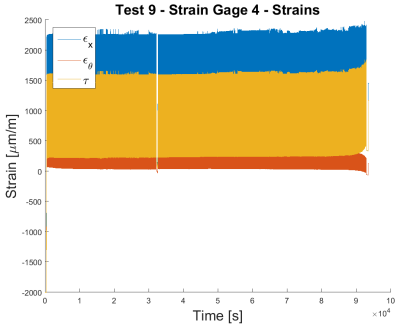

Figure A.130: Test 9, Gage 4 - Strain

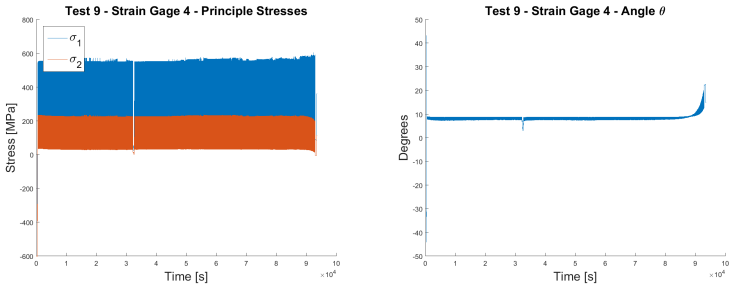

(a) Principle Stress (b) Angle

Figure A.131: Test 9, Gage 4 - Principle Stress - Angle

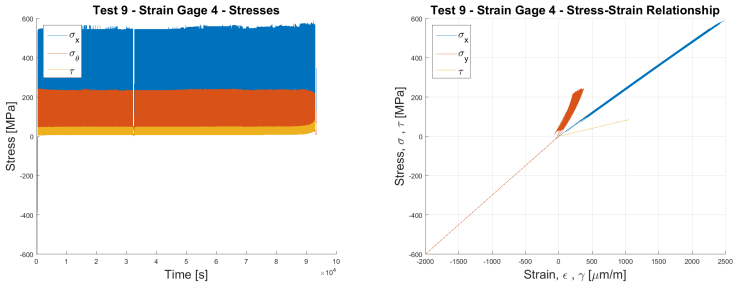

(a) Stress (b) Stress-Strain

Figure A.132: Test 9, Gage 4 - Stress - Stress-Strain

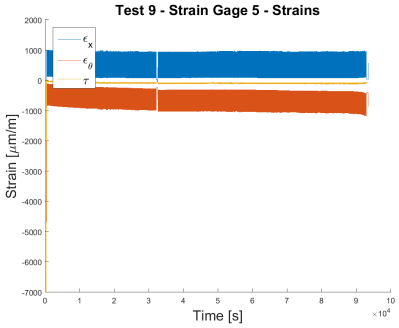

Figure A.133: Test 9, Gage 5 - Strain

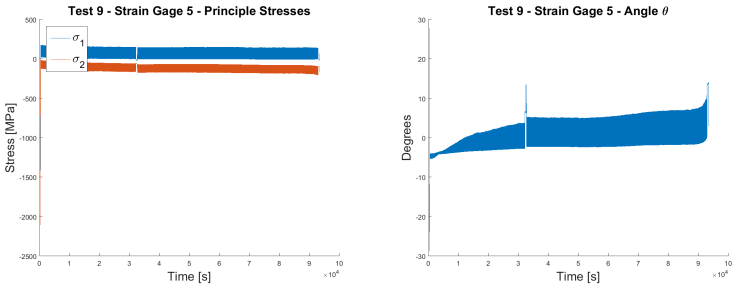

(a) Principle Stress (b) Angle

Figure A.134: Test 9, Gage 5 - Principle Stress - Angle

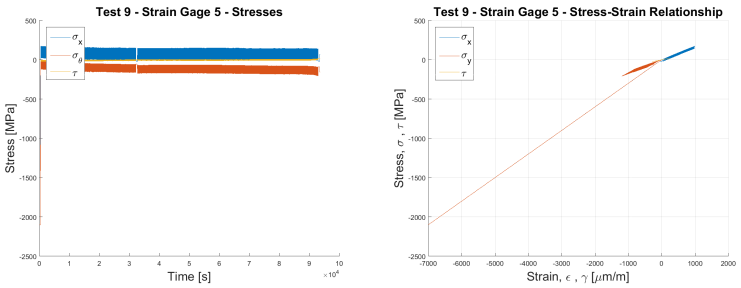

(a) Stress (b) Stress-Strain

Figure A.135: Test 9, Gage 5 - Stress - Stress-Strain

Strain Gage, Test 10

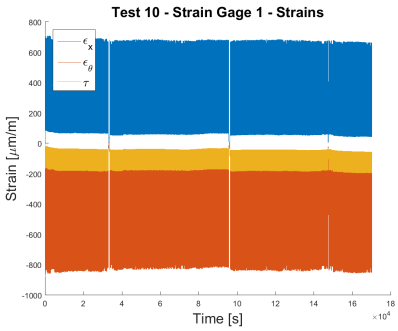

Figure A.136: Test 10, Gage 1 - Strain

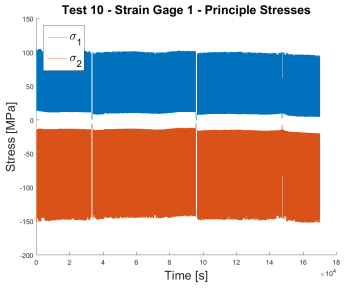

(a) Principle Stress

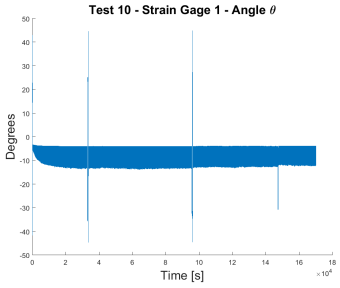

(b) Angle

Figure A.137: Test 10, Gage 1 - Principle Stress - Angle

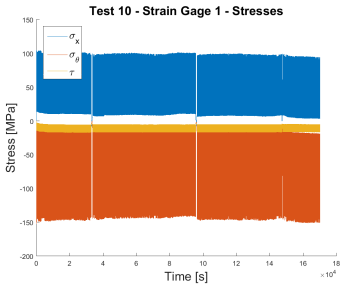

(a) Stress

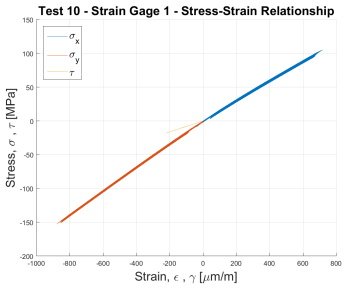

(b) Stress-Strain

Figure A.138: Test 10, Gage 1 - Stress - Stress-Strain

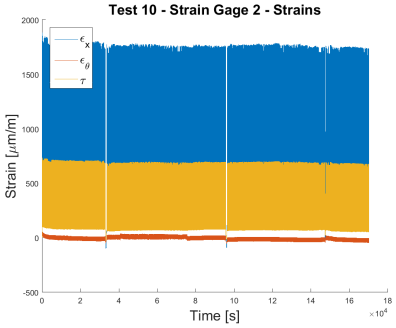

Figure A.139: Test 10, Gage 2 - Strain

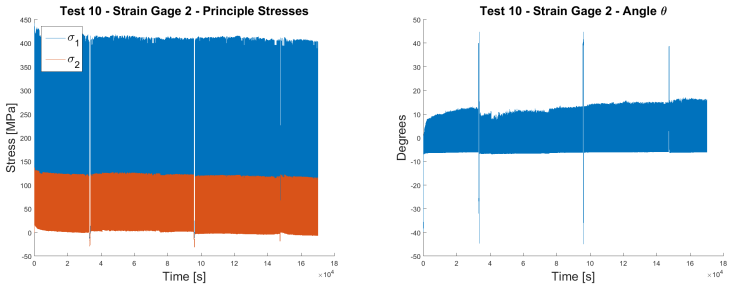

(a) Principle Stress (b) Angle

Figure A.140: Test 10, Gage 2 - Principle Stress - Angle

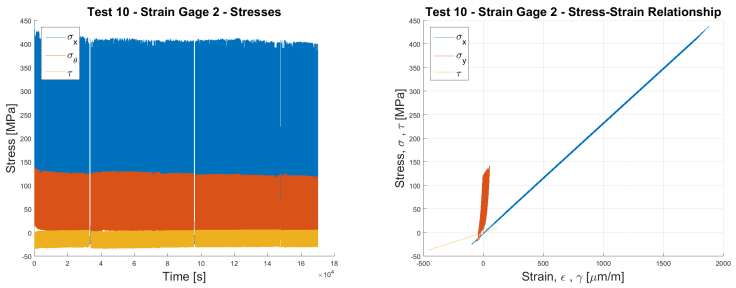

(a) Stress (b) Stress-Strain

Figure A.141: Test 10, Gage 2 - Stress - Stress-Strain

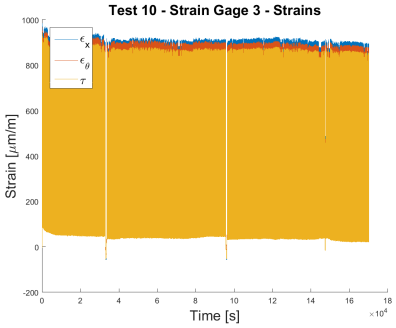

Figure A.142: Test 10, Gage 3 - Strain

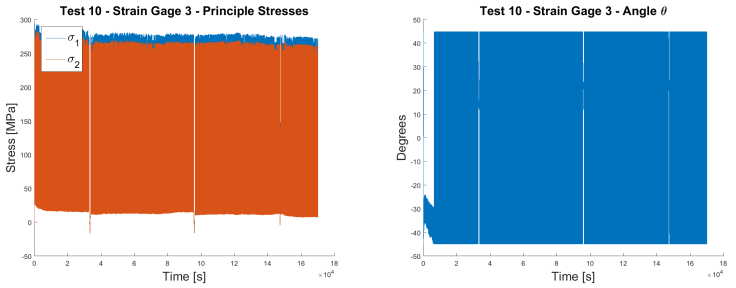

(a) Principle Stress (b) Angle

Figure A.143: Test 10, Gage 3 - Principle Stress - Angle

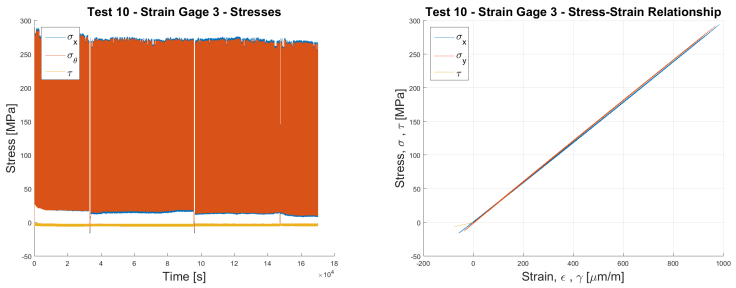

(a) Stress (b) Stress-Strain

Figure A.144: Test 10, Gage 3 - Stress - Stress-Strain

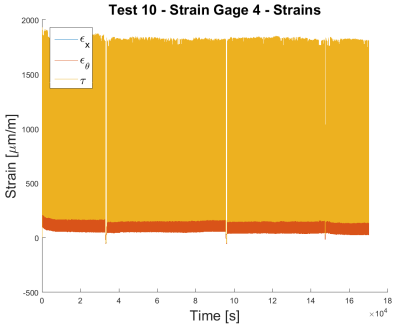

Figure A.145: Test 10, Gage 4 - Strain

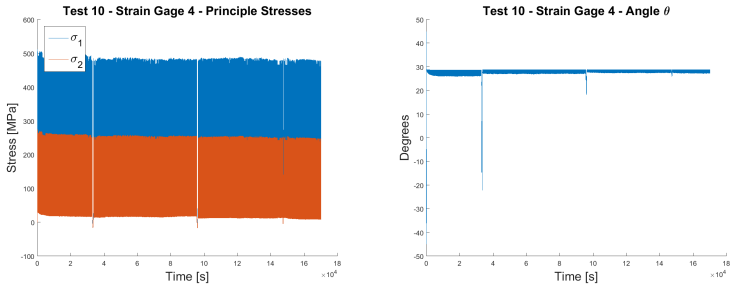

(a) Principle Stress (b) Angle

Figure A.146: Test 10, Gage 4 - Principle Stress - Angle

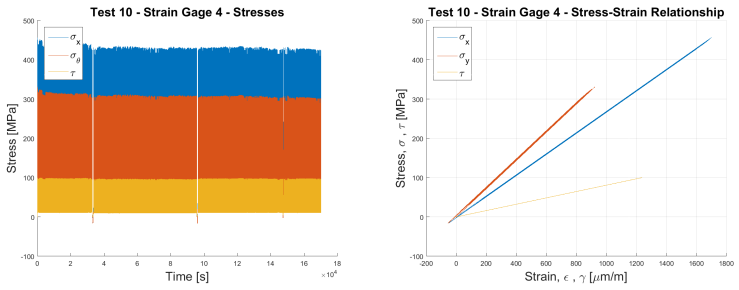

(a) Stress (b) Stress-Strain

Figure A.147: Test 10, Gage 4 - Stress - Stress-Strain

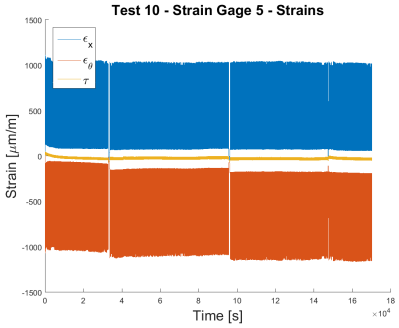

Figure A.148: Test 10, Gage 5 - Strain

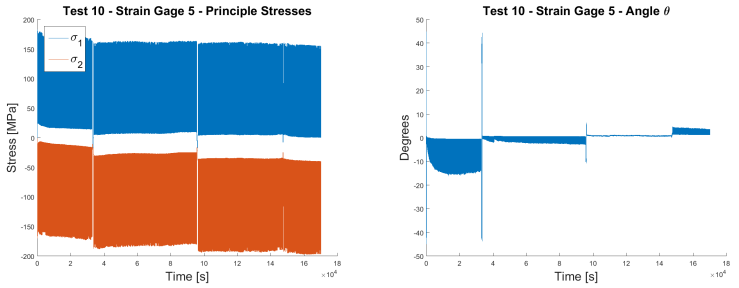

(a) Principle Stress (b) Angle

Figure A.149: Test 10, Gage 5 - Principle Stress - Angle

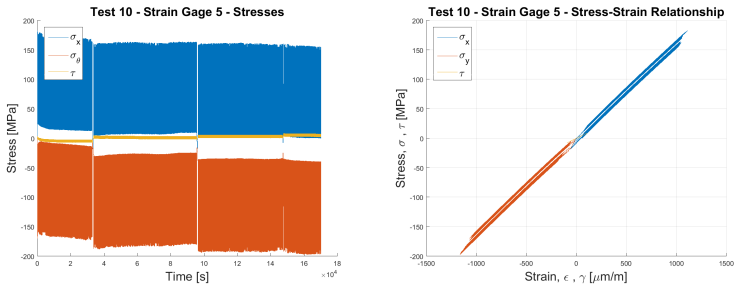

(a) Stress (b) Stress-Strain

Figure A.150: Test 10, Gage 5 - Stress - Stress-Strain

LVDT Data

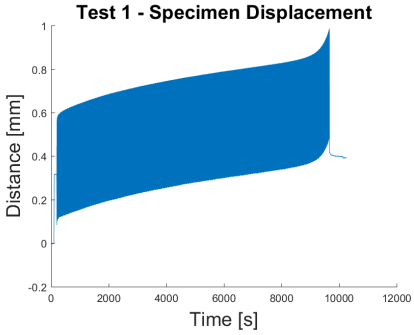

Figure A.151: Dent Displacement for Test 1

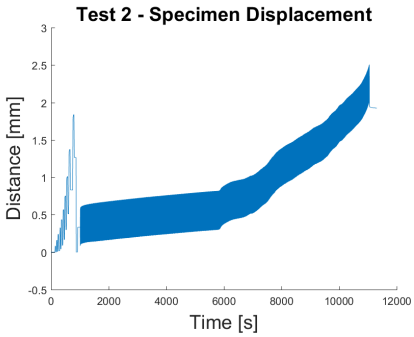

Figure A.152: Dent Displacement for Test 2

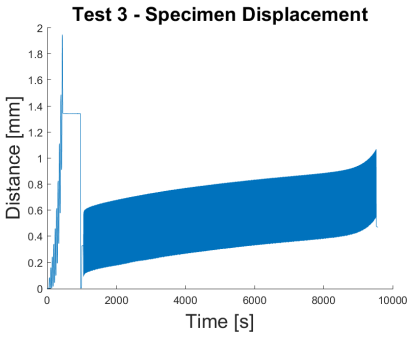

Figure A.153: Dent Displacement for Test 3

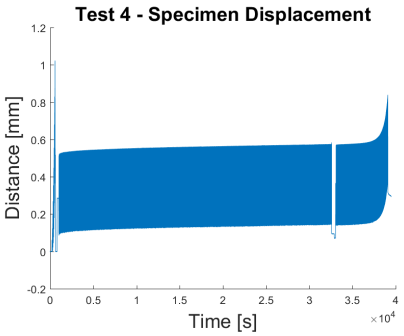

Figure A.154: Dent Displacement for Test 4

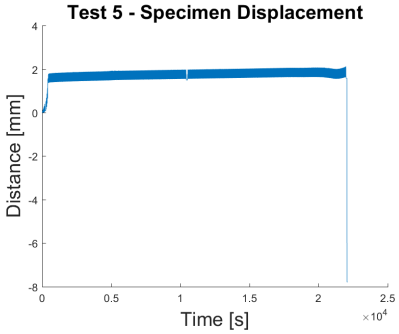

Figure A.155: Dent Displacement for Test 5

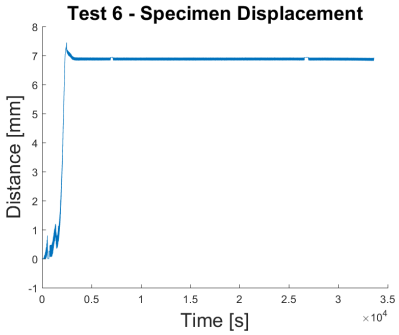

Figure A.156: Dent Displacement for Test 6

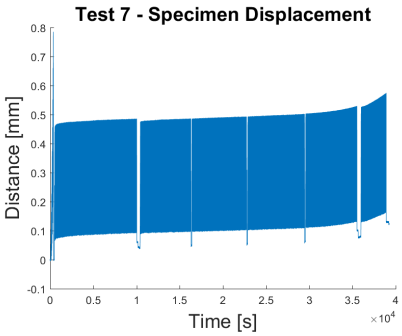

Figure A.157: Dent Displacement for Test 7

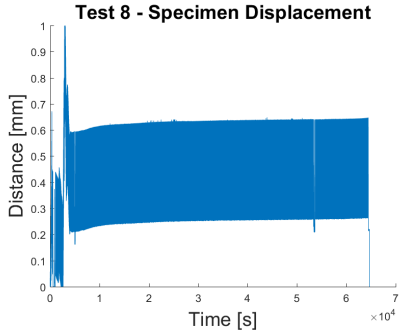

Figure A.158: Dent Displacement for Test 8

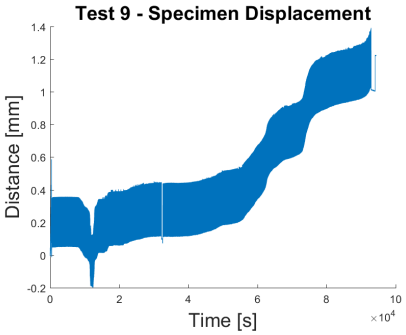

Figure A.159: Dent Displacement for Test 9

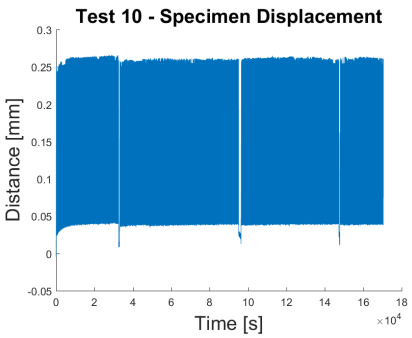

Figure A.160: Dent Displacement for Test 10